Review

Research Progress in Graphene-Based Adsorbents for Wastewater Treatment: Preparation, Adsorption Properties and Mechanisms for Inorganic and Organic Pollutants

Guangqian Li [1], Ruiling Du [1], Zhanfang Cao [1], Changxin Li [2], Jianrong Xue [3], Xin Ma [1,*] and Shuai Wang [1,*]

[1] Hunan Provincial Key Laboratory of Efficient and Clean Utilization of Manganese Resources, College of Chemistry and Chemical Engineering, Central South University, Changsha 410083, China; 15567133352@163.com (G.L.); 13856761570@163.com (R.D.); zfcao1980@csu.edu.cn (Z.C.)

[2] College of Safety Science and Engineering, Nanjing Tech University, Nanjing 211816, China; lichangxin20160706@163.com

[3] College of Chemistry and Chemical Engineering, Hunan University of Science and Technology, Xiangtan 411201, China; jianrongxue@hnust.edu.cn

* Correspondence: maxin2013@csu.edu.cn (X.M.); wangshuai@csu.edu.cn (S.W.); Tel.: +86-731-88879616 (S.W. & X.M.)

Abstract: Graphene-based adsorbents show great potential for application in the field of environmental pollution treatment due to their unique two-dimensional structure, high specific surface area, and tunable surface chemistry. This paper reviews the research on the application of graphene and its derivatives as novel adsorbents in the field of wastewater treatment in recent years, focusing on the preparation and functionalization of graphene-based adsorbents, as well as their adsorption performance and mechanism of action in the removal of inorganic and organic pollutants, and provides an outlook on the future directions of the research on graphene-based adsorbents. The analysis in this paper focuses on the functionalization of graphene-based adsorbents by introducing magnetic particles, hybridization with other materials, and grafting with polymers. The modified graphene-based adsorbents showed significant adsorption and removal of pollutants and were easy to recycle and regenerate. The adsorption of pollutants on graphene-based adsorbents is mainly carried out through π–π interaction, hydrogen bonding, and electrostatic interaction, which is related to the structure of the pollutants. Future research directions on graphene-based adsorbents should focus on in-depth adsorption mechanism studies and the development of cost-effective graphene-based adsorbents for wastewater treatment.

**Keywords:** graphene; adsorbent; ion exchange; adsorption; wastewater treatment

1. Introduction

With the rapid development of industry and the fast increase in population, the problem of increasing pollutants in water bodies is becoming more and more serious. The pollutants in water can be divided into inorganic pollutants and organic pollutants, among which inorganic pollutants mainly include heavy metals, rare metals, and non-metallic inorganic compounds such as fluorides and phosphates, and so on, while organic pollutants mainly include organic dyes, antibiotics and other organic pharmaceuticals, aromatic compounds, etc. These pollutants not only cause certain damage to our environment but also have many adverse effects on human health [1–4]. The issue of pollution of the water environment has slowly come to affect people's daily lives in all aspects. Therefore, addressing the issue of contaminated water and making it cleaner and safer water is a current focus and concern for people in general [5]. When the concentration of pollutants in the human body is higher than the maximum limit that the human body can withstand, these toxic pollutants will have negative impacts on health, with the more serious impacts even leading to cancer [6–8]. As such, the phenomenon of water pollution is a challenge that needs to

be urgently resolved in order to prevent the environment from becoming more hazardous to humans. Thus, the establishment of cost-effective strategies to remove pollutants from wastewater is a global requirement. Today, chemical precipitation [9], ion exchange and adsorption [10], solvent extraction [11], membrane separation [12], electrocatalysts [13], etc., are used for the separation of pollutants in wastewater, among which ion exchange and adsorption are widely used for their advantages relating to easy operation, high efficiency, environmental friendliness, low cost, and the good reusability of adsorbents [14–17]. Carbon materials are popular commodity adsorption materials, such as activated carbon, which has been widely used in wastewater treatment [18–21]. However, the adsorption capacity of activated carbon is limited by its surface characteristics and pore structure, and issues may arise, such as blockages and difficulties in regeneration during its use. In comparison, graphene-based adsorbents demonstrate a wider application potential in the field of wastewater treatment due to their unique structure and excellent chemical stability.

Graphene can be viewed as the basic unit of carbon materials, which can be enclosed, curled, and stacked to form other carbon nanomaterials in other dimensions, such as zero-dimensional fullerenes, one-dimensional carbon nanotubes, and three-dimensional (3D) graphite, as shown in Figure 1a. One-dimensional carbon-based nanomaterials, such as carbon nanotubes (CNTs) and carbon nanofibers (CNFs), have attracted much attention due to their nanoscale dimensions and homogeneous microporous structures with large surface areas. In particular, CNFs are a class of lightweight carbon nanomaterials with excellent specific surface area properties [22]. Until recently, however, CNFs have been mainly associated with catalysis [23], with very few reports of their use as adsorbents. Two-dimensional graphene crystals are formed from closely packed carbon atoms, with a thickness of one carbon atom for each layer of the crystal. The surface is not completely flat, with local microscopic wrinkles and corrugations. However, the hydrophobicity of graphene sometimes hinders its application in water and wastewater treatment. Figure 1b–e represents the molecular structures of graphite, graphene, GO, and rGO, respectively. Among them, graphene oxide (GO) is an important derivative of graphene with a high theoretical specific surface area and a structure similar to that of graphene [24,25], and the structural layers of GO are rich in oxygen-containing functional groups, such as C=O, C–OH, –COOH, and C–O–C [26,27]. Among them, the hydroxyl and epoxy groups are mainly distributed inside the lamellar structure of graphite oxide, while carbonyl and carboxyl groups are mainly distributed at the edges [28–30], as shown in Figure 1d. These functional groups provide good adhesion sites for the adsorption of pollutants in water and have broad application prospects in the field of wastewater treatment [31]. GO materials can also be used as carriers and combined with other materials to form composites, thus improving the performance of the materials themselves. GO-based composites are novel materials that can further improve the adsorption properties and selectivity of graphene through functionalized modification of GO to form new active groups and topologies. The functionalized modification of graphene serves mainly to retain the good physicochemical properties of GO, while effectively compensating for its application limitations. In conclusion, GO and its composites are typical carbon-based adsorbent materials that can effectively remove toxic pollutants from water [32–34].

The aim of this paper is to review recent research advances in the use of graphene and its derivatives for the removal of heavy metals and organic pollutants from water and wastewater. The discussion will focus on the preparation methods and functionalization strategies for graphene-based adsorbents, as well as their performance and mechanism of action in practical applications. Through a comprehensive analysis of the existing literature, this paper will reveal the prospects for the application of graphene in the field of environmental adsorption, and it will point out the problems in the current research and future development directions.
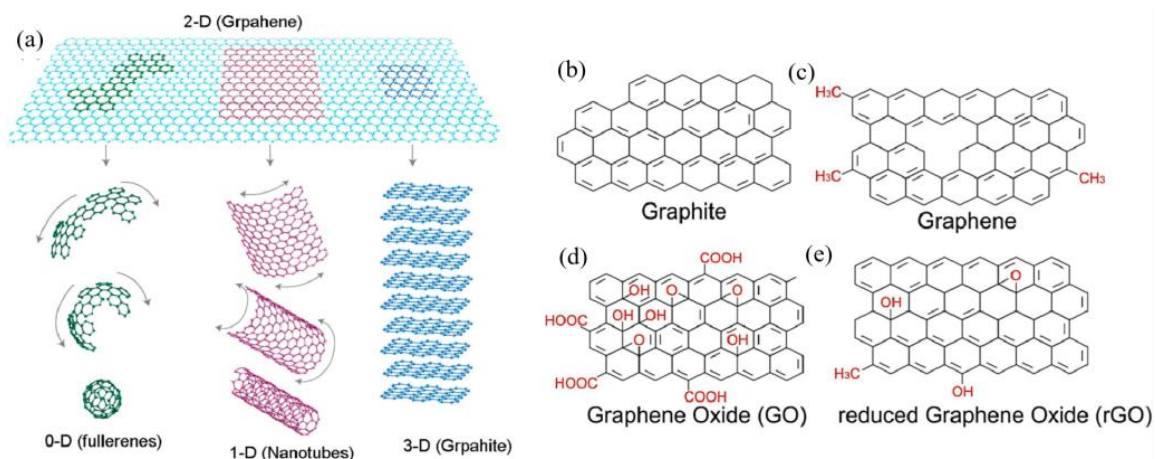
Figure 1. (**a**) Carbon allotropes: graphene to fullerene, nanotubes and graphite. Reprinted with permission from reference [35]. Copyright 2007, Springer Nature. The molecular structure of (**b**) graphite, (**c**) graphene, (**d**) GO, and (**e**) rGO [36]. Copyright Taylor and Francis, 2022.

2. Preparation of Graphene and Its Derivatives

2.1. Preparation of Graphene and GO

2.1.1. Graphene

Graphene has an sp^2 carbon lattice with an extremely high specific surface area, excellent electrical and thermal conductivity, and superior mechanical strength [37]. These properties enable graphene to show great potential for applications in a wide range of fields, including electronic devices, energy storage, composite materials, and environmental governance [38]. Graphene is often referred to as the material of the future due to its chemical stability and many other key advantages [39].

Figure 2 illustrates the two main methods of graphene synthesis: bottom-up and top-down methods [40]. Bottom-up methods involve the continuous growth of graphene through methods that break the chemical bonds of carbon-containing compounds and deposit carbon atoms on a substrate. Bottom-up methods include techniques such as chemical vapor deposition (CVD) [41] and epitaxial growth [42], which build graphene structures at the atomic or molecular level. In contrast, top-down methods are used to obtain graphene from bulk graphite by breaking the van der Waals forces between graphite layers with the help of external forces. Top-down methods include the reduction of graphene oxide via the Hummers method and the modified Hummers method to obtain reduced graphene oxide (rGO) [43]. There are also techniques such as ultrasonic exfoliation [44], ball-milling exfoliation [45], and electrochemical exfoliation [46]. In addition, there are techniques using graphene composites combined with nanoparticles (NPs), such as graphene encapsulation, graphene anchoring, and hybrid hybridization, through which sandwich structures and laminated hybrid NPs are prepared. For the analysis of their physicochemical properties, a variety of microscopic (e.g., scanning electron microscopy, transmission electron microscopy, atomic-force microscopy) and spectroscopic (e.g., X-ray photoelectron spectroscopy, X-ray absorption spectroscopy, Raman spectroscopy, Fourier transform infrared spectroscopy) techniques can be used [47]. Overall, the top-down preparation of graphene is inexpensive, simple, energy-efficient, and easy to scale up.
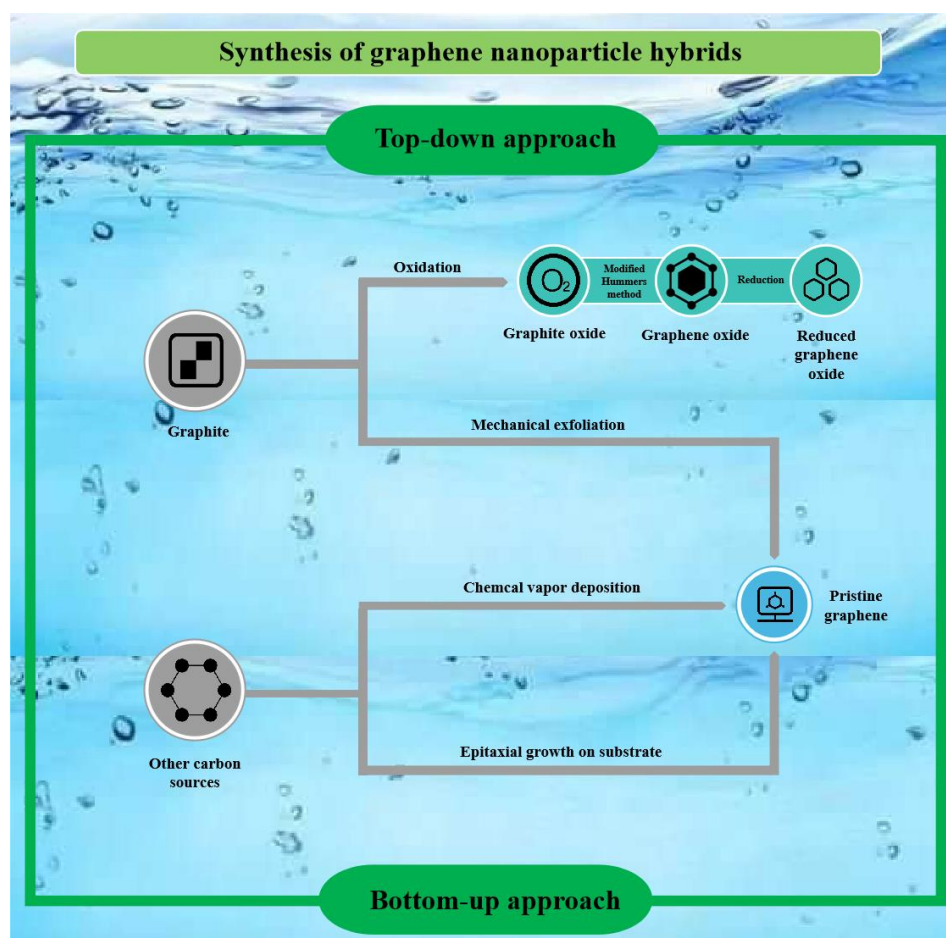
Figure 2. Synthesis of graphene nanoparticle hybrids.

2.1.2. Graphene Oxide

GO has a lower production cost, larger-scale production, and easier processing compared to graphene. It is used as a precursor for the preparation of rGO.

In the conventional Hummers method of preparing GO, it is necessary to reduce residual potassium permanganate with hydrogen peroxide, which is both risky and difficult to control. The use of strong oxidizing agents poses a danger, so a great deal of research has been conducted to find safe and straightforward methods for reducing the risk while preparing high-quality GO. Among them, the Hummers method is the focus of related research. Marcano et al. [48] produced GO using H_2SO_4, H_3PO_4, and $KMnO_4$, while Peng et al. [49] used K_2FeO_4 instead of $KMnO_4$ to reduce the risk caused by high valent manganese ions. Ye et al. [50] designed a microfluidic oxidation method to solve the problems of a long reaction time and poor safety. Zhu et al. [51], meanwhile, prepared acid-less GO by recycling waste acid to reduce environmental pollution. However, the process of adding hydrogen peroxide was still required. Zhou et al. [52] prepared GO without hydrogen peroxide, thus avoiding the high risk of a sharp exothermic reduction reaction due to the quenching reaction with the addition of hydrogen peroxide, whereby they induced the spontaneous reduction of high valent manganese ions by simply adjusting the reaction temperature/time and the amount of concentrated sulfuric acid. It was noteworthy that they achieved a C/O ratio of 1.986, which is lower than that of commercial GO. To promote environmental sustainability, many researchers have explored new production methods for synthesizing GO that offer economic and environmental benefits. Recent researchers have begun to focus on synthesizing GO using alternative, low-cost, carbon-rich materials, including coconut shells, bagasse, tea leaves, pine leaves, and waste tires, rather than graphite. These new preparation methods offer economic and environmental

benefits [53,54]. Many applications can be realized by using waste carbon and converting it into GO [55,56].

### 2.2. Preparation of GO Derivatives

2.2.1. GO Inorganic Composites

GO inorganic composites play a crucial role in wastewater treatment. These composites endow graphene with unique properties, which not only improve the treatment efficiency and effectiveness but also expand the range of applications.

What is widely studied currently is the modification of GO onto magnetic nanoparticles to separate GO from water using gravity or applied magnetic force [57]. Figure 3a shows an efficient procedure for the preparation of magnetically reduced GO composites (MN–CCG) though ultrasonication of a suspension of iron(II) sulfate ($FeSO_4$) with GO in ethanol [58]. The method starts by mixing a GO powder suspension with Fe (II) sulfate, and then ethanol is added for stirring. After sonication, the color of the mixture changes from the original dispersed system to a black precipitate, which indicates the formation of MN–CCG. The MN–CCG composites show scalability and industrial compatibility for the remediation of pollutants.

A number of studies have been conducted on the application of Fe_3O_4/GO and MnO_2/GO in the removal of organic pollutants. Wang et al. [59] prepared Fe_3O_4/GO magnetic composites by sufficiently mixing GO, $FeCl_2$, and $FeCl_3$, adding ammonia drop by drop to adjust the pH to 9 with N_2 being passed through the mixture, and then aging the mixture for 3 h. Chong et al. [60] first synthesized Fe_3O_4/GO though a similar classical co-precipitation method and then proposed preparing Fe^0/Fe_3O_4/GO composites by using a one-step reduction method and investigated the removal properties of typical dyes. As shown in Figure 3b, Fe^0/Fe_3O_4/GO composites were prepared though this method, which has a cumbersome process and needs the toxic chemical hydrazine hydrate in the preparation of Fe^0/Fe_3O_4/GO, as is the case for the one-step reduction method, and at the same time, the new approach maintained the good properties of Fe^0/Fe_3O_4/GO. Das et al. [61] successfully synthesized GO iron nanohybrid (GFeN) materials by modifying iron/iron oxide (Fe/Fe_xO_y) nanoparticles on the surface of GO using a sol–gel process, and they studied these materials' efficiency and performance in removing arsenic from water. Mosleh et al. [62] synthesized iron-containing GO-doped lanthanum titanate ($LaTiO_3$) nanoparticles (FeGO–TiLa) for the effective removal of harmful lead ions from water samples. By utilizing ultrasonic techniques, La(III) ions were coordinated with oxygen-containing ligands to achieve the surface modification of GO through soft–soft interactions. The synthesis of magnetic graphene-oxide-doped titanium lanthanide oxide nanoparticles is shown in Figure 3c. Pan et al. [63] used a mixture of $MnCl_2 \cdot 4H_2O$, $KMnO_4$, and GO to obtain α–MnO_2/GO composites (α–GOM_2) thought an in situ redox reaction. The specific surface area of α-GOM_2 was 2001 $m^2 \cdot g^{-1}$, which was higher than that of GO (1711 $m^2 \cdot g^{-1}$).

GO composites with non-magnetic inorganic materials such as SiO_2, ZnO, and molecular sieves can adsorb pollutants in wastewater very well. Bagbi et al. [64] synthesized and characterized mesoporous silica nanoparticle-decorated GO nanosheets ($MSiO_2$–GO) for the removal of Pb(II) from water. Magnesium dioxide nanoparticles were prepared from ethyl orthosilicate (TEOS) though an ultrasonic method, and GO sheets were prepared using a modified Hummers method. Singh et al. [65] prepared a composite material consisting of zinc oxide (ZnO) nanoparticles and GO through a solvothermal method, and they showed that the material can be used as an adsorbent for the removal of hexavalent chromium ions from an aqueous solution. Li et al. [66] employed the mesoporous material SBA-15 covalently linked with GO to prepare GO–SBA–15. GO–SBA–15 showed good adsorption selectivity for Pb(II) in the presence of Li(I), Na(I), K(I), Ca(II), Mg(II), Cd(II), Cr(III), Co(II), Hg(II), As(III), Mn(II), Ni(II), and Zn(II) ions together.
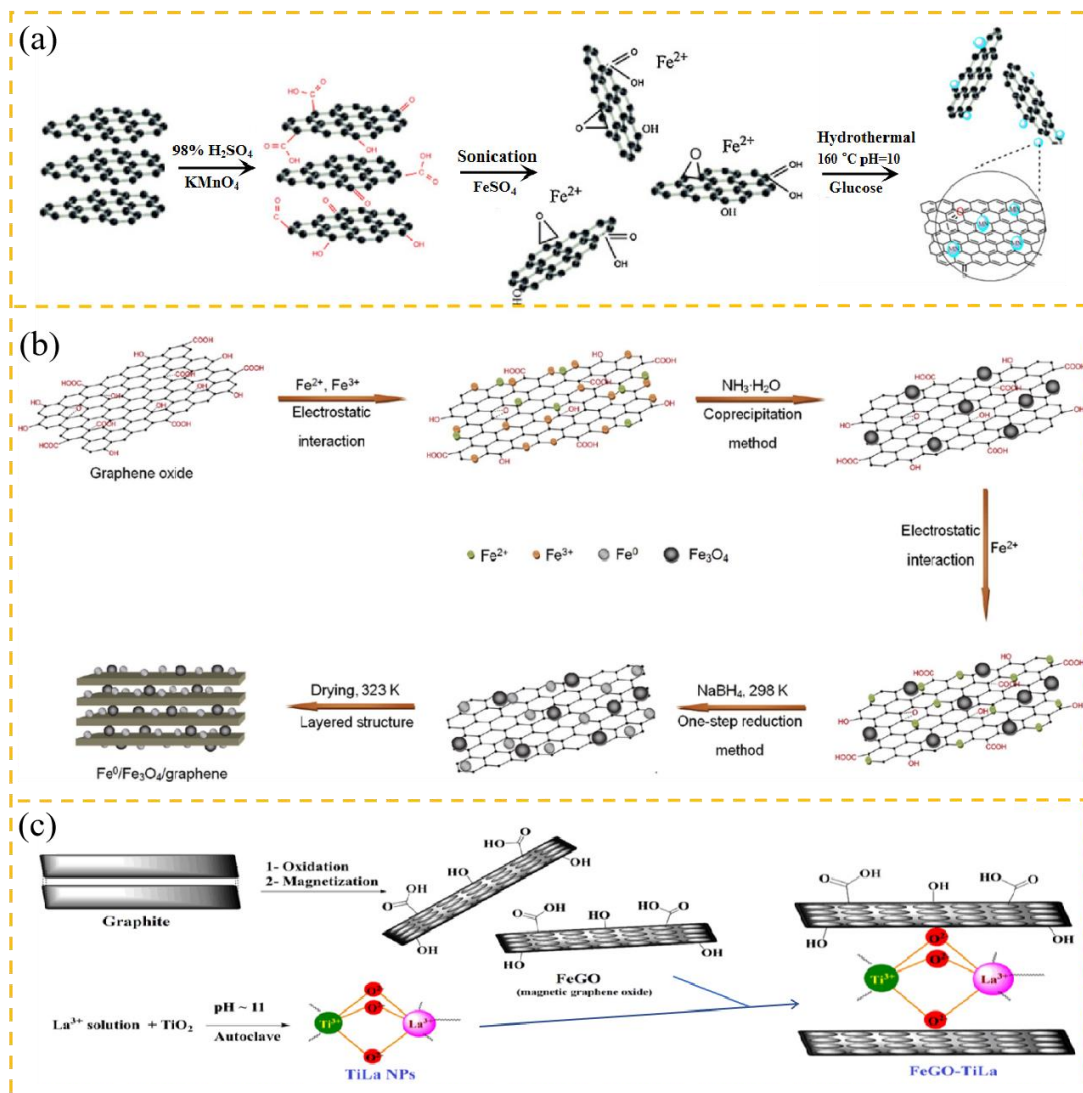
Figure 3. (**a**) Experimental method for synthesizing magnetic GO though the hydrothermal method. Reprinted with permission from reference [58]. Copyright 2011, Elsevier. (**b**) Preparation of $Fe^0/Fe_3O_4/GO$. Reprinted with permission from reference [60]. Copyright 2016, Elsevier. (**c**) Magnetic graphene oxide dopes titanium lanthanum oxide nanoparticle synthesis. Reprinted with permission from reference [62]. Copyright 2022, Elsevier.

2.2.2. GO Polymer Composites

GO, when composited with other polymeric materials, can significantly increase the adsorption capacity for specific pollutants. Such composites typically exhibit higher adsorption capacities and faster adsorption rates. Though the selection of polymer materials with different functions, GO composites can be functionally customized to remove different types of pollutants from wastewater in a targeted manner.

There are a large number of –OH and –NH$_2$ in chitosan (CS), and these functional groups can combine with oxygen-containing groups on GO through hydrogen bonding or other interactions to improve the stability and functionality of the composites. Li et al. [67] successfully developed GO/CS composites (GCs) though the dropwise addition of GO hydrosol onto the surface of CS. The prepared adsorbent was used for simulated static adsorption of copper, lead, and cadmium ions in 50 mg·L^{-1} simulated wastewater. Sherlala et al. [68] prepared CS magnetic GO nanocomposites (CMGO) by using a chemical coprecipitation method, and they studied their adsorption properties for removing arsenic from water.

However, the CS/GO composites showed a low adsorption capacity and poor selectivity. Therefore, it seems necessary to graft specific functional groups on CS/GO composites (CGs) to enhance their adsorption performance for pollutants in wastewater. Xia et al. [69] used GO, CS, and phytic acid as raw materials to directly prepare a novel CS/GO composite containing phytic acid (PCG) though a hydrothermal reaction for the removal of uranium (VI) from an aqueous solution where the phytic-acid-containing CS/GO composite was prepared as shown in Figure 4a. The FTIR and XPS survey spectra of GO, CG, and PCG are shown in Figure 4b,c, demonstrating the successful synthesis of PCG. The results showed that the PCG produced via chemical bonding of the hydroxyl group in the phytic acid molecule with the amino group in CS had a porous structure with a lamellar surface, good thermal stability, and chelating ability for uranium (VI). Zhou et al. [6] prepared a novel composite polyamide oxime/GO/CS composite (PAO/GO/CS) though crosslinking and in situ polymerization, and the synthesis route is shown in Figure 4d. The FTIR and XRD analysis of PAO/GO/CS and its precursor composites before adsorption of U(VI) are shown in Figure 4e,f. This indicates that the amidoxime groups were successfully grafted onto the surface of GO/CS. The resulting defects in uranium (VI) adsorption could be compensated by grafting amidoxime on the surface of GO/CS. According to the characterization and density-functional theory (DFT), uranium (VI) was spontaneously adsorbed onto the oxygen-containing groups in PAO/GO/CS mainly though chemisorption. Zhang et al. [70] prepared a GO suspension by using the improved Hummers method combined with ultrasonic dispersion technology, and then they successfully synthesized a new material, GEC, through covalent binding and electrostatic interaction with CS and EDTA-2Na.

GO can also be composited with other polymeric materials such as sodium alginate, resins, polyethyleneimine, and polyamide dendritic polymers. Abd-Elhamid et al. [71] studied a new strategy for modifying GO with sodium alginate (SA) using ethyl orthosilicate (TEOS) as a binding agent. The GO–sodium alginate composites contained a high number of carboxylate (–COO–Na$^+$) groups, which can interact with metal ions quickly and efficiently. The preparation of GO–SA is shown in Figure 5a. Ma et al. [72] utilized Amberlite IRC748 resin to modify GO to prepare a multifunctional composite adsorbent (IRC748–GO), and the mode of IRC748–GO synthesis is shown in Figure 5b. Arshad et al. [73], meanwhile, synthesized a composite of polyethyleneimine and GO, which showed an excellent adsorption capacity and stability for heavy metal ions such as Pb(II), Hg(II), and Cd(II) in an aqueous solution. Peer et al. [74] prepared a magnetic GO–polyamide dendrimer (mGO–PAMAM) composite by using a "grafting" strategy and investigated its adsorption behavior on Cu(II), Pb(II), and Cd(II). Moreover, Ma et al. [75] synthesized graphene-loaded Fe$_3$O$_4$ nanoparticles as carriers and ethylenediamine and methyl acrylate as functional monomers by using stepwise growth chemistry to synthesize polyamide amide dendritic polymer-functionalized magnetic GO with different generations of polyamide amide dendritic polymers (MGO–PAMAM). The synthesis process of MGO–PAMAM is shown in Figure 5c.
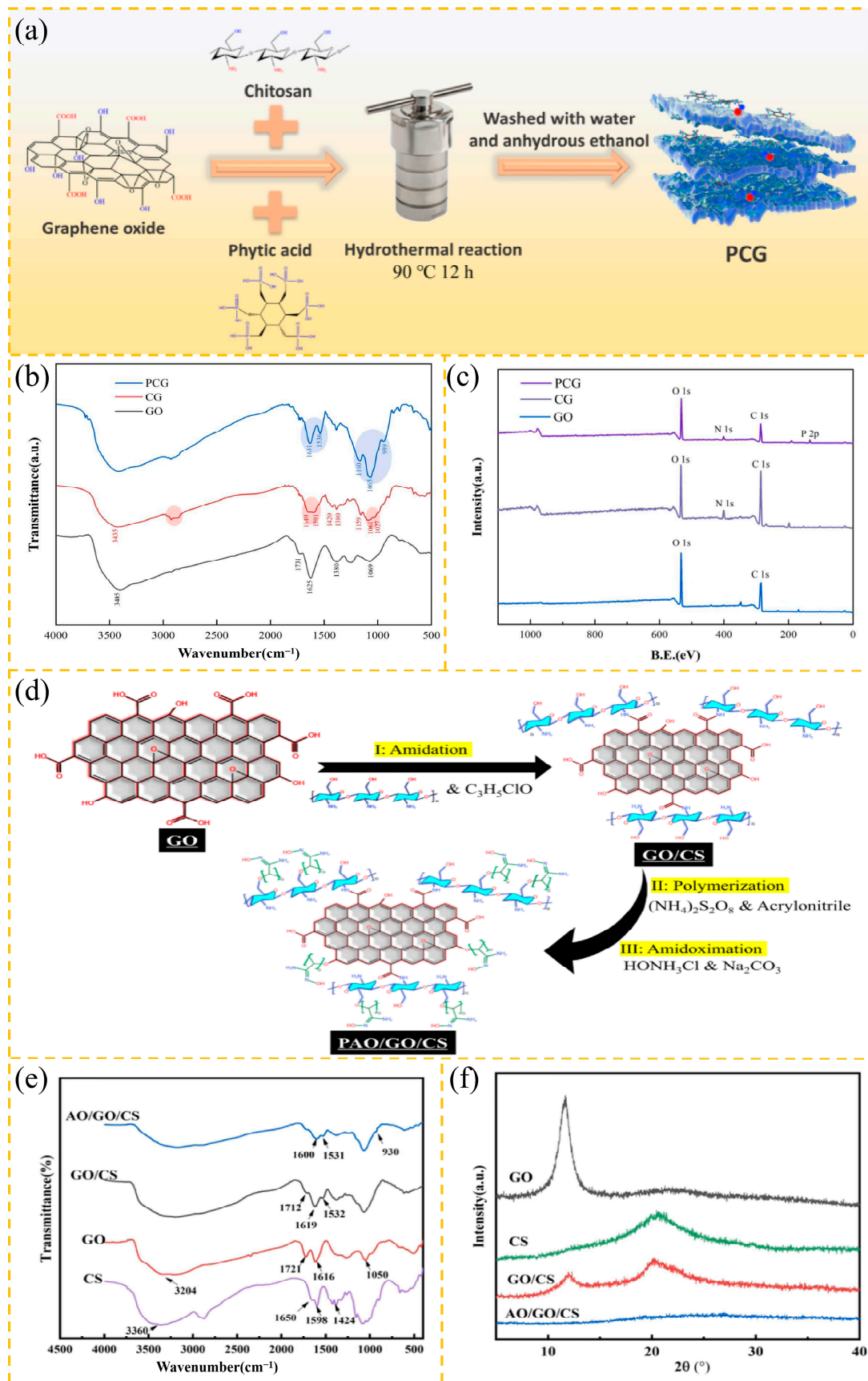
Figure 4. (**a**) Flowchart for the preparation of CS/GO composites containing phytic acid. (**b**) FTIR spectra of GO, CG, and PCG. (**c**) XPS survey spectra of GO, CG, and PCG. Reprinted with permission

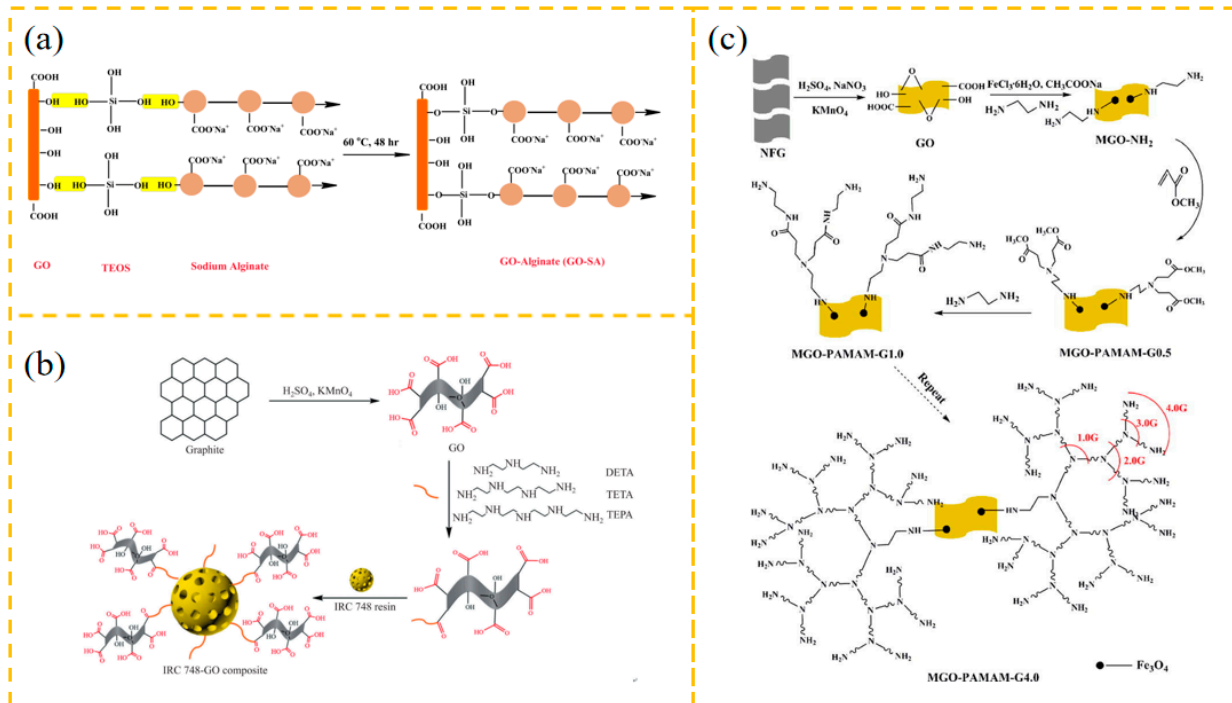from reference [69]. Copyright 2022, Elsevier. (**d**) Roadmap for synthesizing PAO/GO/CS composites. (**e**) FTIR spectra and (**f**) XRD spectra of PAO/GO/CS and its precursor composites. Reprinted with permission from reference [6]. Copyright 2021, Elsevier.

Figure 5. (**a**) Preparation of GO–SA adsorbent [71]. Copyright 2016, Springer Nature. (**b**) Synthesis of IRC748–GO composite. Reprinted with permission from reference [72]. Copyright 2024, Springer Nature. (**c**) Synthesis process of MGO-PAMAM. Reprinted with permission from reference [75]. Copyright 2024, Elsevier.

2.3. Preparation of 3D Graphene-Based Adsorbents

Due to π–π interaction, GO is easily stacked and aggregated, which greatly reduces the adsorption capacity and limits its further application, and the need for centrifugal and magnetic separation techniques complicates the material recovery process. Instead, assembling graphene nanosheets into 3D monolithic porous macrostructures prevents agglomeration and promotes mass transfer. This bulky structure also facilitates their collection and manipulation in water, which may open up a new avenue for graphene materials, one that works toward developing green and sustainable catalysis. 3D GO materials not only have a high specific surface area and porous structure [76], which enhance the adsorption capacity, but also can be effectively reused through a simple recycling process without any loss of material due to their 3D structure, which further expands the scope of GO applications. The preparation method for 3D GO and its composites and their application in the field of water treatment has come to form a hot spot of current research [77]. A large number of literature studies have shown that 3D graphene with such structures can effectively adsorb organic solvents [78], dyes [79], heavy metals [80], and antibiotics [81] in water.

2.3.1. Graphene Foam

Graphene foam is a material with a stable honeycomb structure made from tubular graphene through specific physical and chemical means. This material has a large specific surface area, light weight, and has high mechanical strength. As an advanced 3D-structured carbon material, graphene foam has a variety of remarkable structural properties and a wide range of preparation methods, which give it great potential for application in many fields.

Foamed graphene via freeze-drying, chemical vapor deposition, hydrothermal methods and so on. Jayanthi et al. [82] employed a freeze-drying technique to prepare porous 3D graphene foam. The material has a macroporous structure that allows the diffusion of pollutants within its pores, which is effective in the adsorption of Rhodamine B, malachite green, and acridine yellow and avoids the problem of decreasing adsorption capacity due to the stacking of single layers of graphene. Lei et al. [83] obtained a graphene oxide foam (GOF) by using chemical vapor deposition. This material has a high surface area ($578.4 \text{ m}^2 \cdot \text{g}^{-1}$), is rich in oxygen-containing functional groups, and its adsorption capacities of Zn(II), Cd(II), Pb(II), and Fe(III) were higher than those of activated carbon, CNs, carbon foam, and GO adsorbents.

2.3.2. Graphene Sponge

Graphene sponge (GS) is a material constructed from two-dimensional graphene nanosheets built on top of each other, which can effectively impede agglomeration between graphene sheet layers and has excellent properties such as a large specific surface area, high mechanical strength, good electrical conductivity, large adsorption capacity, and good thermal stability.

Graphene sponge preparation methods include the hydrothermal method, freeze-drying, chemical vapor deposition, physical mixing, and so on. Wu et al. [84] found that GO can be hydrothermally reduced by glucose to form a graphene sponge for the adsorption of various organic solvents. During hydrothermal treatment, graphene sheets were reduced by glucose and formed a 3D porous structure. Bagoole et al. [85] used a modified Hummers method to synthesize GO solutions, followed by high-pressure hydrothermal treatment, freeze-drying, and chemical vapor-phase functionalization to prepare 3D graphene sponges. The surface-functionalized materials proved to have an excellent performance in terms of high-efficiency adsorption. These findings provide a valuable reference for the future development of novel separation materials. Yu et al. [81], meanwhile, prepared a magnetic GO sponge (MGOS) for the adsorption of tetracycline by freeze-drying dispersion of Fe_3O_4 nanoparticles and GO. The small size and negative surface charge of Fe_3O_4, the high degree of oxidation of graphene, and freeze-drying were responsible for the high adsorption capacity of MGOS. The adsorption behavior of tetracycline on MGOS suggests that MGOS holds promise for the remediation of tetracycline-based pollutants. Maimaiti et al. [86] designed a magnetic Fe_3O_4/TiO_2/graphene sponge (MFTGS) with a good regeneration ability in efforts to remove dyes. Fe_3O_4 was mixed with GO, and then tetrabutyl titanate was hydrolyzed to deposit titanium dioxide on the Fe_3O_4/GO mixture. The results showed that an MFTGS has the potential to remove dye contaminants from aqueous environments and can be regenerated through simple washing conditions. To further reduce the cost, Sun et al. [87] developed a flexible one-pot method to synthesize a novel amino-functionalized graphene sponge sorbent (AFGS) by taking advantage of the low-cost and super-hydrophilicity of the commercially available melamine sponge (MF), in which the graphene nanosheets were assembled into a 3D network on the backbone of the melamine sponge with the assistance of ethylenediamine. The formation process and morphology of AFGS, which is different from graphene sponge, are shown in Figure 6. Figure 6a shows that the MF backbone formed a 3D porous structure. Under the conventional dip-coating method (Route 1 and Figure 6b,c), the surface of the sponge skeleton was encapsulated by graphene fragments. The SEM image of graphene sponge at high magnification (Figure 6c) is shown. In contrast, the AFGS obtained by route 2 showed a leafy graphene structure grown on spongy branches (Figure 6d). The size of leafy graphene sheets is about tens to hundreds of micrometers (Figure 6e).
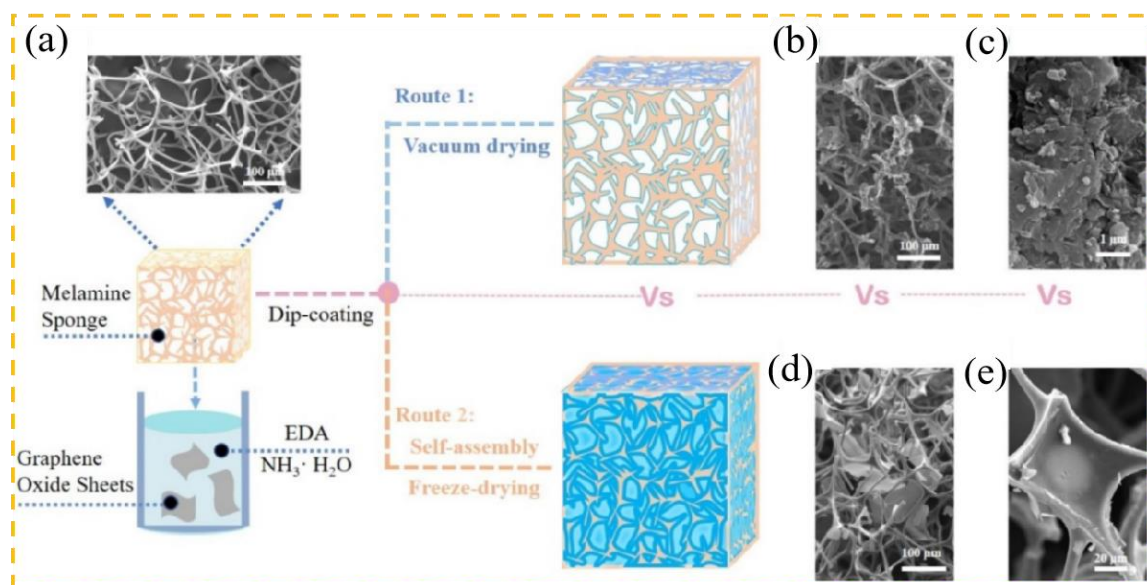
Figure 6. (**a**) Synthetic route and SEM images of melamine sponge. (**b**,**c**) SEM images of graphene sponge at low magnification and high magnification. (**d**,**e**) SEM images of AFGS at low magnification and high magnification. Reprinted with permission from reference [87]. Copyright 2021, Elsevier.

2.3.3. Graphene Gel

Graphene is highly hydrophobic and has a low adsorption capacity. In order to maintain a stable dispersion of graphene-based adsorbent materials, various methods have been employed to synthesize 3D graphene-based gels, such as hydrothermal reduction [88], chemical reduction [89], and chemical vapor deposition [90].

Hydrogels have attracted much attention due to their simple synthesis, ease of handling, low cost, and high adsorption efficiency [91]. Hydrogels can absorb large amounts of liquids and low-molecular-weight compounds without losing their original shape [92]. Due to their unique functionality, reusability, and high adsorption capacity, hydrogels are considered ideal adsorbents for future adsorption processes [93]. Developing hydrogel-based adsorbents for the adsorption of various aquatic pollutants has now become a focus of research. Taye et al. [94] prepared a hydrogel named water hyacinth leaf protein concentrate/GO (WHLPC/GO) using a one-step hydrothermal method for the treatment of Cr(VI) hexavalent chromium in wastewater. The material consisted of a combination of water hyacinth leaf protein concentrate (WHLPC) and GO, of which WHLPC accounted for about 90%. Sahraei et al. [80] prepared novel magnetic biosorbent hydrogel spheres using modified biopolymers, gum tragacanth (GT), poly(vinyl alcohol) (PVA), and GO, using the gel method to remove a variety of target pollutants, and they found that these spheres to be promising for a wide range of applications in the simultaneous removal of various pollutants from water. The preparation method is shown in Figure 7a. Yao et al. [95] synthesized tannic-acid-functionalized graphene (TA-rGO) in a simple and green method. A pH-responsive TA-functionalized graphene hydrogel (TRGAA) was synthesized though a random copolymerization reaction in the presence of TA-rGO using 2-acrylamido-2-methyl-1-propanesulfonic acid (AMPSA) and acrylic acid (AA) as raw materials, and the synthesis of TRGAA hydrogel is shown in Figure 7b.

Graphene aerogels are a class of monolithic materials with a well-developed pore structure. These 3D porous materials have the advantages of low density, low thermal conductivity, and well-developed pores. They also have an interconnected porous structure, high specific surface area, high pore volume, thermal and electrical conductivity, and environmentally friendly properties [96,97]. The methods to prepare them include the freeze-drying method, chemical reduction self-assembly method, and so on. Deng et al. [98] prepared a phosphoric-acid-modified aloe/CS aerogel (CS/AL-AP) though self-assembly

with CS, phosphoric acid, and aloe vera powder, achieved by using vacuum freeze-drying. CS/AL-AP was prepared as shown in Figure 7c. Nundy et al. [99], meanwhile, fabricated 3D, porous, lamellar rGO aerogel to explore their potential for antimony removal from wastewater, where the process was the synthesis of rGO aerogels from graphite flakes using the modified Hummers method, as shown in Figure 7d.
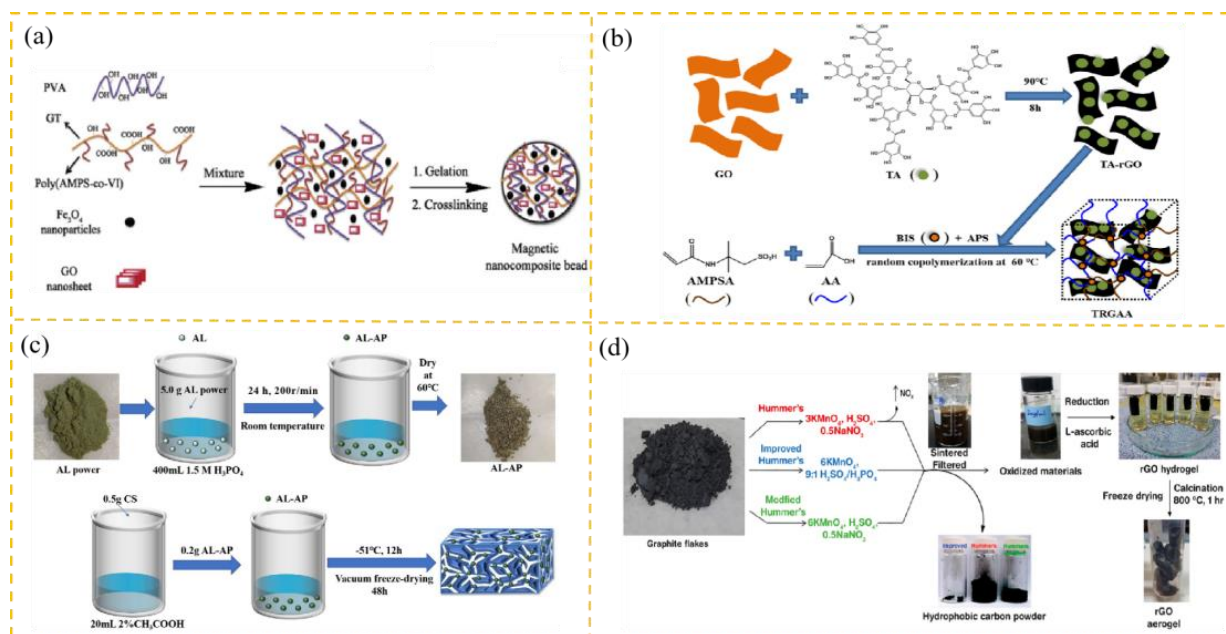
Figure 7. (**a**) Preparation of magnetic biosorbent hydrogel spheres. Reprinted with permission from reference [80]. Copyright 2017, Elsevier. (**b**) Synthesis of TRGAA hydrogel. Reprinted with permission from reference [95]. Copyright 2021, Elsevier. (**c**) Preparation of CS/AL-AP. Reprinted with permission from reference [98]. Copyright 2022, Springer Nature. (**d**) Synthesis of rGO aerogels from graphite flakes using a modified Hummers method. Reprinted with permission from reference [99]. Copyright 2021, Elsevier.

3. Adsorption of Inorganic Pollutants with Graphene-Based Adsorbents

3.1. Heavy Metals

The current environmental issue of heavy metal pollution, classified as an inorganic pollutant, is prevalent and has detrimental effects. The main heavy metal ions, including arsenic, chromium, lead, selenium, and mercury, are persistent and toxic substances that pose a significant threat to organisms and the environment. They enter the ecosystem through various industrial processes, mining activities, and inappropriate waste disposal [100]. Heavy metals are difficult to degrade, easy to accumulate, and have high toxicity after entering a water body. Heavy metals accumulate in animals and plants throughout the water body, and eventually, they pass to humans through the food chain. A large amount of heavy metal accumulation in organisms will affect their physiological activities, resulting in chronic poisoning and even death. Heavy metal pollution of water bodies is, thus, an environmental problem that needs to be solved urgently. If there is no effective, comprehensive treatment of polluted water bodies, the ecological environment will suffer serious damage and human health will be seriously harmed [101,102].

3.1.1. Arsenic

The high toxicity of arsenic renders it one of the prominent contaminants in various environmental pollutants. Arsenic can infiltrate the human body through the food chain or water, exerting toxic effects by influencing metabolic enzymes, inducing lipid peroxidation, causing genetic damage, and altering gene expression. The widespread concern over the

detrimental effects caused by arsenic pollution necessitates urgent measures for its removal from various water bodies.

Various treatment techniques for arsenic removal have been investigated. These include physicochemical processes such as adsorption [103], precipitation [104], and membrane separation [105]. Among them, adsorption is considered an economical and simple operational technique for arsenic remediation. Various materials can be used as possible adsorbents for the removal of arsenic. Although commercial activated carbon has been used for As(V) adsorption, its adsorption capacity is low, reaching a maximum of only 4.96 mg·g^{-1} at pH 7 and 25 °C [106]. Elsewhere, GO has received attention as a potential adsorbent for arsenic removal. The presence of functional groups such as hydroxyl, carboxyl, and epoxy groups promotes the adsorption of arsenic on the GO surface. However, the use of GO faces certain challenges, such as self-agglomeration and difficulties in the post-processing separation of nanoparticles [107]. Therefore, GO has been modified with different materials to improve its performance. Meanwhile, iron-oxide-derived adsorbents have received great attention in arsenic removal due to their excellent arsenic adsorption properties compared to other types of adsorbents [108]. Das et al. [61] used the inorganic composite material GFeN for the adsorption of As(III) and As(V) with very high adsorption capacities of 306.10 $\pm$ 9.92 mg·g^{-1} and 431.41 $\pm$ 25.95 mg·g^{-1}, respectively. These findings highlight the great potential of GFeN as a highly efficient arsenic removal material. Figure 8a illustrates the potential mechanism of arsenic removal by GFeN. Initially, arsenic ions in water make contact with the nanohybrid surface, forming an arsenic flux gradient between the solution and the adsorbent surface. Subsequently, electrostatic adsorption and surface complexation result in arsenic adsorption onto the GFeN surface. Furthermore, the arsenic absorbed on the GFeN surface is transformed and stabilized in the nanohybrid material. Figure 8b,c also illustrates that the arsenic removal from GFeN is not controlled by electrostatic forces alone; instead, surface complexation plays an important role, making it effective over a wide pH range. Qu et al. [109] investigated the adsorption removal performance of As(V) from simulated arsenic-containing wastewater using iron nitrate–graphene (FG) nanocomposites. The adsorption data demonstrated that, under optimal conditions, the removal efficiency of As(V) was as high as 99%, with the treated arsenic content reduced to a remarkably low level of 9.4 μg·L^{-1}. As shown in Figure 8d,e, the main mechanism for the removal of As(V) from water by graphene involves the interaction of arsenic ions with carboxyl, hydroxyl, and other oxygen-containing functional groups on the graphene surface. In addition, electrostatic adsorption, ion exchange and complexation also contribute to this process. These surface hydroxyl groups enhance the electron density on the graphene surface, making it charged and forming hydrogen bonds with hydrated As(III) and As(V) ions. In an aqueous environment, these ions are held together by charge attraction and hydrogen bonding. As(V) removal maintained above 95% under both acidic and alkaline conditions, as shown in Figure 8f.

In addition to iron-derived adsorbents, there are other materials that have been used to improve the performance of graphene-based adsorbents and reduce the difficulty of post-processing separation for arsenic removal. Sherlala et al. [68] used CMGO for arsenic adsorption and showed that its adsorption capacity and removal efficiency were as high as 45 mg·g^{-1} and 61%, respectively. The adsorption mechanism is mainly through the complexation reaction between the surface functional groups of CMGO (e.g., –NH$_2$, –OH, –OH$_2$) and As(III). Such surface complexes can be formed with monodentate bonds or exosphere complexes. The superparamagnetic nature of the nanocomposites enables them to separate and recycle nanoparticles using external magnetic fields. Thus, the developed nanocomposites have potential for arsenic remediation.
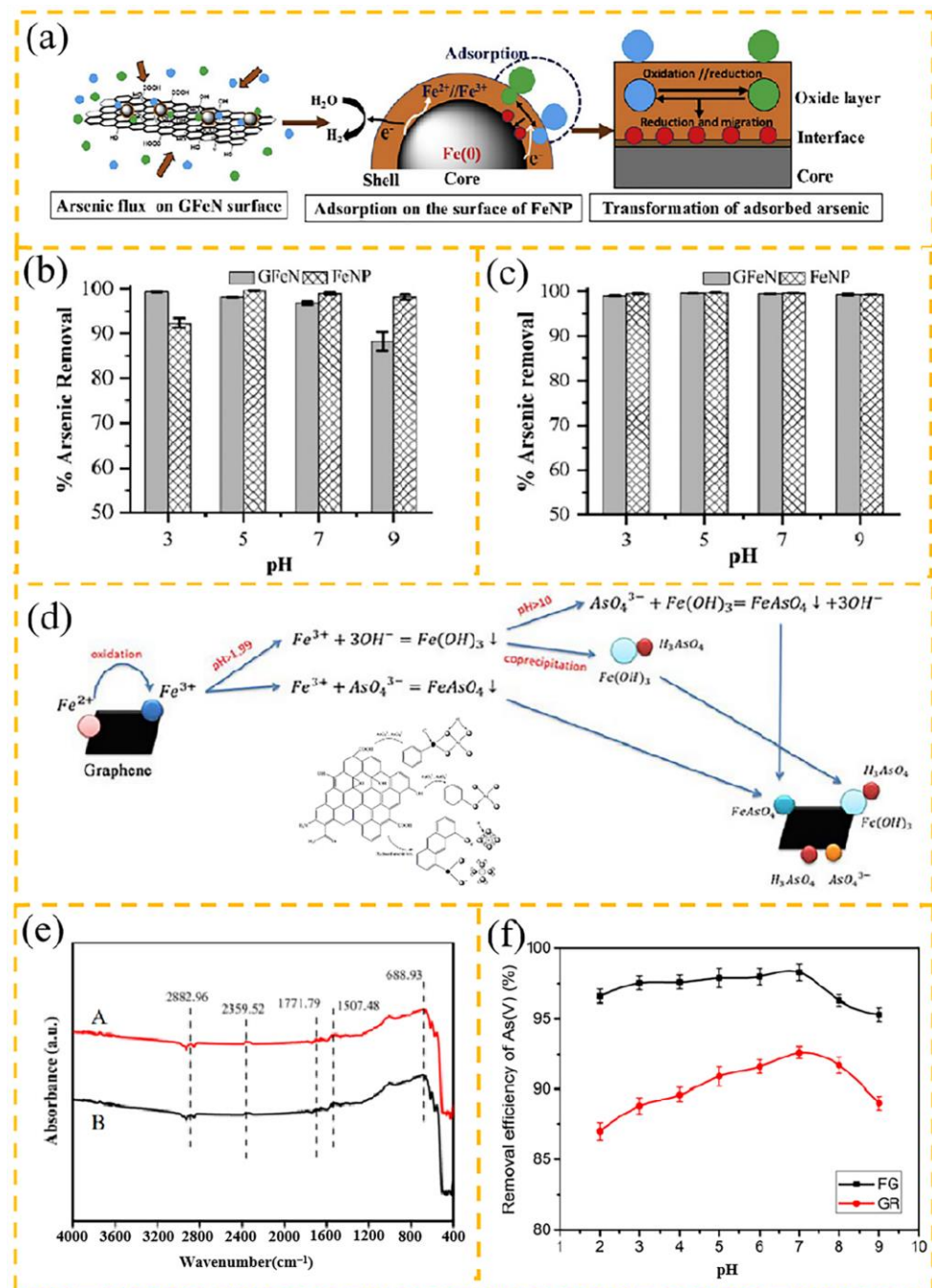
Figure 8. (**a**) The possible mechanism for arsenic removal by GFeN. Arsenic removal at different pH: (**b**) As(V) and (**c**) As(III). Reprinted with permission from reference [61]. Copyright 2020, Elsevier. (**d**) The removal mechanism of arsenic via ferric salt loaded on the surface of ferric nitrate-graphene (FG). (**e**) Fourier transform infrared spectra of the A fresh and B used ferric nitrate-graphene (FG) adsorbents. (**f**) Effect of pH on the adsorption of As(V). FG, ferric nitrate-graphene; GR, blank graphene. Reprinted with permission from reference [109]. Copyright 2019, John Wiley and Sons.

3.1.2. Chromium

Chromium exists in the environment mainly in the forms of chromium(III) and chromium(VI). The toxicity of chromium(VI) is higher than that of chromium(III) due to its elevated water solubility, fluidity, permeability, oxidation potential, and carcinogenic properties. According to the American Conference of Governmental Industrial Hygienists (ACGIH), the recommended concentrations for water-soluble and water-insoluble

chromium(VI) compounds should not exceed 0.05 mg·m^{-3} and 0.01 mg·m^{-3}, respectively [110]. The presence of chromium(VI) in water poses significant risks to the kidneys, nervous system, lungs, and liver of mammals [111]. Given the severe toxicity associated with chromium(VI), it is imperative to prioritize the removal of this compound from water sources.

Various researchers have reported and investigated low-cost adsorbents for the removal of Cr(VI) from wastewater, such as orange peels [112], industrial wastes [113], biochar [114], etc. However, all these adsorbents have limited applicability due to their low adsorption capacity, poor selectivity, and lack of regeneration. Mondal et al. [115] concluded that graphene oxide can be used as an effective alternative to remove Cr(VI) from aqueous solutions. To make GO more appropriate for this application, it was chemically modified. Singh et al. [65] used the inorganic composite material ZnO–GO for the removal of Cr(VI) from aqueous solutions. The researchers delved into the adsorption characteristics of the material, including the kinetic, isothermal, and thermodynamic behaviors related to hexavalent chromium. The experimental data demonstrate that at a pH of 8.02, with an initial Cr(VI) concentration of 5 mg·L^{-1} and an adsorbent dose of 2 g·L^{-1}, the maximum adsorption efficiency is achieved. Additionally, the adsorption of Cr(VI) on the ZnO–GO surface follows a chemisorption process, as evidenced by the pseudo-second-order kinetic model. The utilization of ZnO–GO nanocomposites for Cr(VI) removal in water treatment demonstrates remarkable efficiency and feasibility, thereby having significant implications for the advancement of novel environmentally friendly materials.

There has been increasing attention paid to potential biosorbents for the removal of heavy metal ions in water treatment, such as CS [116], which possesses amine and hydroxyl groups that can remove heavy metal ions by forming stable metal chelates [117]. However, CS is only soluble in acidic solutions, which limits its application in the removal of heavy metal ions from aqueous media. Zhang et al. [70] addressed this limitation by crosslinking CS to adsorb Cr(VI) using the polymer composite GEC; the maximum adsorption of Cr(VI) by GEC under optimized conditions (pH 2, contact time 90 min) was 86.17 mg·g^{-1}. Based on the pH results, the adsorption mechanism can be mainly explained as follows: the NH$_2$ and OH reactive groups in GEC, which can be protonated in an acidic solution, give a positive charge to the GEC surface. Therefore, hexavalent chromium binds to GEC through the strong electrostatic attraction between the protonated groups of GEC and the negatively charged hexavalent chromium material.

The interest in the synthesis of graphene hydrogels for the removal of heavy metals has been growing in recent years. This is due to the high removal efficiency, reusability, and biocompatibility of hydrogels [118]. Hydrogels are 3D polymer networks capable of absorbing large amounts of water but insoluble in water. Interestingly, water hyacinth has been used as a precursor for the preparation of activated carbon, proteins, bioelectrodes, and hydrogels for different applications, including adsorbent materials for Cr(VI) removal [119]. Kumar et al. [120] used dried fenugreek root powder for Cr(VI) adsorption with a maximum adsorption capacity of only 1.28 mg/g. Worku et al. [121] used water-hyacinth-based activated carbon to adsorb Cr(VI), but its adsorption capacity was also low; a simple method to modify water hyacinth is still needed to obtain a higher adsorption capacity. Taye et al. [94] remediated Cr(VI) in wastewater with WHLPC/GO hydrogel. The experimental results showed that the adsorption of Cr(VI) was spontaneous and endothermic. The study of different factors revealed that the highest adsorption capacity of 322.00 mg·g^{-1} was achieved under optimum conditions, i.e., pH 1.0 and an equilibrium contact time of 420 min. The results of that study not only demonstrated the efficient adsorption capacity of the hydrogel materials but also highlighted their potential application in environmental treatment, especially in the reduction of toxic heavy metal emissions from industrial activities.

3.1.3. Lead

The presence of lead in water poses a significant threat to human health and various biological systems [122]. The US Environmental Protection Agency sets the acceptable

concentration of Pb in drinking water at 15 $\mu g \cdot L^{-1}$ [123]. The treatment of Pb ions in wastewater is essential prior to their discharge into environmental water sources [124].

In recent years, graphene-based adsorbents have attracted researchers' attention as potential adsorbents for heavy metal removal from water and wastewater [125]. However, the current cost of pure graphite is still high. Therefore, recycling of graphite is very important. In an investigation aimed at finding a cost-effective method, it was proposed that waste-derived GO offers a better solution for the removal of toxic Pb from aqueous solutions [126]. The adsorption and removal of Pb(II) from water were investigated by Azam et al. [127], who prepared GO from graphite rods of waste dry cell batteries. The experimental results showed that the removal of Pb(II) (10 ppm) by GO was up to 98.87% at pH 4, a contact time of 20 min, and an adsorbent dosage of 0.25 $g \cdot L^{-1}$, and the maximum adsorption capacity was calculated to be 55.80 $mg \cdot g^{-1}$ at 20 °C. The possible adsorption mechanism of Pb(II) on the GO surface in an aqueous solution is shown in Figure 9a. The adsorption of cationic heavy metals such as lead on the GO surface mainly involves electrostatic attraction between opposite charges, and the FTIR spectra of graphite and GO before and after Pb adsorption are shown in Figure 9b, confirming the mechanism.
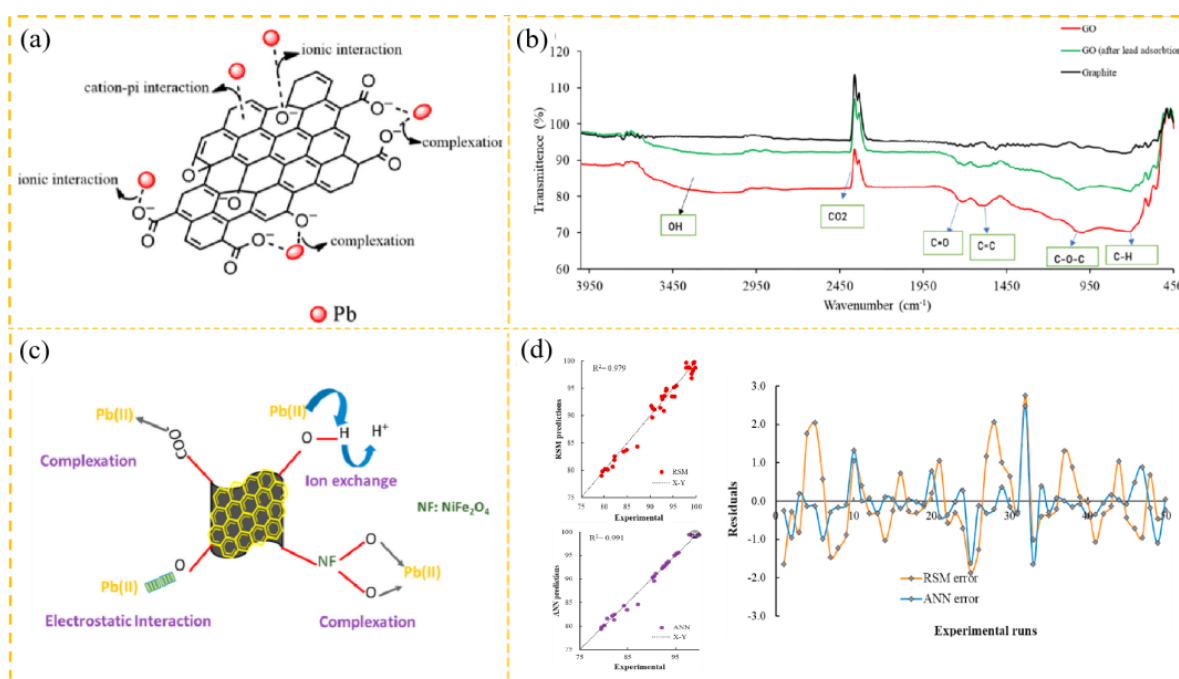
Figure 9. (**a**) The possible adsorption mechanism of Pb(II) on the GO surface from an aqueous solution. (**b**) FTIR spectrum of graphite powder, GO, and lead-adsorbed GO. Reprinted with permission from reference [127]. Copyright 2022, Elsevier. (**c**) Schematic representation of predominant mechanism for adsorption removal of Pb(II) with rGNF. (**d**) Comparison of performance of RSM and ANN predictions. Reprinted with permission from reference [124]. Copyright 2022, Elsevier.

Researchers have developed a number of novel GO composite adsorbents in order to increase the adsorption capacity. GO-functionalized binary metal oxides have been used as adsorbents due to their high stability, porosity, and high adsorption capacity for heavy metal ions. Mosleh et al. [62] used FeGO–TiLa to effectively remove harmful Pb(II) from water samples. The adsorption results showed that FeGO–TiLa removed up to 93% of Pb(II), which was significantly better than the results obtained for pure TiLa nanoparticles (81%) and magnetic GO (74%). Isothermal modeling analysis showed that the Langmuir model provided a better fit with the experimental data compared to the Freundlich model, thus indicating the existence of a monolayer physisorption mechanism. Kinetic studies also showed that the adsorption process follows a quasi-second-order rate equation. The adsorption of Pb(II) on FeGO flakes may be attributed to the coordination or complexation

with oxygen-containing groups and non-covalent interactions between π–cations. Manganese oxides, moreover, have recently attracted a great deal of attention due to their low zero-charge potential, high surface area, negative charge-rich and strong surface activity, and various other properties. Lingamdinne et al. [128] investigated the adsorption mechanism of Pb(II) on these composites using composites of rGO and manganese oxide (Mn_3O_4). The adsorption of cationic heavy metals, such as Pb(II), from aqueous solutions onto the GO surface primarily involves electrostatic attraction between opposite charges (cation–π interaction and ion interaction) and surface complexation. Under optimized conditions (pH 4, adsorbent dose 0.5 g·L^{-1}, contact time 60 min, temperature 25 ± 2 °C), the maximum adsorption capacity of the prepared rGO–Mn_3O_4 composite material for Pb(II) was determined to be 130.28 ± 0.52 mg·g^{-1}, indicating a high efficiency in terms of adsorption performance. Furthermore, thermodynamic analysis revealed that the adsorption process is spontaneous and endothermic in nature.

The above studies did not use mathematical modeling techniques to optimize the intermittent adsorption process and the interactive effects of various variables on the removal efficiency. Mathematical and statistical methods are useful for planning experiments, detecting the effects of different independent process factors, and recommending ideal settings to obtain the best possible results. Narayana et al. [124] investigated the optimum values of independent process variables for maximum removal efficiency of Pb(II) from magnetic rGO reverse spinel nickel ferrite (rGNF) nanocomposites using response surface methodology (RSM) and artificial neural network (ANN). As shown in Figure 9c, surface complexation was identified as the main mechanism for the removal of Pb(II) via rGNF adsorption. The maximum removal efficiency of 99.8% was achieved when the initial concentration was 15 mg·L^{-1}, the adsorbent dosage was 0.55 g·L^{-1}, the treatment time was 100 min, the pH was maintained at 5, and the treatment temperature was 30 °C. The performance predicted by the RSM and ANN is shown in Figure 9d. It can be observed that both data-driven model predictions gave good predictions that were comparable to the experimental values; however, the ANN predictions were superior.

3.1.4. Copper and Cobalt

Electroplating wastewater mainly contains copper, cobalt, and other metals, which can cause a large amount of water pollution if not treated properly. When the human body ingests food contaminated with copper ions, acute copper ion poisoning may be triggered. Excessive intake of cobalt ions will also seriously jeopardize human health [129]. The adsorption of copper and cobalt thus plays an important role in environmental management. It may also contribute to the recycling of copper, cobalt, and nickel metals, which have irreplaceable roles as important non-ferrous metals in many fields in contemporary industrial development.

In order to increase the reusability and stability of graphene-based composite adsorbent materials for the adsorption of copper ions, GO was functionalized with Amberlite IRC 748 resin. Ma et al. [72] performed adsorption experiments of Cu(II) on an IRC748–GO composite. The adsorption process conformed to the quasi-secondary kinetic model, and the adsorption isotherm conformed to the Langmuir isotherm, with a maximum adsorption capacity of 127.22 mg·g^{-1} for Cu(II). The adsorption was investigated by using infrared spectroscopy, scanning electron microscopy, X–ray photoelectron spectroscopy, and an adsorption isotherm, and the results showed that the carboxyl groups in IRC748–GO composite produced effective complexation of Cu(II).

Functionalization of GO with inorganic complexes can also enhance the adsorption capacities of Cu(II) and Co(II). Ranjith et al. [130] adsorbed Cu(II) and Co(II) ions in water using zinc oxide nanorod–rGO (ZnO NR–rGO) nanocomposite. The results showed that the adsorbent was adsorbed at a solution adsorbent dosage of 10 mg, metal ion concentration of 10 mg/L, and pH of 6.0, and the maximum adsorption capacities for Cu(II) and Co(II) were 67.399 and 36.354 mg·g^{-1}, respectively.

3.1.5. Selenium

Selenium pollution is a significant environmental concern, with selenium being present in water as a result of human activities such as coal combustion, mining operations, and crude oil processing. During the power generation process, solid waste and flue gas are released into the environment, leading to elevated concentrations of selenium in water in the forms of selenite (Se(IV)) and selenate (Se(VI)) [131]. It is estimated that approximately 80,000 tons of selenium are discharged into soil and water annually worldwide due to human activities. This subsequently affects animals, plants, and ecosystems, resulting in severe environmental and health consequences [132,133]. The recommended guidelines by the World Health Organization (WHO) and limits set by the Environmental Protection Agency (EPA) are 40 $\mu g \cdot L^{-1}$ and 50 $\mu g \cdot L^{-1}$, respectively [134,135]. Therefore, it is imperative to develop efficient technologies for selenium removal. By applying an adsorption technique, the pollution of water and soil with selenium can be reduced, and the ecosystem can be protected.

Although activated carbon as an adsorbent is applied for the adsorption of selenium from wastewater, it is not very efficient for selenium species investigated; it is reported that Se(IV) was adsorbed almost not at all (only 4%) at pH 6, and only 42% of Se(VI) was collected [136]. Activated carbon was modified, but the adsorption capacity remained low [137]. Recently, graphene oxide was found to selectively adsorb metal ions [138]. More studies were conducted to modify GO to adsorb metal ions. For instance, Xiao et al. [139] investigated the adsorption performance of selenium with polyamide-amide-functionalized GO (PAMAM–GO) material. The mapping of Se is illustrated in Figure 10a,b, indicating that Se was adsorbed on graphene oxide functionalized with a silane coupling agent. The maximum removal capacities for Se(VI) and Se(IV) were 77.9 $mg \cdot g^{-1}$ and 60.9 $mg \cdot g^{-1}$, respectively, at pH 6. It was shown that the chemically modified GO could effectively enhance the adsorption performance of selenium in water, especially at a lower pH, where its selective adsorption performance for Se(VI) is more prominent. As such, this chemically modified GO provides an effective material solution for the treatment of selenium-containing wastewater. According to analysis, one or two of the amine groups may interact with a selenium–oxygen anion, and the adsorption mechanism of PAMAM–GO on Se(IV) and Se(VI) is shown in Figure 10c. Lu et al. [140] used poly(allylamine)-modified magnetic GO (PAA–MGO) material for the adsorption removal of selenium from water, especially for Se(VI) and Se(IV). The adsorption results showed that the maximum adsorption capacities of PAA–MGO were 120.1 $mg \cdot g^{-1}$ for Se(IV) and 83.7 $mg \cdot g^{-1}$ for Se(VI) at pH 5.8. In addition, the effect of pH on selenium adsorption was investigated, and it was found that the selenium adsorption was favorable under acidic conditions, with an optimal pH of 3.1.

Currently, nano zero-valent iron (nZVI) seems a promising reductant and adsorbent for Se(IV) removal because of its large specific surface area and high reactivity [134]. Sun et al. [141] investigated the efficiency of the removal of selenate (Se(IV)) by this nZVI/rGO composite by loading GO prepared via the modified Hummers method on nZVI. The adsorption results showed that the removal ratio reached 99% when the loading ratio was 10%, the dose was 0.3 $g \cdot L^{-1}$, and the initial pH was 3. The influencing factors of nZVI/rGO on the removal ratio of Se(IV) are shown in Figure 10e,f. The isothermal adsorption was consistent with the Langmuir isothermal model, and the maximum adsorption capacity was as high as 173.53 $mg \cdot g^{-1}$. The process of Se(IV) removal by nZVI/rGO consisted of the following two main steps: (1) Se(IV) in aqueous solution was rapidly adsorbed on the surface of the material to form surface complexes. (2) Se(IV) first diffused on the surface of the material, underwent internal diffusion after a period of reaction, and finally reduced to Se(0). At the same time, Fe(0) was oxidized to Fe(II), and Fe(II) was oxidized to hydroxide precipitate covering the particle surface. The mechanism of Se(IV) removal by NZVI/rGO is shown in Figure 10d.
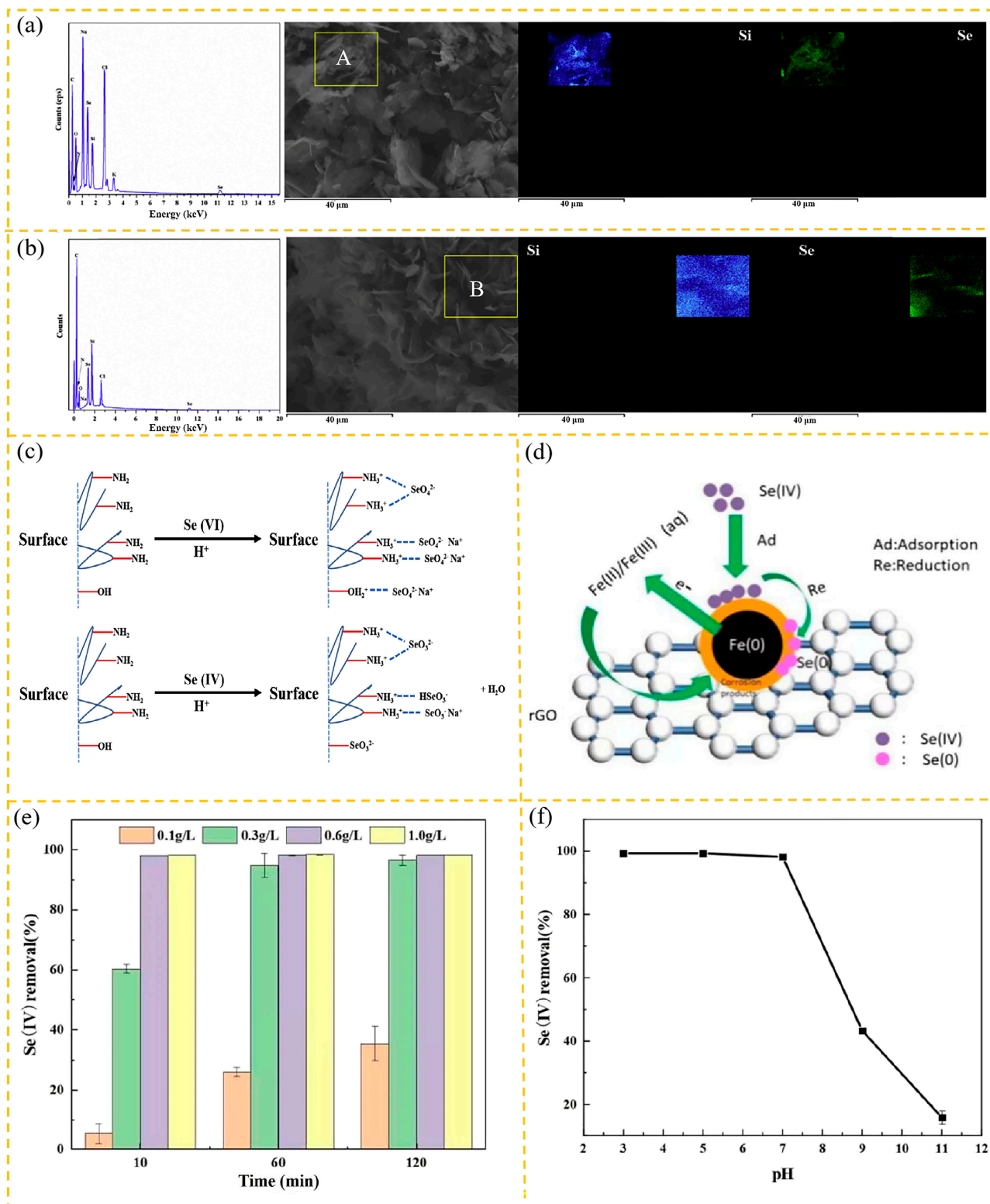
Figure 10. EDS spectra of PAMAM-GO after the adsorption of (**a**) selenate and (**b**) selenite ions. The scanned results of Si and Se in the yellow boxes (A and B) are shown on the right sides. (**c**) Schematic illustration of adsorption mechanisms for Se(IV) and Se(VI) on PAMAM-GO. Reprinted with permission from reference [139]. Copyright 2016, Elsevier. (**d**) Mechanism diagram of Se(IV) removal by nZVI/rGO. Influence of Se(IV) removal efficiency by nZVI/rGO: (**e**) contact time and dosage; (**f**) pH. Reprinted with permission from reference [141]. Copyright 2022, Springer Nature.

3.1.6. Summary of Adsorption of Heavy Metal Ions

A summary is given herein for a more intuitive comparison of the adsorption performances of various graphene-based adsorbents for heavy metal ions (see Table 1).

Table 1. Adsorption capacities of graphene-based adsorbents for selected heavy metal ions.

Adsorbent		Heavy Metal Ion	Adsorption Conditions	Adsorption Capacity/ Removal Efficiency	Reference
Material	Form				
CMGO	Powder	As(III)	pH = 7.3, 25 °C, 4 h	45 mg·g^{-1}	[68]
Fe$_3$O$_4$–GO	Powder	As(III)	pH = 7, 25 °C, 12 h	85 mg·g^{-1}	[142]
		As(V)	pH = 7, 25 °C, 12 h	38 mg·g^{-1}	
Fe$_3$O$_4$–rGO	Powder	As(III)	pH = 7, 25 °C, 12 h	57 mg·g^{-1}	[142]
		As(V)	pH = 7, 25 °C, 12 h	12 mg·g^{-1}	
Fe$_3$O$_4$–GO	Aerogel	As(V)	Neutral pH, 25 °C, 12 h	40.048 mg·g^{-1}	[143]
Fe$_3$O$_4$–rGO	Powder	As(III)	pH = 7, 30 °C, 2 h	0.81 mg·g^{-1}	[144]
GO	Powder	As(III)	pH = 7, 30 °C, 2 h	0.70 mg·g^{-1}	[144]
rGO	Powder	As(III)	pH = 7, 30 °C, 2 h	0.68 mg·g^{-1}	[144]
Co–rGO	Powder	As(III)	pH = 7, 30 °C, 2 h	0.75 mg·g^{-1}	[144]
GFeN	Powder	As(III)	pH = 7, 22 ± 2 °C	306.10 ± 9.92 mg·g^{-1}	[61]
		As(V)	pH = 7, 22 ± 2 °C	431.41 ± 25.95 mg·g^{-1}	
FG	Powder	As(V)	pH = 7, 35 °C	112.4 mg·g^{-1}	[109]
TAIGO	Powder	Hg(II)	Natural pH, 15 min	23.81 mg·g^{-1}	[145]
GO	Powder	Cr(VI)	pH = 4	1.222 mg·g^{-1}	[115]
ZnO–GO	Powder	Cr(VI)	Neutral pH, 303 K	96%	[65]
GEC	Powder	Cr(VI)	pH = 2, 25 °C	86.17 mg·g^{-1}	[70]
MCGO–IL	Powder	Cr(VI)	pH = 3, 30 °C	145.35 mg·g^{-1}	[146]
GONF	Powder	Cr(III)	pH = 4, 298 ± 2 K	45.5 mg·g^{-1}	[147]
		Pb(II)	pH = 5–6, 298 ± 2 K	25.0 mg·g^{-1}	
WHLPC/GO	Hydrogel	Cr(VI)	pH = 1, 7 h	322.00 mg·g^{-1}	[94]
AFGS	Sponge	Cr(VI)	pH > 4, 25 °C	166.46 mg·g^{-1}	[87]
M–PAS–GO	Powder	Cr(VI)	pH = 3.2, 25 °C	46.48 mg·g^{-1}	[148]
rGNF	Powder	Pb(II)	pH = 5, 30 °C, 100 min	99.8%	[124]
GO	Powder	Pb(II)	pH = 4, 25 °C, 20 min	98.87%	[127]
rGO–Mn$_3$O$_4$	Powder	Pb(II)	pH = 4, 25 ± 2 °C, 60 min	130.28 ± 0.52 mg·g^{-1}	[128]
MCGO	Powder	Pb(II)	pH = 5, 1 h	50.23 mg·g^{-1}	[149]
FeGO–TiLa	Powder	Pb(II)	pH = 5, 2 h	112 mg·g^{-1}	[62]
MSiO$_2$–GO	Powder	Pb(II)	pH = 6, 25 °C	90.48%	[64]
Magnetic GO	Powder	Cd(II)	pH = 7, 45 °C	128.2 mg·g^{-1}	[150]
		Pb(II)	pH = 7, 45 °C	385.1 mg·g^{-1}	
ZnO NR–rGO	Powder	Co(II)	pH = 6	36.354 mg·g^{-1}	[130]
		Cu(II)	pH = 6	67.399 mg·g^{-1}	
AMGO	Powder	Cr(VI)	pH = 2	123.4 mg·g^{-1}	[151]
TSCGO	Powder	Hg(II)	pH = 6, 298 K	933.2 mg·g^{-1}	[152]
		Pb(II)	pH = 5, 298 K	890.4 mg·g^{-1}	
GOFH	Powder	As(V)	pH = 4, 298 K	160 mg·g^{-1}	[153]
		Cr(VI)	pH = 4, 298 K	66 mg·g^{-1}	
IRC748–GO	Powder	Cu(II)	pH = 5.81, 30 °C	127.22 mg·g^{-1}	[72]
CMC/SA/GO@Fe$_3$O$_4$	Powder	Cu(II)	pH = 5, 30 °C	55.96 mg·g^{-1}	[154]
		Cd(II)	pH = 6, 30 °C	86.28 mg·g^{-1}	
		Pb(II)	pH = 5, 30 °C	189.04 mg·g^{-1}	
GO–EDTA–CS	Powder	Cu(II)	pH = 5.1, room temperature	130 ± 2.80 mg·g^{-1}	[155]
		Hg(II)	pH = 5.1, room temperature	324 ± 3.30 mg·g^{-1}	
GO/CS	Powder	Cu(II)	pH = 5, 313.15 K, 210 min	269 mg·g^{-1}	[156]
GO/CS	Powder	Cu(II)	pH = 6, 20 °C	60.7 mg·g^{-1}	[67]
		Cr(VI)	pH = 6, 20 °C	48.7 mg·g^{-1}	
		Pb(II)	pH = 6, 20 °C	32.3 mg·g^{-1}	

Table 1. *Cont.*

Adsorbent		Heavy Metal Ion	Adsorption Conditions	Adsorption Capacity/ Removal Efficiency	Reference
Material	Form				
mGO–PAMAM	Powder	Cu(II)	pH = 7, 25 °C	353.59 mg·g^{-1}	[74]
		Cd(II)	pH = 6, 25 °C	435.85 mg·g^{-1}	
		Pb(II)	pH = 7, 25 °C	326.729 mg·g^{-1}	
GO–SA	Powder	Pb(II)	pH = 4, 25 °C	887.21 mg·g^{-1}	[71]
		Zn(II)	pH = 5, 25 °C	161.25 mg·g^{-1}	
		Cd(II)	pH = 7, 25 °C	139.62 mg·g^{-1}	
GO–sand	Powder	Pb(II)	pH = 6, 298 K	289.68 mg·g^{-1}	[157]
		Cr(III)	pH = 6, 298 K	258.87 mg·g^{-1}	
GO–MBT	Powder	Pb(II)	pH = 6	116.959 mg·g^{-1}	[158]
		Cd(II)	pH = 7	112.99 mg·g^{-1}	
GO–CNC	Powder	Cr(VI)	pH = 5, 105 min	90.74%	[159]
		Ni(II)	pH = 8, 90 min	58.56%	
RGOS	Powder	Pb(II)	pH = 5.0, <10 min	689 mg·g^{-1}	[160]
		Cu(II)	pH = 5.0, <10 min	59 mg·g^{-1}	
		Ni(II)	pH = 5.5, <10 min	66 mg·g^{-1}	
		Cd((II)	pH = 5.0, <10 min	267 mg·g^{-1}	
		Cr(III)	pH = 5.5, <10 min	191 mg·g^{-1}	
GRP–PPY–NP	Powder	Mn(II)	pH = 5.5, 90 min	89%	[161]
ZnO–Gr	Powder	Ni(II)	pH = 8.2, 25 °C	66.66 mg·g^{-1}	[162]
Graphene	Powder	Ni(II)	pH = 8.2, 25 °C	3.78 mg·g^{-1}	[162]
mp–CA/GO	Aerogel	Pb(II)	25 °C, 40 min	368.2 mg·g^{-1}	[163]
		Cu(II)	25 °C, 40 min	98.1 mg·g^{-1}	
		Cd(II)	25 °C, 40 min	183.6 mg·g^{-1}	
GOF	Foam	Zn(II)	pH = 10	326.4 mg·g^{-1}	[83]
		Cd(II)	pH = 10	252.5 mg·g^{-1}	
		Pb(II)	pH = 10	381.3 mg·g^{-1}	
		Fe(III)	pH = 10	587.6 mg·g^{-1}	
rGO	Aerogel	Sb(III)	pH = 6 ± 0.5, 298 K	168.59 mg·g^{-1}	[99]
		Sb(V)	pH = 6 ± 0.5, 298 K	206.72 mg·g^{-1}	
TI/GO@ Fe$_3$O$_4$	Powder	Pb(II)	pH = 5, 293 K	461.00 mg·g^{-1}	[164]
PAMAM–GO	Powder	Se(IV)	pH = 6	60.9 mg·g^{-1}	[139]
		Se(VI)	pH = 6	77.9 mg·g^{-1}	
PAA–MGO	Powder	Se(IV)	pH = 5.8	120.1 mg·g^{-1}	[140]
		Se(VI)	pH = 5.8	83.7 mg·g^{-1}	
NZVI/rGO	Powder	Se(IV)	pH = 3, 25 °C	173.53 mg·g^{-1}	[141]
CTAB@GO	Powder	Se(IV)	pH = 2–3	139.95 mg·g^{-1}	[165]
		Se(VI)	pH = 2–3	468.01 mg·g^{-1}	

3.2. Rare Metals

The presence of rare metals is a particular concern in industrial wastewater treatment because they can cause serious environmental impacts and human health risks even at low concentrations. Accumulation of rare metals in the environment may lead to deterioration of water quality and affect the survival of aquatic organisms.

3.2.1. Radioactive Metals

A large amount of radioactive wastewater containing uranium, thorium, and other radioactive metals is generated during the mining and smelting of rare earth ores. These radioactive metals are difficult to reduce. Therefore, it is important to treat radioactive wastewater and reuse the treated water. Adsorption methods have attracted much attention because of the advantages of high selectivity, fast adsorption rate, and high capacity of adsorption materials such as graphene-based adsorption materials [166,167].

GO and its composites are promising materials for the adsorption of radioactive metals in water. Wu et al. [168] used persimmon-tannin-modified GO/CS (PGC) microspheres to investigate their effective adsorption behavior for U(VI) in aqueous solution. It was shown that the maximum adsorption capacity of PGC microspheres for U(VI) reached 199.13 mg·g^{-1} at 303 K, pH = 5, and initial uranium concentration of 10.00 mg/L, and the removal efficiency was 98.2%. Meanwhile, in order to make up for the lack of U(VI) adsorption on GO/CS, Zhou et al. [6] adsorbed U(VI) with PAO/GO/CS. Langmuir adsorption modeling showed that the maximum adsorption of U(VI) by PAO/GO/CS was 701.5, 821.7, and 1220.0 mg·g^{-1} at 293, 303, and 313 K, respectively. U(VI) was adsorbed spontaneously and predominantly chemisorbed onto oxygen-containing moieties. PAO/GO/CS could realize selective adsorption of common coexisting ions to U(VI) and excellent water separation performance.

It is well known that thorium and uranium often co-exist in some natural minerals such as monazite and thorium ores. Pan et al. [63] synthesized α–GOM$_2$ for the simultaneous removal of thorium/uranium ions from aqueous solutions. The maximum adsorption capacity of α–GOM$_2$ for Th(IV) was 497.5 mg·g^{-1} and 185.2 mg·g^{-1} for U(VI) in the single-component system (Th(IV) or U(VI)), which was higher than that of GO. In the binary-component system (Th(IV)/U(VI)), the saturated adsorption capacity on α–GOM$_2$ was 408.8 mg·g^{-1} for Th(IV) and 66.8 mg·g^{-1} for U(VI), which was also higher than that on GO. Based on the analysis of the XPS data, as shown in Figure 11a,b, it is believed that the adsorption process between Th(IV)/U(VI) and α–GOM$_2$ may involve four kinds of molecular interactions, as shown in Figure 11c, including ligand interactions, electrostatic interactions, cation–π interactions, and Lewis acid–base interactions. These results suggest that α-GOM$_2$ can be used as a potential adsorbent for the removal and separation of Th(IV)/U(VI) ions from aqueous solutions.

Produced by the fission of uranium 235, Cesium 137 is a radionuclide with a half-life of about 30 years. Due to its similarity in chemical properties to potassium ions, it can easily enter the ecosystem and is one of the hazardous substances in wastewater. The transition metal hexacyanoferrate (MHCF) has become a research hotspot because of its high selectivity for cesium ions, but nanoscale MHCF is difficult to recover. To overcome this problem, Kim et al. [169] used HCF–PEI–rGO composite membranes of GO grafted with polyethyleneimine (PEI) and potassium hexacyanoferrate (KCuHCF) nanoparticles for efficient and selective removal of cesium ions, and this composite was capable of efficiently treating radioactive materials. It was shown that the removal efficiency of the HCF–PEI–rGO membrane for Cs(I) exceeded 98%. In addition, the membrane showed stable cesium removal performance even under simulated general groundwater conditions. These results indicate that the HCF–PEI–rGO membrane can be effectively used for the rapid treatment of radiocaesium-contaminated water, which is promising for practical applications. Prussian blue has been investigated for the selective removal of radiocaesium from water due to its similar hydration radius with cesium ions. To address the difficulty of separating Prussian blue from treated solutions, Kadam et al. [170] utilized magnetic graphene oxide Prussian blue (PSMGPB) nanocomposites stabilized with its biopolymer pectin in order to enhance its properties and prevent aggregation and to improve the cesium adsorption efficiency. For PSMGPB nanocomposites, the adsorption capacity for Cs(I) was 1.609 mmol·g^{-1} at an optimal pH of 7 and an optimal adsorption temperature of 30 °C. This enhanced adsorption efficiency was attributed to the separation of pectin-stabilized GO sheets and the improved distribution of magnetite on the GO surface.
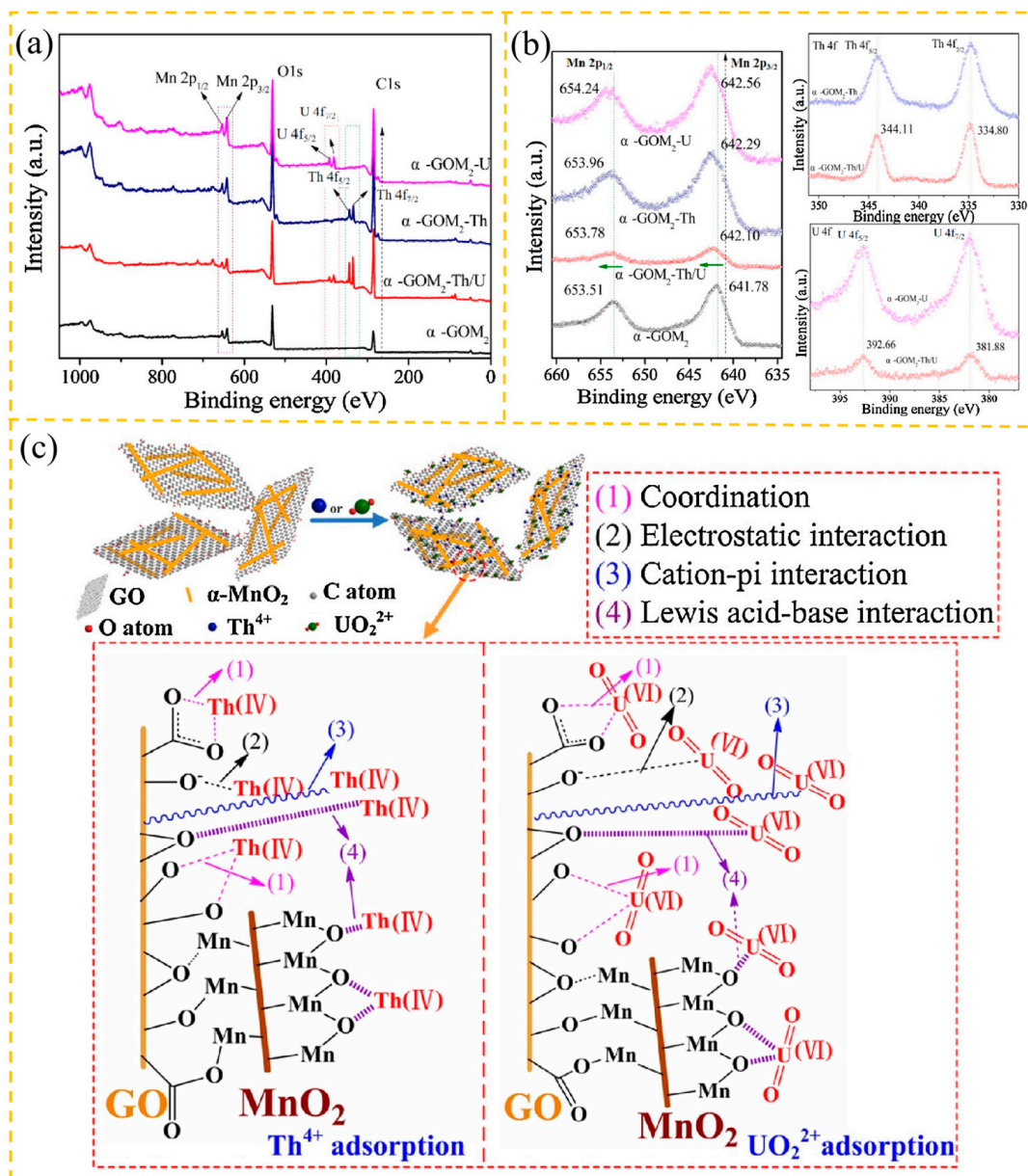
Figure 11. (**a**) XPS survey spectra and (**b**) Mn 2p, Th 4f, and U 4f peaks in the XPS spectra of α–GOM$_2$ before and after adsorbing single Th(IV), single U(VI), and Th(IV)/U(VI). The green arrows indicate the increase in Mn 2p binding energy of α–GOM$_2$ upon adsorption of Th(IV) or U(VI). (**c**) Schematic diagram of possible interaction between Th(IV) or U(VI) and α–GOM$_2$. The yellow arrow and the dotted line box indicate the possible interaction mechanisms in the adsorption of Th(IV) or U(VI) by α–GOM$_2$. Reprinted with permission from reference [63]. Copyright 2016, Elsevier.

3.2.2. Rare Earth Metals

Rare earth metals are mainly derived from ores, which are usually mined in specialized rare earth deposits and extracted through crushing, grinding, chemical treatment, and other steps. Rare earth metals generated during the mining process may enter surface water or groundwater through stormwater flushing or direct discharge. From an environmental perspective, the removal and recovery of rare earth metals can reduce dependence on natural resources and lead to sustainable resource utilization.

Cerium (Ce), as one of the major rare earth ionic pollutants, poses a threat to ecosystems and human health. GO and cellulose are two potential adsorption materials. GO has excellent adsorption properties due to its high specific surface area and abundant functional

groups but at a higher cost. Cellulose is a renewable, low-cost natural polymer, but its adsorption capacity is limited by the limited number of functional groups. By combining GO with modified cellulose, Huang et al. [171] could develop an efficient and low-cost adsorbent (CPAG) for the removal of Ce(III) from water. The results showed that CPAG adsorbed 271.8 mg·g^{-1} of Ce(III) with an adsorption temperature of 25 °C, the pH was 4.2, and the equilibrium contact adsorption time was 25 min. The adsorption mechanism was dominated by the complexation of ion exchange with ionized oxygen-containing functional groups. The composite material combines the advantages of both, improves the adsorption efficiency, reduces the cost, and provides a feasible solution for environmental protection.

Lanthanides, as important fission products, are prominent in environmental impact assessment and high-tech applications. Lanthanum and praseodymium, two of the most common elements, are widely used in various industrial fields, but they also raise concerns about environmental pollution. To address this issue, researchers have developed various adsorbents to remove these elements from water, including modified GO, functional ionic liquids, biomaterials, etc. Abu Elgoud et al. [172] obtained GO–imidazole–FeCN by combining 1-methylimidazole and epichlorohydrin onto graphene oxide, which was further treated with $K_3[Fe(CN)_6]$ composites showed high adsorption affinity for La(III) and Pr(III). In addition, the effects of different parameters on the adsorption process were investigated and the adsorbents were analyzed by various characterization means to optimize their performance and reduce the environmental risks. The experimental adsorption capacities of La(III) and Pr(III) were 785.55 and 867.67 mg·g^{-1}, respectively, and the GO–imidazole–FeCN composites exhibited excellent regeneration–reuse behavior.

3.3. Other Inorganic Pollutants

Inorganic pollutants in wastewater come from a wide variety of sources and have a significant impact on the environment. In addition to heavy metal ions, there are fluoride, phosphate, etc.

3.3.1. Fluorides

Improperly disposed of fluorinated wastes from industrial processes can enter water bodies through surface runoff or infiltration, and fluoride contained in agricultural drainage can also contaminate water sources through surface runoff. People who consume fluoride in excess can lead to the development of dental and skeletal fluorosis [173]. The presence of fluoride can disrupt the balance of aquatic ecosystems, so there is a need to remove fluoride from wastewater.

Current methods for removing fluoride from water, such as precipitation and Al^{3+} co-precipitation, are useful but produce toxic sludge. Therefore, Liu et al. [174] developed more environmentally friendly adsorbents, Zr–MCGO functionalized with $Fe_3O_4/CS/GO$ (MCGO) and zirconium (IV) showed excellent adsorptive properties, was easy to separate, and could be operated over a wide pH range. When comparing the fluoride removal capacity of different adsorbents, it was found that the modified Zr–MCGO showed higher adsorption efficiency than the pristine MC and MCGO. The addition of zirconium significantly enhanced the adsorption capacity from 3.93 mg·g^{-1} to 5.78 mg·g^{-1}. Zr–MCGO outperformed Zr–MC, showing that the synergistic effect of GO and chitosan provided more adsorption sites. It was also shown that pH had a significant effect on the adsorption of fluoride, where the adsorption was better between pH 4.0 and 8.0, while high pH decreased the adsorption efficiency. Rashid et al. [175] studied the performance of a GO–CeO_2 nanocomposite for the adsorption removal of excess fluoride from drinking water. The adsorption data revealed that the maximum capacity of the nanocomplex for fluorine ion adsorption at pH 6.5 was 8.61 mg·g^{-1}, which increased to 16.07 mg·g^{-1} at pH 4.0. The experimental results showed that it played a major role in the rapid trapping of aqueous fluoride by ion exchange with ultrafast kinetic properties (<1 min), and the diagram of the mechanism of rapid capture of aqueous fluoride by ion exchange is shown in Figure 12a,

and based on the adsorption behavior and XPS data, as shown in Figure 12b,c, it is proposed that the removal of fluoride by GO–CeO$_2$ is carried out in two steps.
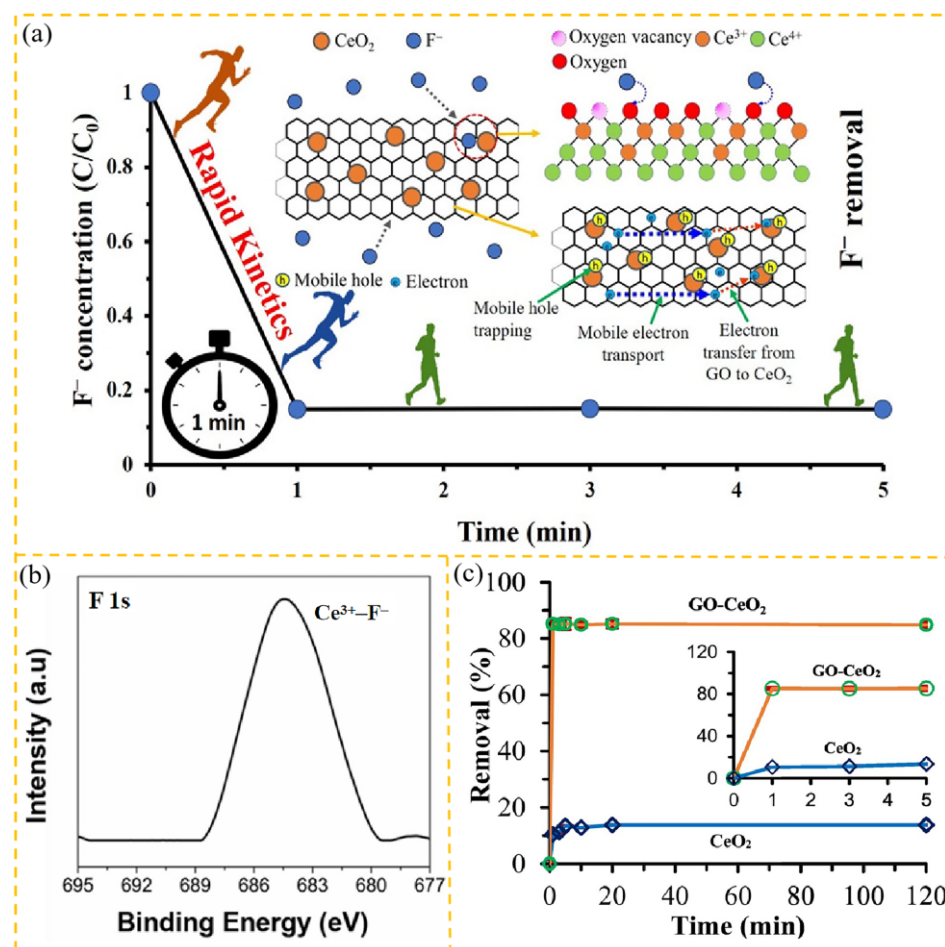

Figure 12. (**a**) Diagram of the mechanism of rapid capture of aqueous fluoride by ion exchange. (**b**) High-resolution XPS of F 1s spectrum after fluoride adsorption. (**c**) Fluoride removal by only CeO$_2$ NPs; the plot for fluoride removal by GO–CeO$_2$ is also shown for ease of comparison (Inset: Initial 5 min data zoomed in). Reprinted with permission from reference [175]. Copyright 2021, Elsevier.

3.3.2. Phosphates

Phosphates are widely available compounds in nature and human society, and they play an important role in many biological processes and industrial applications. However, phosphates from over-applied fertilizers enter rivers and lakes through farm drainage and surface runoff, and phosphate-containing detergents and other household cleaning products enter water bodies through municipal sewage systems. And phosphate is one of the major contributors to the eutrophication of water bodies, which leads to a decline in aquatic biodiversity and deterioration of water quality. In this context, control measures can be used, such as the adsorption and removal of phosphorus.

In order to effectively remove phosphate, Vasudevan et al. [176] tested the ability of graphene to adsorb phosphate from an aqueous solution by examining the experimental parameters, including pH, concentration, and temperature, and evaluated the associated adsorption isotherms, kinetics, and thermodynamic properties based on the experimental data. The experimental results showed that graphene is an excellent phosphate adsorbent with an adsorption capacity of up to 89.37 mg·g^{-1} under the experimental conditions of an initial phosphate concentration of 100 mg·L^{-1} and a temperature of 303 K. The results showed that graphene is an excellent phosphate adsorbent with a high adsorption capacity of up to 89.37 mg·g^{-1}.

To enhance the adsorption capacity as well as reusability of graphene adsorbent material, Eltaweil et al. [177] prepared a reusable lanthanum doped aminated graphene oxide/aminated chitosan microspheres (La-AmGO@AmCs) for the efficient removal of phosphate ions. The adsorption kinetic process conformed to the quasi-secondary kinetics and the proposed Langmuir model fitting, and the adsorption isotherm conformed to the Langmuir model fitting, with the maximum adsorption capacity of 125.00 mg·g^{-1}. The removal rates of La-AmGO@AmCs microspheres were all above 86% after reuse five times. The adsorption mechanisms of LaAmGO@AmCs on phosphate ions include electrostatic interaction, intrasphere complexation, Lewis acid-base interaction, ion exchange, protonation, precipitation, and hydrogen bonding. The experimental results showed that the La-AmGO@AmCs microspheres could be used for the removal and recovery of phosphorus from wastewater. Wang et al. [178] researched the performance of a 3D graphene/La(OH)$_3$-nanorod aerogel for the removal and recovery of phosphate from wastewater. The adsorption data revealed that GLA-10 exhibited a maximum phosphorus adsorption capacity of 76.85 mg·g^{-1}. The mechanism of phosphorus adsorption by GLA-10 can be divided into three stages, as shown in Figure 13a: (1) the –OH on the surface of La(OH)$_3$ is replaced by phosphate into the solution; (2) the exchanged phosphates form an inner-sphere ligand with La; and (3) the LaP coordination complex was transformed into LaPO$_4$-0.5H$_2$O crystals. The anomalous selectivity was further confirmed by comparing the XPS spectra before and after adsorption even in the presence of high concentrations of dissolved organic matter or various competing anions, as shown in Figure 13b,c.
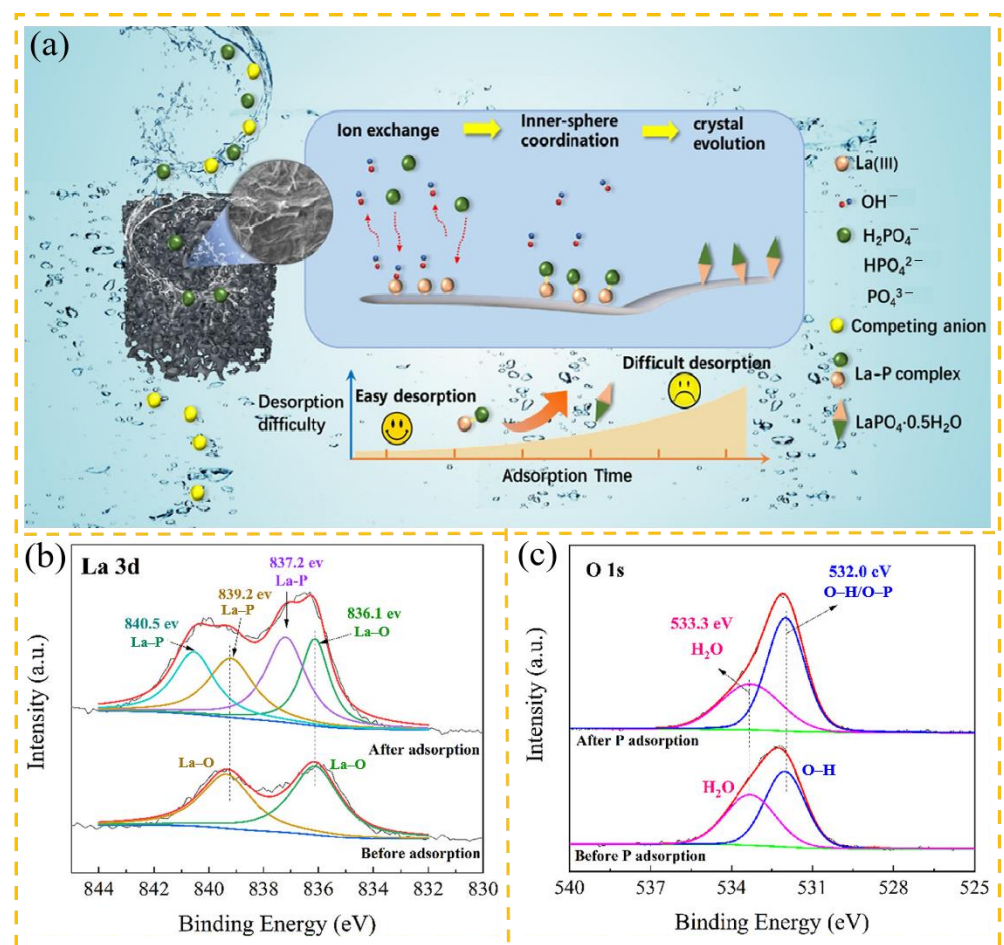
Figure 13. (**a**) Schematic illustration for the process of P adsorption by GLA-10. La 3d (**b**) and (**c**) O 1s XPS spectra of GLA-10 before and after P adsorption. Reprinted with permission from reference [178]. Copyright 2022, Elsevier.

4. Adsorption of Organic Pollutants with Graphene-Based Adsorbents

4.1. Organic Dyes

The presence of organic dyes in aquatic environments poses a significant threat to aquatic animals and plants [179]. Dye-containing wastewater obstructs light penetration, weakens photosynthesis in aquatic plants and algae, and reduces dissolved oxygen levels, which ultimately results in water eutrophication [180]. Dyes in wastewater are categorized into two main groups: cationic dyes and anionic dyes. When treating these dye wastewaters, different technologies and methods are required to target the removal of these dye ions. Many researchers have used different methods to remove organic dyes [181], and adsorption has been found to be easier than these methods and is thus promising for dye removal.

4.1.1. Organic Cationic Dyes

Cationic dyes such as rhodamine B (RhB), malachite green (MG), ethyl violet (EV), methylene blue (MB), nile blue (NB), and crystal violet (CV) are widely used in various industries such as food, textiles, cosmetics, paper, paint, printing, and others [182]. Due to their poor biodegradability, the discharge of dye-containing wastewater into water bodies leads to serious water pollution.

A carbon-based material with superhydrophobicity, porous graphene (PG), has been used as an effective adsorbent for dye removal [183]. Recently, a new technique was demonstrated for a greener approach to synthesizing PG, and the efficacy of this new green PG for the removal of seven emerging contaminants, such as RhB, was investigated for the first time [184]. The rGO–ZnS nanocomposites were used as adsorbent materials for two dyes, MG and EV [185]. The removal rate was rapid during the first 20 min. This fast initial adsorption process is due to the high number of available active sites on the nanocomposites. The adsorption data for both dyes fit well with the pseudo-second-order kinetic model, with adsorption capacities of 27.54 mg·g^{-1} and 20.04 mg·g^{-1} for MG and EV, respectively.

GO contains active surface oxygen-containing group pairs with a high capacity for the adsorption of organic dyes. Jayawardena et al. [186] investigated the adsorption performance of GO for the removal of MB from an aqueous solution by synthesizing GO with different degrees of oxidation. The results showed that the optimized GO materials had very high adsorption capacities, with the most effective samples having adsorption capacities of 2294 mg·g^{-1} at pH 7 and 2301 mg·g^{-1} at pH 12. By comparing the properties of the GO materials before and after adsorption, it was found that the removal of MB is affected by a number of factors, including the porosity of the materials, electrostatic attraction, hydrogen bonding, and π–π interaction. In addition, the best-performing GO materials showed excellent reproducibility, as they maintained a removal efficiency of more than 90% after five cycles. Li et al. [27] adsorbed MB using a magnetic humic acid/GO composite (MHAGO). The results of their adsorption experiments demonstrated that 30 mg of MHAGO adsorbent can treat 100 mL of aqueous solution containing 5.0 mg·L^{-1} MB at 45 °C, achieving a maximum MB adsorption capacity of approximately 59.00 mg·g^{-1}. The effects of the initial MB concentration and pH on MB adsorption onto MHAGO are shown in Figure 14a,b. The mechanism for this adsorption by MHAGO is illustrated in Figure 14c, revealing a potential involvement of hydrogen bonds and π–π interactions during the process. As an innovative biological adsorbent, MHAGO exhibits exceptional performance in dye wastewater treatment, providing valuable insights for future research on recyclability and reuse.

In order to find effective adsorbents that can remove and adsorb dyes quickly, many research groups have investigated GO composites as adsorbents. Dang et al. [187] used carbon foam/CNTs/GO (CF/CNTs/GO) and investigated the adsorption properties of this material for MB. The experimental results showed that the prepared CF/CNTs/GO adsorbents exhibited remarkable removal efficiency (73%) and capacity (146 mg·g^{-1}) for MB.
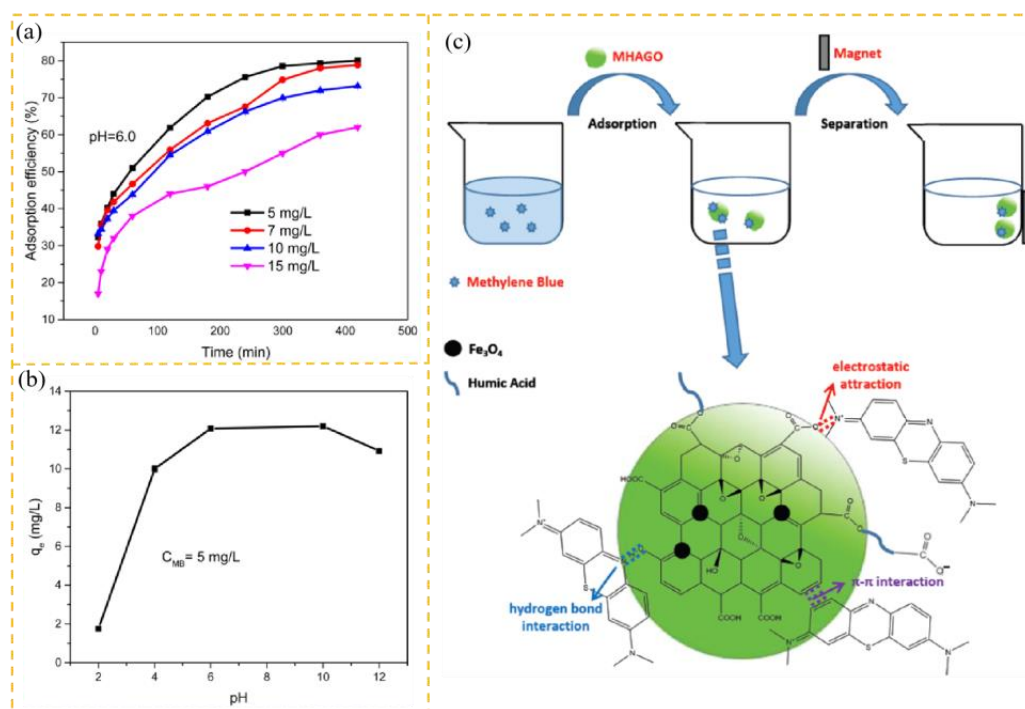
Figure 14. (**a**) Effect of contact time and initial MB concentration on adsorption efficiency of MHAGO for MB. (**b**) Effect of pH on equilibrium adsorption capacity of MHAGO for MB. (**c**) Schematic illustration of adsorption mechanisms for MHAGO. Reprinted with permission from reference [27]. Copyright 2021, Elsevier.

4.1.2. Organic Anionic Dyes

Anionic dyes such as Congo red (GR), orange G (OG), methyl orange (MO), and bromophenol blue (BB) have good water solubility, which allows them to penetrate the fibers uniformly during the dyeing process. Some anionic dyes are considered mutagenic and carcinogenic, and long-term exposure may increase the risk of cancer. Therefore, the development and adoption of effective dye wastewater treatment technologies is the key to reducing these hazards.

CR is a chemical substance with a complex aromatic composition that is not easily degraded. Rashad et al. [188] investigated the adsorption process of CR dye on the surface of mixed-phase copper oxide-graphene heterostructured nanocomposites. The results showed that the compound achieved 75% adsorption efficiency for CR. In order to reduce the adsorption cost, Zheng et al. [189] used CR as a dye pollutant model and obtained the raw material from used lithium-ion batteries, and investigated the effects of graphene aerogel input, initial concentration of pollutant, initial pH, temperature, and adsorption time on the adsorption of CR. The experimental results showed that the adsorption rate was as high as 99% under the optimal conditions. The adsorption process was multimolecular layer adsorption, and the quasi-second-order kinetic equation indicated that the adsorption might be chemisorption. The maximum adsorption capacity was 53.91 mg·g^{-1}.

OG is a compound with acidic dye properties that is mainly used to color textiles, food, and pharmaceuticals. Since its molecule contains sulfonate groups that dissociate in water to form negatively charged anions, it can affect water quality and ecosystem balance when discharged directly into water bodies without treatment. GO has received much attention due to its excellent surface properties in the adsorption of dye wastewater. Yang et al. [190] used 3-aminopropyltriethoxysilane modified GO (AS–GO) to remove OG. The results showed that AS–GO had good adsorption capacity for OG. During the reaction process, the maximum adsorption capacity of OG was 576.6 mg·g^{-1} at an initial OG concentration of 100 mg·L^{-1}, an initial adsorbent dose of 2.5 g·L^{-1}, T = 313 K, and pH = 3. The reaction mechanism is shown in Figure 15a. The FTIR spectra proved the

existence of π–π and hydrogen bonding interactions, as shown in Figure 15b. The XRD of AS–GO and AS–GO–OG showed no significant changes, indicating the stability of the adsorbent, as shown in Figure 15c. After four desorption–adsorption cycles, the removal rate remained above 86%, as shown in Figure 15d.
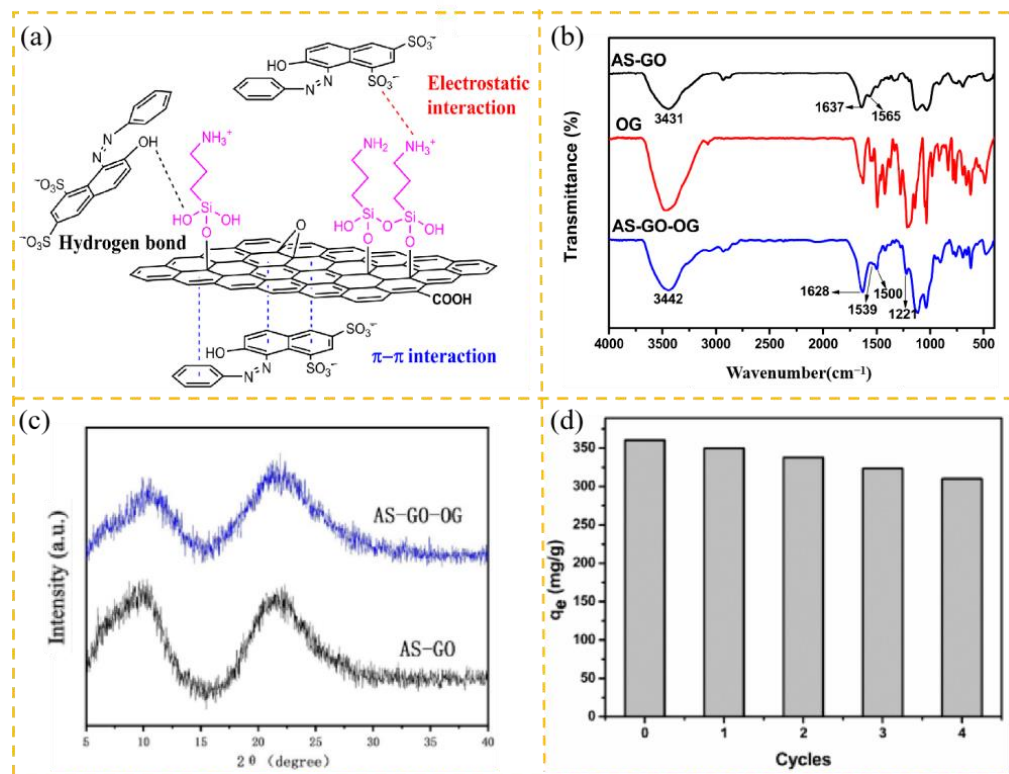
Figure 15. (**a**) Schematic illustration of adsorption mechanisms by AS−GO. (**b**) FTIR spectra of AS–GO, OG, and AS−GO−OG. (**c**) XRD spectra of AS−GO and AS−GO−OG. (**d**) Effect of regeneration cycle on equilibrium adsorption capacity of AS–GO for OG [190]. Copyright 2022, MDPI.

MO belongs to azo compounds, which may lead to color changes in water bodies after entering the water body, affecting not only water quality and aesthetics but also the survival of aquatic organisms. Labiadh et al. [191] investigated the performance of free-standing 3D graphene nano-edge as an effective adsorbent for the removal of MO from aqueous solution. This graphene material exhibits excellent MO absorption over a wide pH range from 2 to 11. It was found that the π–π interactions and hydrogen bonding existing between MO and graphene edges were responsible for the substantial adsorption of MO. Three kinetic models, Frendluich, Temkin, and Langmuir, were used to evaluate the experimental equilibrium data, among which the latter provided the best fit for the adsorption process, according to which the adsorption capacity of the monolayer was derived as 27.932 mg·g^{-1}.

4.1.3. Summary of Adsorption of Organic Dyes

A summary is given herein for a more intuitive comparison of the adsorption performances of various graphene-based adsorbents for dye (see Table 2).

Table 2. Adsorption capacities of graphene-based adsorbents for selected dye.

Adsorbent		Organic Dye	Adsorption Conditions	Adsorption Capacity (mg·g^{-1})	Reference
Material	Form				
GO	Powder	MB	pH = 12	2301	[186]
MHAGO	Powder	MB	pH = 6.0, 45 °C	59.00	[27]
β-CD/GO	Powder	MB	30 °C, 1 h	76.4	[192]
RL–GO	Powder	MB	pH = 11, 318 K	581.40	[193]
GO–TSC–GO	Powder	MB	pH > 7, 25 °C, 120 min	596.642	[194]
GO	Powder	MB	pH > 7, 25 °C, 120 min	196.8	[194]
GO/DETA/MnFe$_2$O$_4$@SiO$_2$	Powder	MB	pH = 7, 25 °C	243.91	[195]
MFTGS	Sponge	MB	308 K, 10 min	224	[86]
CF/CNTs/GO	Foam	MB	C$_0$ = 100 mg·L^{-1}	146	[187]
APAM/DTPA–CS/GO	Aerogel	MB	303 K, 95 min	652.99	[196]
GO/PEI	Aerogel	MB	pH = 10.5, 25 ± 1 °C	249.6	[197]
		MO	pH = 2.0, 25 ± 1 °C	331.0	
CS/GO	Aerogel	MB	pH = 8, 293 K	437.29	[198]
CGZ-3	Aerogel	MB	pH = 9, 298 K	427.35	[199]
M−rGO	Aerogel	MB	298 K	450.90	[200]
GO-MMT/SA	Aerogel	MB	60 min	150.66	[201]
TA–rGO	Hydrogel	MB	25 °C	1000	[95]
GO–EDTA–CS	Powder	MB	pH = 8.3, room temperature	141 ± 6.60 mg·g^{-1}	[155]
		CV	pH = 8.3, room temperature	121 ± 3.50 mg·g^{-1}	
CS/GO	Powder	RhB	pH = 4, 25 °C	858.0	[202]
rGO–ZnS	Powder	MG	25 °C	27.54	[185]
		EV	25 °C	20.04	
Ag–rGO	Powder	NB	pH = 6, 30 °C	36.8	[203]
rGO	Powder	NB	pH = 6, 30 °C	20	[203]
GO	Powder	NB	pH = 6, 30 °C	8.8	[203]
Ag$_2$O–Al$_2$O$_3$–ZrO$_2$–rGO	Powder	CR	30 °C, 90 min	333.32	[204]
CS/GO	Powder	CR	pH = 7, 300 K	182.5	[205]
		MB	pH = 7, 300 K	219.3	
Graphene	Aerogel	CR	pH = 2, 60 °C	53.91	[189]
CTAB–GO	Powder	CR	pH = 3, 298 K	2767	[206]
G/SnO$_2$	Powder	CR	pH = 2–4, 318 K	359.71	[207]
AS–GO	Powder	OG	pH = 3, 313 K	576.6	[190]
3D graphene	Powder	MO	pH = 2–11, 20 °C	27.932	[191]
GONs	Powder	MO	pH = 6.7, 298 K	179.21	[208]
		BB	pH = 6.7, 298 K	236.42	

4.2. Pharmaceuticals

4.2.1. Antibiotics

The main types of antibiotics found in the water environment include tetracycline, sulfonamides, and fluoroquinolones [209,210]. During the production, transportation, and usage of pharmaceutical antibiotics, a significant amount is released into the environment. Due to their stability and limited natural degradation, coupled with their continuous discharge from sewage treatment plants into the ecological environment, water pollution caused by antibiotic contamination has become increasingly severe. Such contamination can cause serious harm [211,212], while unnecessary ingestion of antibiotics by humans can result in toxicity [213,214]. Therefore, it is crucial to address antibiotic contamination. With the increasing social awareness of the need for environmental protection and the continuous progress of related technologies, the application of antibiotic adsorption technology has broad prospects and deserves continuous attention and in-depth research. Many researchers have used graphene-based adsorbents to adsorb antibiotics in water for environmental protection. The adsorption results for antibiotics by selected graphene-based adsorbents are shown in Table 3.

Table 3. Adsorption results of antibiotics by graphene-based adsorbents.

Adsorbent		Antibiotic	Adsorption Conditions	Adsorption Capacity/Removal Efficiency	Reference
Material	**Form**				
Graphene	Powder	Sulfamethoxazole	pH = 7, 298 K	181.3 $\mu g \cdot g^{-1}$	[215]
		Sulfamethazine	pH = 7, 298 K	196.3 $\mu g \cdot g^{-1}$	
		Sulfadiazine	pH = 7, 298 K	184.9 $\mu g \cdot g^{-1}$	
		Cefalexin	pH = 7, 298 K	207.2 $\mu g \cdot g^{-1}$	
		Olfloxain	pH = 7, 298 K	199.2 $\mu g \cdot g^{-1}$	
		Amoxicillin	pH = 7, 298 K	198.2 $\mu g \cdot g^{-1}$	
		Tetracycline	pH = 7, 298 K	200.2 $\mu g \cdot g^{-1}$	
GO	Powder	Sulfamethazine	pH = 5	240 $mg \cdot g^{-1}$	[216]
		Ciprofloxacin	pH = 9	379 $mg \cdot g^{-1}$	
GO	Powder	Doxycycline	pH = 6, 25 °C	116.5099 $mg \cdot g^{-1}$	[217]
		Ciprofloxacin	pH = 6, 25 °C	156.7634 $mg \cdot g^{-1}$	
		Tetracycline	pH = 6, 25 °C	80.980 $mg \cdot g^{-1}$	
GO	Powder	Chlortetracycline	pH = 5, 298 K	218.60 $mg \cdot g^{-1}$	[218]
		Tetracycline	pH = 5, 308 K	182.91 $mg \cdot g^{-1}$	
		Oxytetracycline	pH = 5, 308 K	176.62 $mg \cdot g^{-1}$	
SGO	Powder	Sparfloxacin	pH = 5.5, 25 °C	1428.57 $\mu mol \cdot g^{-1}$	[219]
GO/α–ATP	Powder	Tetracycline	pH = 5, 55 °C	38.73 $mg \cdot g^{-1}$	[220]
CS–GO	Powder	Metronidazole	Neutral pH, 298 K	29.76 $mg \cdot g^{-1}$	[221]
		Ciprofloxacin	Neutral pH, 298 K	102.04 $mg \cdot g^{-1}$	
CD–DGO	Powder	Sulfamethoxazole	pH = 2, 35 °C	144.2804 $mg \cdot g^{-1}$	[222]
		Sulfadiazine	pH = 2, 35 °C	152.2888 $mg \cdot g^{-1}$	
MGO	Powder	Erythromycin	pH = 3, 298 K	285.71 $mg \cdot g^{-1}$	[223]
TS–GO	Powder	Ciprofloxacin	pH = 5, 25 °C	769.23 $mg \cdot g^{-1}$	[224]
		Amoxicillin	pH = 3, 25 °C	625 $mg \cdot g^{-1}$	
GO–CNF	Aerogel	Doxycycline	25 °C	469.7 $mg \cdot g^{-1}$	[225]
		Chlortetracycline	25 °C	396.5 $mg \cdot g^{-1}$	
		Oxytetracycline	25 °C	386.5 $mg \cdot g^{-1}$	
		Tetracycline	25 °C	343.8 $mg \cdot g^{-1}$	
Alginate/rGO	Hydrogel	Tetracycline	pH = 8, 298 K	290.70 $mg \cdot g^{-1}$	[226]
		Ciprofloxacin	pH = 8, 298 K	344.83 $mg \cdot g^{-1}$	

Adsorption by activated carbon, graphene, and GO is one of the most attractive methods to remove antibiotics [84,227], but the pH has a strong influence on the adsorption of antibiotics. Li et al. [218] utilized GO as the main material to explore the adsorption performance of GO on tetracycline antibiotics under different pH conditions, and the experimental results showed that the pH is an important factor affecting the adsorption performance of GO. The functional groups on the surface of GO may change at a high pH, which affects its interaction with antibiotics. The adsorption results showed that the maximum adsorption capacity of GO for the three antibiotics was achieved at pH 5, with the highest adsorption capacity of 167.0 $mg \cdot g^{-1}$ for chloro-tetracycline. This finding is of great significance for understanding and optimizing the ability of GO to remove antibiotics from water in practical water treatment processes. To achieve better adsorption, GO polymers have been used as antibiotic adsorbents. Yu et al. [222] prepared a novel ternary composite, β-cyclodextrin/dopamine hydrochloride–GO (CD–DGO), and investigated its adsorption properties on sulfonamide antibiotics (sulfonamides). The effects of different doses of the composite, the ratio of the components, and the pH of the solution on the adsorption capacity were experimentally evaluated. The results showed that the maximum adsorption capacities of CD–DGO for sulfamethoxazole (SMX) and sulfadiazine (SDZ) were 144 $mg \cdot g^{-1}$ and 152 $mg \cdot g^{-1}$ at pH = 2, respectively.

For easier separation of nanomaterials from water after adsorption, the preparation of nanomaterial hydrogels and polymer composite hydrogels proved to be useful. Zhuang et al. [226] investigated the performance of adsorption for the removal of antibiotics from water using modified alginate/graphene bi-network porous hydrogels. It was shown that hydrogen bonding had a greater effect on adsorption than carboxyl groups. The adsorption results revealed maximum capacities of 290.70 mg·g^{-1} for tetracycline and 344.83 mg·g^{-1} for ciprofloxacin in the modified hydrogel. Antibiotic adsorption is not only of great significance for protecting the environment and promoting sustainable development but also plays a key role in enhancing economic benefits, safeguarding public health, promoting scientific research, and strengthening environmental monitoring and management.

4.2.2. Other Organic Pharmaceuticals

In addition to antibiotics, there are other medications whose dangers should not be overlooked, such as sulfamethoxazole, carbamazepine, ketoprofen, valsartan, diclofenac, and amphetamines (ATDs). Most of these drugs originate from synthesis or extraction processes in the pharmaceutical industry. Entry into water sources through improper handling or discharge may lead to contamination. Removal of these drugs is necessary to ensure that water quality is safe and meets regulatory requirements.

Granular activated carbon (GAC) is widely used for the removal of active pharmaceutical ingredients (APIs), but these adsorbents suffer from degraded performance and expensive regeneration due to the presence of natural organic macromolecules (NOMs) [228,229]. A stable, self-regenerating adsorbent, metal oxide nanocomposite (S–MGC) containing TiO$_2$ and SiO$_2$ combined with 3D GO, which adsorbs APIs and is regenerated by light, was used by Fu et al. Removal of APIs in a variety of environments, including five model APIs: sulfamethoxazole, carbamazepine, ketoprofen, valsartan, and diclofenac. In the absence of TiO$_2$/SiO$_2$, the adsorption performance of 3D GO (CGB) was superior to that of GAC, while S–MGCs further enhanced the adsorption capacity of CGB.

ATDs are harmful in a variety of ways, primarily including damage to the blood system, nervous system, skin, and liver. Cao et al. [230] used deep eutectic solvent-functionalized composites (ZMG–DES) as adsorbents for the adsorption of three typical ATDs (MDMA, MAM, and AM). The adsorption schematic is shown in Figure 16a. The results of batch experiments showed that the maximum adsorption of MDMA (933.652 μg·g^{-1}) was 2.3 and 2.8 times higher than that of MAM (412.849 μg·g^{-1} and AM (328.652 μg·g^{-1}), respectively. The affected in different environments as shown in Figure 16b–d. ZMG–DES exhibited a fast adsorption rate (within 1 h), good affinity (96.76%, 74.33%, and 61.35% removal, respectively), and excellent reusability (five cycles) for MDMA, MAM, and AM. Quantum chemical theory and Multiwfn were used to study the weak interactions, especially the differences in H-bonding. In addition, mechanisms such as π–π, van der Waals forces, hydrophobic interactions, and electrostatic attraction were involved in the adsorption.
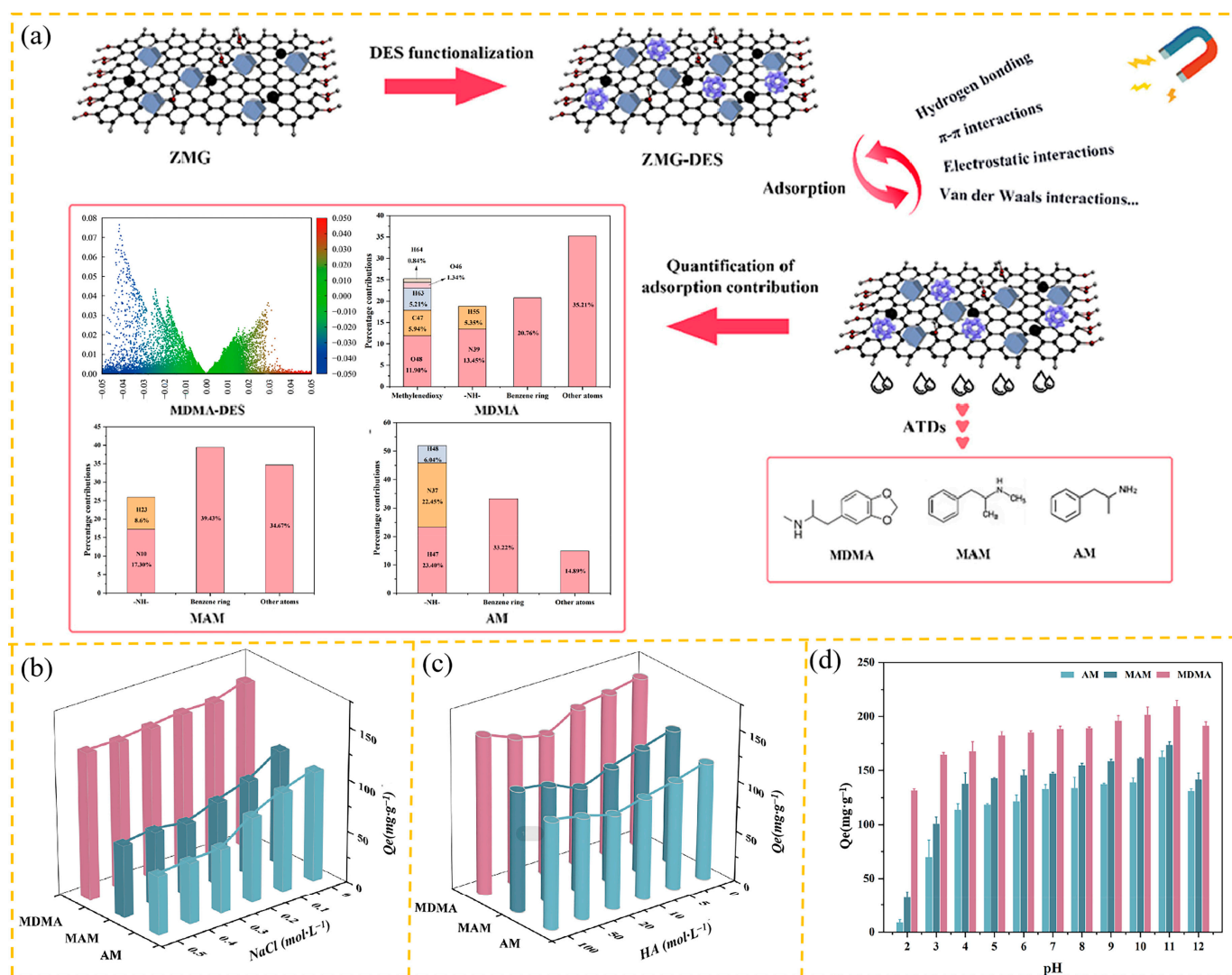
Figure 16. (**a**) Schematic diagram of ZMG–DES adsorbed ATDs. Effects of (**b**) NaCl concentration, (**c**) HA concentration, (**d**) solution pH of three ATD adsorption on ZMG–DES. Reprinted with permission from reference [230]. Copyright 2024, Elsevier.

4.3. Aromatic Pollutants

Most aromatic compounds are recognized as toxic pollutants, among which phenolic compounds such as phenol, nitrobenzene, bisphenol A, and triclosan, as well as polycyclic aromatic hydrocarbons such as anthracene (ANT), 2-methyl anthraquinone (2-MAQ), quinoline, are of great concern.

Phenolic compounds are highly toxic and can cause skin burns, respiratory irritation, and poisoning in humans. They seriously pollute water bodies, disrupt the ecological balance, and affect food safety. Phenol is toxic and tends to accumulate in the food chain, inducing heart disease and leukemia, thus posing an irreversible risk to public health [231]. In order to develop a recyclable and efficient adsorbent for the adsorption of phenol, Cui et al. [232] used 3D nitrogen-doped graphene oxide aerogel (NGOA) for the adsorption of phenol and the static saturated adsorption capacity for phenol reached 108.19 mg·g^{-1}, which was significantly higher than that of most adsorbents. Importantly, monolithic NGOA can be easily separated and recovered after adsorption saturation. Finally, the adsorption mechanism of phenol on NGOA was proposed, as shown in Figure 17a. The adsorption of phenol on NGOA mainly consists of porous adsorption, π–π interactions, hydrogen bonding, and electrostatic gravitational forces, which are physical adsorption. Nitrophenols are highly toxic and may cause central nervous system damage and organ

dysfunction with prolonged exposure, requiring stringent safety measures to minimize their impact on human health and the environment. In order to remove nitrobenzene, Severo et al. [233] used a 3D graphene sponge material (WS-Graphene) and used it to adsorb o- and p-nitrophenol from wastewater, as shown in Figure 17b. When the concentration of both adsorbents was fixed at 700 mg·L^{-1}, the adsorption process of both nitrophenols was very rapid, reaching equilibrium in less than 5 min. In addition, the maximum adsorption capacities were 1842 mg·g^{-1} for o-nitrophenol and 879.6 mg·g^{-1} for p-nitrophenol at 30 °C. For the removal of bisphenol A (BPA) and triclosan (TCS), Wang et al. [234] investigated the adsorption behavior of BPA and TCS on graphene and compared it with activated carbon, and the adsorption schematic is shown in Figure 17c. The maximum adsorption capacities of BPA on both graphene and activated carbon reached about 2 mg·g^{-1}. In contrast, the strong partitioning capacity of TCS on graphene indicated that graphene material can be used for the removal of TCS from wastewater. This phenomenon should be attributed to the establishment of electrostatic repulsion between anionic BPA (or TCS) molecules and graphene (or activated carbon) surfaces at higher pH conditions.

Polycyclic aromatic hydrocarbons (PAHs) are a class of compounds consisting of two or more benzene rings attached to each other. They are widely present in the environment, mainly from incomplete combustion of fossil fuels and wood, spills of petroleum products, etc. PAHs are acutely and chronically toxic to aquatic organisms and are capable of affecting growth, reproduction, and the immune system of living organisms. Song et al. [235] used nitrogen-doped rGO (NRGO) for the removal of PAHs and their oxygen derivatives in aqueous solutions (OPAHs). NRGO showed significant adsorption efficiency for ANT and 2-MAQ. At 298 K and pH = 7, the adsorption capacity of NRGO was 5.77 mg·g^{-1} for ANT and 9.29 mg·g^{-1} for 2-MAQ, which increased more than 2.76 and 2.29 times, respectively, compared with GO and 1.4 times compared with rGO. Based on the characterization results and adsorption experiments, intra-particle diffusion, hydrophobic effects, and π–π interactions may be simultaneously involved in the adsorption process. This work provides ideas for the application of NRGO in the environment and the possibility of removing low concentrations of PAHs and OPAHs from wastewater.

Quinoline is a nitrogen-containing heterocyclic compound, and its presence in wastewater is potentially harmful in various ways. After entering the water body, quinoline may persist in the aqueous environment for a long period and cause persistent effects on the water quality due to its chemical stability. An effective method for the removal of quinoline is adsorption. Kang et al. [236] worked on the adsorption properties of a nitrogen-doped hollow carbon nanospheres/graphene composite aerogel (HCNS/NGA) for quinoline. The results of the adsorption study revealed that HCNS/NGA exhibited a high adsorption capacity for quinoline, reaching 138.37 ± 2.58 mg·g^{-1} at 298 K, demonstrating significant potential for practical applications. The adsorption of quinoline molecules on HCNS/NGA may be the result of the synergistic effect of multiple mechanisms, among which physical adsorption may be dominant, and the mechanism is shown in Figure 17d.
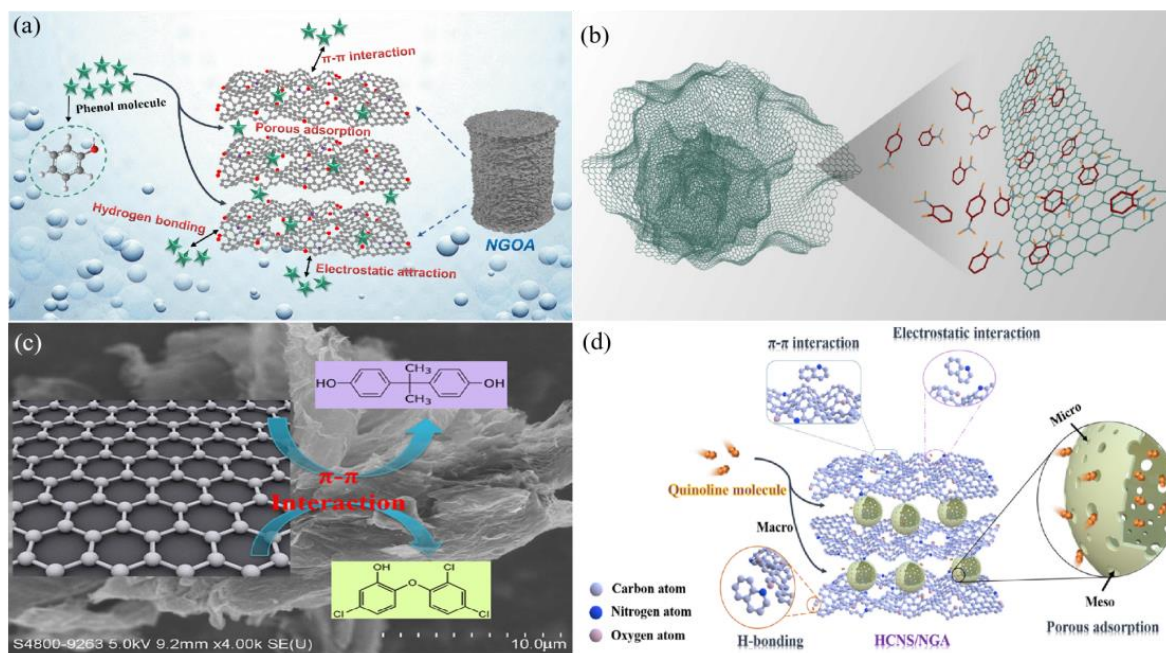
Figure 17. (**a**) The adsorption mechanism of phenol on NGOA. Reprinted with permission from reference [232]. Copyright 2023, Elsevier. (**b**) Schematic diagram of nitrophenol adsorption by WS-Graphene. Reprinted with permission from reference [233]. Copyright 2023, Elsevier. (**c**) Schematic diagram of BPA and TCS adsorption by graphene [234]. Copyright 2017, ACS. (**d**) Schematic illustration of the possible interaction between HCNS/NGA and quinoline molecules. Reprinted with permission from reference [236]. Copyright 2021, Elsevier.

5. Conclusions and Prospects

Graphene, as a two-dimensional material, exhibits considerable research and application potential in the field of adsorbent materials due to its unique physical and chemical properties, such as the high hydrophobicity of graphene materials, good adsorption affinity for organic pollutants, and huge specific surface area. In particular, GO contains abundant oxygen-containing functional groups and hydroxyl and epoxy groups, which provide good adsorption of pollutants in adsorbent water, and its adsorption performance and recycling rate can be improved though chemical or physical modification. There are two main methods for graphene synthesis: bottom-up methods and top-down methods. This paper describes the main preparation methods of graphene and its derivatives, as well as the main preparation methods of 3D graphene. The rapid development of the preparation technology of graphene and its derivatives has enabled a variety of high-performance graphene-based adsorbents to effectively remove toxic pollutants from wastewater, such as heavy metals, rare metals, organic dyes, and pharmaceuticals, with fast kinetics and excellent adsorption performance. Further functionalization of these graphene-based adsorbents through the introduction of specific functional groups or the incorporation of other nanomaterials is expected to significantly improve their performance in removing heavy metals and organic pollutants. This paper further summarized the adsorption results obtained in recent years regarding graphene-based adsorbents on inorganic and organic pollutants, as well as the adsorption mechanisms in recent years.

In the future, continuous production of graphene-based adsorbents using low-cost raw materials has the potential to reduce their cost in the future. Large-scale preparation of cost-effective graphene-based adsorbents for wastewater treatment still requires further research. The application of graphene-based adsorbents in wastewater treatment plants is expected to be a breakthrough for future research. The research directions on graphene-based adsorbents will be directed toward developing more environmentally friendly methods for graphene preparation, reducing the utilization of hazardous chemicals, minimizing

production costs, and enhancing the sustainability of graphene. By precisely manipulating the layer count, pore size distribution, and surface properties of graphene, it is possible to design graphene-based materials with enhanced selectivity and adsorption capacities. Innovative functionalization strategies, such as biomolecular modification and magnetic nanoparticle incorporation, are being explored to augment the performance of graphene-based materials in specific applications. A comprehensive understanding of the interaction mechanism between graphene-based materials and pollutants offers theoretical guidance for the development of more efficient adsorbents. Graphene-based adsorbents hold significant potential for application in the field of environmental purification. Through continuous technological innovation and extensive research, they are expected to address current environmental issues and make substantial contributions to safeguarding human health and preserving the ecological environment.

References

1. Sarath, N.G.; Puthur, J.T. Heavy metal pollution assessment in a mangrove ecosystem scheduled as a community reserve. *Wetl. Ecol. Manag.* **2021**, *29*, 719–730. [CrossRef]
2. Liu, M.; Zhang, L.; Wang, M.; Wang, X.; Cui, H.; Wei, J.; Li, X. The role of metal-organic frameworks in removing emerging contaminants in wastewater. *J. Clean. Prod.* **2023**, *429*, 139526. [CrossRef]
3. Wójcik, G. Sorption behaviors of light lanthanides(III) (La(III), Ce(III), Pr(III), Nd(III)) and Cr(III) using nitrolite. *Materials* **2020**, *13*, 2256. [CrossRef] [PubMed]
4. Vergara-Araya, M.; Oeltze, H.; Radeva, J.; Roth, A.G.; Göbbert, C.; Niestroj-Pahl, R.; Dähne, L.; Wiese, J. Operation of hybrid membranes for the removal of pharmaceuticals and pollutants from water and wastewater. *Membranes* **2022**, *12*, 502. [CrossRef]
5. Duan, G.; Cao, Z.; Zhong, H.; Ma, X.; Wang, S. Highly efficient poly(6-acryloylamino-N-hydroxyhexanamide) resin for adsorption of heavy metal ions. *J. Environ. Manag.* **2022**, *308*, 114631. [CrossRef]
6. Zhou, S.; Xie, Y.; Zhu, F.; Gao, Y.; Liu, Y.; Tang, Z.; Duan, Y. Amidoxime modified chitosan/graphene oxide composite for efficient adsorption of U(VI) from aqueous solutions. *J. Environ. Chem. Eng.* **2021**, *9*, 106363. [CrossRef]
7. Tang, X.; Xue, H.; Li, J.; Wang, S.; Yu, J.; Zeng, T. Degradation of bisphenol A by nitrogen-rich ZIF-8-derived carbon materials-activated peroxymonosulfate. *Toxics* **2024**, *12*, 359. [CrossRef]
8. Cui, Y.; Li, S.; Yu, N.; Yu, X.; Ji, X.; Wang, L. Highly biocompatible hemoglobin-stabilized gold nanoparticles for an enhanced catalytic reduction of 4-nitrophenol. *Inorganics* **2024**, *12*, 136. [CrossRef]
9. Benalia, M.C.; Youcef, L.; Bouaziz, M.G.; Achour, S.; Menasra, H. Removal of heavy metals from industrial wastewater by chemical precipitation: Mechanisms and sludge characterization. *Arab. J. Sci. Eng.* **2022**, *47*, 5587–5599. [CrossRef]
10. Wang, L.; Luo, Y.; Li, H.; Yu, D.; Wang, Y.; Wang, W.; Wu, M. Preparation and selective adsorption of surface-imprinted microspheres based on hyperbranched polyamide-functionalized sodium alginate for the removal of Sb(III). *Colloids Surf. A Physicochem. Eng. Asp.* **2020**, *585*, 124106. [CrossRef]
11. Wang, S.; Li, J.; Narita, H.; Tanaka, M. Solvent extraction equilibrium modeling for the separation of ammonia, nickel(II), and copper(II) from the loaded LIX84-I. *Miner. Eng.* **2021**, *172*, 107132. [CrossRef]
12. Pei, J.; Huang, L.; Jiang, H.; Liu, H.; Liu, X.; Hu, X. Inhibitory effect of hydrogen ion on the copper ions separation from acid solution across graphene oxide membranes. *Sep. Purif. Technol.* **2019**, *210*, 651–658. [CrossRef]
13. Wang, J.; Yang, F.; Wang, S.; Zhong, H.; Wu, Z.-k.; Cao, Z.-f. Reactivation of nano-Fe₃O₄/diethanolamine/rGO catalyst by using electric field in Fenton reaction. *J. Taiwan Inst. Chem. Eng.* **2019**, *99*, 113–122. [CrossRef]
14. Jiang, C.-L.; Wang, R.; Chen, X.; Zheng, L.-G.; Cheng, H. Preparation of chitosan modified fly ash under acid condition and its adsorption mechanism for Cr(VI) in water. *J. Cent. South Univ.* **2021**, *28*, 1652–1664. [CrossRef]

15. Shi, T.-S.; Jiang, F.; Wang, P.; Yue, T.; Sun, W. Deep purification of As(V) in drinking water by silica gel loaded with FeOOH and MnO$_2$. *J. Cent. South Univ.* **2021**, *28*, 1692–1706. [CrossRef]

16. Qiu, S.; Yan, L.; Jing, C. Simultaneous removal of arsenic and antimony from mining wastewater using granular TiO$_2$: Batch and field column studies. *J. Environ. Sci.* **2019**, *75*, 269–276. [CrossRef] [PubMed]

17. Guo, X.; Wu, Z.; He, M.; Meng, X.; Jin, X.; Qiu, N.; Zhang, J. Adsorption of antimony onto iron oxyhydroxides: Adsorption behavior and surface structure. *J. Hazard. Mater.* **2014**, *276*, 339–345. [CrossRef]

18. Ighalo, J.O.; Iwuozor, K.O.; Igwegbe, C.A.; Adeniyi, A.G. Verification of pore size effect on aqueous-phase adsorption kinetics: A case study of methylene blue. *Colloids Surf. A Physicochem. Eng. Asp.* **2021**, *626*, 127119. [CrossRef]

19. Alshabib, M.; Oluwadamilare, M.A.; Tanimu, A.; Abdulazeez, I.; Alhooshani, K.; Ganiyu, S.A. Experimental and DFT investigation of ceria-nanocomposite decorated AC derived from groundnut shell for efficient removal of methylene-blue from wastewater effluent. *Appl. Surf. Sci.* **2021**, *536*, 147749. [CrossRef]

20. Yu, W.; Xu, J.; Li, J.; Zhu, S.; Xie, J.; Zhou, Z.; Wang, B.; Li, J.; Chen, K. Hollow structured kapok fiber-based hierarchical porous biocarbons for ultrahigh adsorption of organic dyes. *Ind. Eng. Chem. Res.* **2022**, *61*, 4114–4124. [CrossRef]

21. Chen, Q.; Zhang, Q.; Yang, Y.; Wang, Q.; He, Y.; Dong, N. Synergetic effect on methylene blue adsorption to biochar with gentian violet in dyeing and printing wastewater under competitive adsorption mechanism. *Case Stud. Therm. Eng.* **2021**, *26*, 101099. [CrossRef]

22. Park, C.; Engel, E.S.; Crowe, A.; Gilbert, T.R.; Rodriguez, N.M. Use of carbon nanofibers in the removal of organic solvents from water. *Langmuir* **2000**, *16*, 8050–8056. [CrossRef]

23. Mishakov, I.V.; Bauman, Y.I.; Brzhezinskaya, M.; Netskina, O.V.; Shubin, Y.V.; Kibis, L.S.; Stoyanovskii, V.O.; Larionov, K.B.; Serkova, A.N.; Vedyagin, A.A. Water purification from chlorobenzenes using heteroatom-functionalized carbon nanofibers produced on self-organizing Ni-Pd catalyst. *J. Environ. Chem. Eng.* **2022**, *10*, 107873. [CrossRef]

24. Dehghani, Z.; Ostovari, F.; Sharifi, S. A comparison of the crystal structure and optical properties of reduced graphene oxide and aminated graphene nanosheets for optoelectronic device applications. *Optik* **2023**, *274*, 170551. [CrossRef]

25. Kim, J.B.; Koo, S.H.; Kim, I.H.; Kim, J.T.; Kim, J.G.; Jayaraman, B.; Lim, J.; Kim, S.O. Characteristic dual-domain composite structure of reduced graphene oxide and its application to higher specific capacitance. *Chem. Eng. J.* **2022**, *446*, 137390. [CrossRef]

26. Bryan, M.Y.K.; Chai, P.V.; Law, J.Y.; Mahmoudi, E. Graphene oxide-chitosan composite material as adsorbent in removing methylene blue dye from synthetic wastewater. *Mater. Today Proc.* **2022**, *64*, 1587–1596. [CrossRef]

27. Li, D.; Hua, T.; Yuan, J.; Xu, F. Methylene blue adsorption from an aqueous solution by a magnetic graphene oxide/humic acid composite. *Colloids Surf. A Physicochem. Eng. Asp.* **2021**, *627*, 127171. [CrossRef]

28. Hua, Y.; Li, F.; Hu, N.; Fu, S.-Y. Frictional characteristics of graphene oxide-modified continuous glass fiber reinforced epoxy composite. *Compos. Sci. Technol.* **2022**, *223*, 109446. [CrossRef]

29. Jun, S.-Y.; Park, S.H.; Sohn, M.K.; Kim, S.; Lee, J.M.; Kong, D.S.; Lee, T.-Y.; Jung, J.H.; Kim, M.-S.; Yoo, S.; et al. Reduction time effect on the dielectric characteristics of reduced-graphene-oxide--encapsulated barium titanate powder fillers. *Carbon* **2022**, *199*, 23–32. [CrossRef]

30. Anandaraj, C.; Venkatapathy, R.; Bharath Sabarish, V.C.; Kalaivani, P.; Durairajan, A.; Graça, M.P.; Valente, M.A.; Gajendiran, J.; Gokul Raj, S.; Ramesh Kumar, G. Structural characteristics, optical, electrical and electrochemical sensing properties of graphene and multi walled carbon nanotube admixtured bismuth iron oxide composite ceramics. *Ceram. Int.* **2021**, *47*, 28042–28049. [CrossRef]

31. Hu, H.; Wen, W.; Ou, J.Z. Construction of adsorbents with graphene and its derivatives for wastewater treatment: A review. *Environ. Sci. Nano* **2022**, *9*, 3226–3276. [CrossRef]

32. Wang, Y.; Gai, Z.; Guo, F.; Zhang, M.; Zhang, L.; Xia, G.; Chai, X.; Ren, Y.; Zhang, X.; Jiang, X. A diamond/graphene/diamond eectrode for waste water treatment. *Nanomaterials* **2023**, *13*, 3043. [CrossRef] [PubMed]

33. Faysal Hossain, M.D.; Akther, N.; Zhou, Y. Recent advancements in graphene adsorbents for wastewater treatment: Current status and challenges. *Chin. Chem. Lett.* **2020**, *31*, 2525–2538. [CrossRef]

34. Asif, F.C.; Saha, G.C. Graphene-like carbon structure synthesis from biomass pyrolysis: A critical review on feedstock–process–properties relationship. *C* **2023**, *9*, 31. [CrossRef]

35. Geim, A.K.; Novoselov, K.S. The rise of graphene. *Nat. Mater.* **2007**, *6*, 183–191. [CrossRef] [PubMed]

36. Laraba, S.R.; Luo, W.; Rezzoug, A.; Zahra, Q.u.a.; Zhang, S.; Wu, B.; Chen, W.; Xiao, L.; Yang, Y.; Wei, J.; et al. Graphene-based composites for biomedical applications. *Green Chem. Lett. Rev.* **2022**, *15*, 724–748. [CrossRef]

37. Brzhezinskaya, M.; Irzhak, A.; Irzhak, D.; Kang, T.W.; Kononenko, O.; Matveev, V.; Panin, G.; Roshchupkin, D. Direct growth of graphene film on piezoelectric La$_3$Ga$_{5.5}$Ta$_{0.5}$O$_{14}$ crystal. *Phys. Status Solidi (RRL)—Rapid Res. Lett.* **2016**, *10*, 639–644. [CrossRef]

38. Kononenko, O.; Brzhezinskaya, M.; Zotov, A.; Korepanov, V.; Levashov, V.; Matveev, V.; Roshchupkin, D. Influence of numerous Moiré superlattices on transport properties of twisted multilayer graphene. *Carbon* **2022**, *194*, 52–61. [CrossRef]

39. Santhiran, A.; Iyngaran, P.; Abiman, P.; Kuganathan, N. Graphene synthesis and its recent advances in applications—A review. *C* **2021**, *7*, 76. [CrossRef]

40. Jana, A.; Scheer, E.; Polarz, S. Synthesis of graphene–transition metal oxide hybrid nanoparticles and their application in various fields. *Beilstein J. Nanotechnol.* **2017**, *8*, 688–714. [CrossRef]

41. Pedrazzetti, L.; Gibertini, E.; Bizzoni, F.; Russo, V.; Lucotti, A.; Nobili, L.; Magagnin, L. Graphene growth on electroformed copper substrates by atmospheric pressure CVD. *Materials* **2022**, *15*, 1572. [CrossRef] [PubMed]

42. Sun, L.; Chen, B.; Wang, W.; Li, Y.; Zeng, X.; Liu, H.; Liang, Y.; Zhao, Z.; Cai, A.; Zhang, R.; et al. Toward epitaxial growth of misorientation-free graphene on Cu(III) foils. *ACS Nano* **2022**, *16*, 285–294. [CrossRef]

43. Olorunkosebi, A.A.; Eleruja, M.A.; Adedeji, A.V.; Olofinjana, B.; Fasakin, O.; Omotoso, E.; Oyedotun, K.O.; Ajayi, E.O.B.; Manyala, N. Optimization of graphene oxide through various Hummers' methods and comparative reduction using green approach. *Diam. Relat. Mater.* **2021**, *117*, 108456. [CrossRef]

44. Vacacela Gomez, C.; Guevara, M.; Tene, T.; Villamagua, L.; Usca, G.T.; Maldonado, F.; Tapia, C.; Cataldo, A.; Bellucci, S.; Caputi, L.S. The liquid exfoliation of graphene in polar solvents. *Appl. Surf. Sci.* **2021**, *546*, 149046. [CrossRef]

45. Tan, H.; Navik, R.; Liu, Z.; Xiang, Q.; Zhao, Y. Scalable massive production of defect-free few-layer graphene by ball-milling in series with shearing exfoliation in supercritical CO_2. *J. Supercrit. Fluids* **2022**, *181*, 105496. [CrossRef]

46. Edison, T.N.J.I.; Atchudan, R.; Karthik, N.; Chandrasekaran, P.; Perumal, S.; Arunachalam, P.; Raja, P.B.; Sethuraman, M.G.; Lee, Y.R. Electrochemically exfoliated graphene sheets as electrode material for aqueous symmetric supercapacitors. *Surf. Coat. Technol.* **2021**, *416*, 127150. [CrossRef]

47. Rabchinskii, M.K.; Sysoev, V.V.; Glukhova, O.E.; Brzhezinskaya, M.; Stolyarova, D.Y.; Varezhnikov, A.S.; Solomatin, M.A.; Barkov, P.V.; Kirilenko, D.A.; Pavlov, S.I.; et al. Guiding graphene derivatization for the on-chip multisensor arrays: From the synthesis to the theoretical background. *Adv. Mater. Technol.* **2022**, *7*, 2101250. [CrossRef]

48. Marcano, D.C.; Kosynkin, D.V.; Berlin, J.M.; Sinitskii, A.; Sun, Z.; Slesarev, A.; Alemany, L.B.; Lu, W.; Tour, J.M. Improved synthesis of graphene oxide. *ACS Nano* **2010**, *4*, 4806–4814. [CrossRef]

49. Peng, L.; Xu, Z.; Liu, Z.; Wei, Y.; Sun, H.; Li, Z.; Zhao, X.; Gao, C. An iron-based green approach to 1-h production of single-layer graphene oxide. *Nat. Commun.* **2015**, *6*, 5716. [CrossRef]

50. Ye, C.; Wang, G.; Yuan, H.; Li, J.; Ni, K.; Pan, F.; Guo, M.; Wu, Y.; Ji, H.; Zhang, F.; et al. Microfluidic oxidation of graphite in two minutes with capability of real-time monitoring. *Adv. Mater.* **2022**, *34*, 2107083. [CrossRef]

51. Zhu, Y.; Kong, G.; Pan, Y.; Liu, L.; Yang, B.; Zhang, S.; Lai, D.; Che, C. An improved Hummers method to synthesize graphene oxide using much less concentrated sulfuric acid. *Chin. Chem. Lett.* **2022**, *33*, 4541–4544. [CrossRef]

52. Zhou, A.; Yu, T.; Liang, X.; Yin, S. H_2O_2-free strategy derived from Hummers method for preparing graphene oxide with high oxidation degree. *FlatChem* **2023**, *38*, 100487. [CrossRef]

53. Sahila Grace, A.; Littis Malar, G.S.P. Synthesis and characterization of graphene oxide from coconut husk ash. *Orient. J. Chem.* **2020**, *36*, 348–352. [CrossRef]

54. Amir Faiz, M.S.; Che Azurahanim, C.A.; Yazid, Y.; Suriani, A.B.; Siti Nurul Ain, M.J. Preparation and characterization of graphene oxide from tea waste and it's photocatalytic application of TiO_2/graphene nanocomposite. *Mater. Res. Express* **2020**, *7*, 015613. [CrossRef]

55. Sujiono, E.H.; Zurnansyah; Zabrian, D.; Dahlan, M.Y.; Amin, B.D.; Samnur; Agus, J. Graphene oxide based coconut shell waste: Synthesis by modified Hummers method and characterization. *Heliyon* **2020**, *6*, e04568. [CrossRef]

56. Tohamy, H.-A.S.; El-Sakhawy, M.; Kamel, S. Development of magnetite/graphene oxide hydrogels from agricultural wastes for water treatment. *J. Alloys Compd.* **2022**, *10*, 1889–1909. [CrossRef]

57. Harres, A.; Garcia, W.J.S.; Salles, T.R.; Bruckmann, F.S.; Sulzenco, J.B.; Schneider, A.D.; Rhoden, C.R.B. Magnetic properties of graphene oxide decorated with magnetite nanoparticles. *Diam. Relat. Mater.* **2023**, *138*, 110238. [CrossRef]

58. Shen, J.; Shi, M.; Ma, H.; Yan, B.; Li, N.; Ye, M. Hydrothermal synthesis of magnetic reduced graphene oxide sheets. *Mater. Res. Bull.* **2011**, *46*, 2077–2083. [CrossRef]

59. Wang, X.; Yu, J. Application of Fe_3O_4/graphene oxide composite for the separation of Cs(I) and Sr(II) from aqueous solution. *J. Radioanal. Nucl. Chem.* **2015**, *303*, 807–813. [CrossRef]

60. Chong, S.; Zhang, G.; Tian, H.; Zhao, H. Rapid degradation of dyes in water by magnetic Fe^0/Fe_3O_4/graphene composites. *J. Environ. Sci.* **2016**, *44*, 148–157. [CrossRef]

61. Das, T.K.; Sakthivel, T.S.; Jeyaranjan, A.; Seal, S.; Bezbaruah, A.N. Ultra-high arsenic adsorption by graphene oxide iron nanohybrid: Removal mechanisms and potential applications. *Chemosphere* **2020**, *253*, 126702. [CrossRef]

62. Mosleh, N.; Joolaei Ahranjani, P.; Parandi, E.; Rashidi Nodeh, H.; Nawrot, N.; Rezania, S.; Sathishkumar, P. Titanium lanthanum three oxides decorated magnetic graphene oxide for adsorption of lead ions from aqueous media. *Environ. Res.* **2022**, *214*, 113831. [CrossRef]

63. Pan, N.; Li, L.; Ding, J.; Li, S.; Wang, R.; Jin, Y.; Wang, X.; Xia, C. Preparation of graphene oxide-manganese dioxide for highly efficient adsorption and separation of Th(IV)/U(VI). *J. Hazard. Mater.* **2016**, *309*, 107–115. [CrossRef]

64. Bagbi, Y.; Solanki, P.R. Fabrication of mesoporous silica nanoparticle-decorated graphene oxide sheets for the effective removal of lead (Pb^{2+}) from water. *ACS Omega* **2023**, *9*, 304–316. [CrossRef]

65. Singh, S.; Anil, A.G.; Khasnabis, S.; Kumar, V.; Nath, B.; Adiga, V.; Kumar Naik, T.S.S.; Subramanian, S.; Kumar, V.; Singh, J.; et al. Sustainable removal of Cr(VI) using graphene oxide-zinc oxide nanohybrid: Adsorption kinetics, isotherms and thermodynamics. *Environ. Res.* **2022**, *203*, 111891. [CrossRef]

66. Li, X.; Wang, Z.; Li, Q.; Ma, J.; Zhu, M. Preparation, characterization, and application of mesoporous silica-grafted graphene oxide for highly selective lead adsorption. *Chem. Eng. J.* **2015**, *273*, 630–637. [CrossRef]

67. Li, L.; Zhao, L.; Ma, J.; Tian, Y. Preparation of graphene oxide/chitosan complex and its adsorption properties for heavy metal ions. *Green Process. Synth.* **2020**, *9*, 294–303. [CrossRef]

68. Sherlala, A.I.A.; Raman, A.A.A.; Bello, M.M.; Buthiyappan, A. Adsorption of arsenic using chitosan magnetic graphene oxide nanocomposite. *J. Environ. Manag.* **2019**, *246*, 547–556. [CrossRef] [PubMed]

69. Xia, H.; Ren, Q.; Lv, J.; Wang, Y.; Feng, Z.; Li, Y.; Wang, C.; Liu, Y.; Wang, Y. Hydrothermal fabrication of phytic acid decorated chitosan-graphene oxide composites for efficient and selective adsorption of uranium (VI). *J. Environ. Chem. Eng.* **2023**, *11*, 110760. [CrossRef]

70. Zhang, L.; Luo, H.; Liu, P.; Fang, W.; Geng, J. A novel modified graphene oxide/chitosan composite used as an adsorbent for Cr(VI) in aqueous solutions. *Int. J. Biol. Macromol.* **2016**, *87*, 586–596. [CrossRef] [PubMed]

71. Abd-Elhamid, A.I.; Elgoud, E.M.A.; Aly, H.F. Alginate modified graphene oxide for rapid and effective sorption of some heavy metal ions from an aqueous solution. *Cellulose* **2022**, *29*, 6231–6245. [CrossRef]

72. Ma, X.; Duan, G.-y.; Huang, J.-q.; Yang, J.; Cao, Z.-f.; Wang, S. Preparation of graphene oxide/polyiminodiacetic acid resin as a high-performance adsorbent for Cu(II). *J. Cent. South Univ.* **2023**, *30*, 3881–3896. [CrossRef]

73. Arshad, F.; Selvaraj, M.; Zain, J.; Banat, F.; Abu Haija, M. Polyethylenimine modified graphene oxide hydrogel composite as an efficient adsorbent for heavy metal ions. *Sep. Purif. Technol.* **2019**, *209*, 870–880. [CrossRef]

74. Peer, F.E.; Bahramifar, N.; Younesi, H. Removal of Cd (II), Pb (II) and Cu (II) ions from aqueous solution by polyamidoamine dendrimer grafted magnetic graphene oxide nanosheets. *J. Taiwan Inst. Chem. Eng.* **2018**, *87*, 225–240. [CrossRef]

75. Ma, Y.-X.; Xing, D.; Shao, W.-J.; Du, X.-Y.; La, P.-Q. Preparation of polyamidoamine dendrimers functionalized magnetic graphene oxide for the adsorption of Hg(II) in aqueous solution. *J. Colloid Interface Sci.* **2017**, *505*, 352–363. [CrossRef]

76. Nardecchia, S.; Carriazo, D.; Ferrer, M.L.; Gutiérrez, M.C.; del Monte, F. Three dimensional macroporous architectures and aerogels built of carbon nanotubes and/or graphene: Synthesis and applications. *Chem. Soc. Rev.* **2013**, *42*, 794–830. [CrossRef]

77. Ren, R.-P.; Li, W.; Lv, Y.-K. A robust, superhydrophobic graphene aerogel as a recyclable sorbent for oils and organic solvents at various temperatures. *J. Colloid Interface Sci.* **2017**, *500*, 63–68. [CrossRef]

78. Wang, Y.; Xie, W.; Liu, H.; Gu, H. Hyperelastic magnetic reduced graphene oxide three-dimensional framework with superb oil and organic solvent adsorption capability. *Adv. Compos. Hybrid Mater.* **2020**, *3*, 473–484. [CrossRef]

79. Tiwari, J.N.; Mahesh, K.; Le, N.H.; Kemp, K.C.; Timilsina, R.; Tiwari, R.N.; Kim, K.S. Reduced graphene oxide-based hydrogels for the efficient capture of dye pollutants from aqueous solutions. *Carbon* **2013**, *56*, 173–182. [CrossRef]

80. Sahraei, R.; Sekhavat Pour, Z.; Ghaemy, M. Novel magnetic bio-sorbent hydrogel beads based on modified gum traga-canth/graphene oxide: Removal of heavy metals and dyes from water. *J. Clean. Prod.* **2017**, *142*, 2973–2984. [CrossRef]

81. Yu, B.; Bai, Y.; Ming, Z.; Yang, H.; Chen, L.; Hu, X.; Feng, S.; Yang, S.-T. Adsorption behaviors of tetracycline on magnetic graphene oxide sponge. *Mater. Chem. Phys.* **2017**, *198*, 283–290. [CrossRef]

82. Jayanthi, S.; KrishnaRao Eswar, N.; Singh, S.A.; Chatterjee, K.; Madras, G.; Sood, A.K. Macroporous three-dimensional graphene oxide foams for dye adsorption and antibacterial applications. *RSC Adv.* **2016**, *6*, 1231–1242. [CrossRef]

83. Lei, Y.; Chen, F.; Luo, Y.; Zhang, L. Synthesis of three-dimensional graphene oxide foam for the removal of heavy metal ions. *Chem. Phys. Lett.* **2014**, *593*, 122–127. [CrossRef]

84. Wu, R.; Yu, B.; Liu, X.; Li, H.; Wang, W.; Chen, L.; Bai, Y.; Ming, Z.; Yang, S.-T. One-pot hydrothermal preparation of graphene sponge for the removal of oils and organic solvents. *Appl. Surf. Sci.* **2016**, *362*, 56–62. [CrossRef]

85. Bagoole, O.; Rahman, M.M.; Shah, S.; Hong, H.; Chen, H.; Al Ghaferi, A.; Younes, H. Functionalized three-dimensional graphene sponges for highly efficient crude and diesel oil adsorption. *Environ. Sci. Pollut. Res.* **2018**, *25*, 23091–23105. [CrossRef]

86. Maimaiti, T.; Hu, R.; Yuan, H.; Liang, C.; Liu, F.; Li, Q.; Lan, S.; Yu, B.; Yang, S.-T. Magnetic Fe_3O_4/TiO_2/graphene sponge for the adsorption of methylene blue in aqueous solution. *Diam. Relat. Mater.* **2022**, *123*, 108811. [CrossRef]

87. Sun, Y.; Yu, F.; Li, L.; Ma, J. Adsorption-reduction synergistic effect for rapid removal of Cr (VI) ions on superelastic NH_2-graphene sponge. *Chem. Eng. J.* **2021**, *421*, 129933. [CrossRef]

88. Myung, Y.; Jung, S.; Tung, T.T.; Tripathi, K.M.; Kim, T. Graphene-based aerogels derived from biomass for energy storage and environmental remediation. *ACS Sustain. Chem. Eng.* **2019**, *7*, 3772–3782. [CrossRef]

89. Kaushik, J.; Gunture; Tripathi, K.M.; Singh, R.; Sonkar, S.K. Thiourea-functionalized graphene aerogel for the aqueous phase sensing of toxic Pb(II) metal ions and H_2O_2. *Chemosphere* **2022**, *287*, 132105. [CrossRef] [PubMed]

90. Lee, B.; Lee, S.; Lee, M.; Jeong, D.H.; Baek, Y.; Yoon, J.; Kim, Y.H. Carbon nanotube-bonded graphene hybrid aerogels and their application to water purification. *Nanoscale* **2015**, *7*, 6782–6789. [CrossRef] [PubMed]

91. Li, S.; Xu, J.; Yao, G.; Liu, H. Self-adhesive, self-healable, and triple-responsive hydrogel doped with polydopamine as an adsorbent toward methylene blue. *Ind. Eng. Chem. Res.* **2019**, *58*, 17075–17087. [CrossRef]

92. Pandey, S.; Do, J.Y.; Kim, J.; Kang, M. Fast and highly efficient removal of dye from aqueous solution using natural locust bean gum based hydrogels as adsorbent. *Int. J. Biol. Macromol.* **2020**, *143*, 60–75. [CrossRef]

93. Gutekunst, S.B.; Siemsen, K.; Huth, S.; Moehring, A.; Hesseler, B.; Timmermann, M.; Paulowicz, I.; Mishra, Y.K.; Siebert, L.; Adelung, R.; et al. 3D hydrogels containing interconnected microchannels of subcellular size for capturing human pathogenic acanthamoeba castellanii. *ACS Biomater. Sci. Eng.* **2019**, *5*, 1784–1792. [CrossRef]

94. Taye, A.; Yifru, A.; Getachew, N.; Mehretie, S.; Admassie, S. Adsorption of hexavalent chromium using water hyacinth leaf protein concentrate/graphene oxide hydrogel. *Environ. Monit. Assess.* **2023**, *195*, 1342. [CrossRef]

95. Yao, G.; Liu, X.; Zhang, G.; Han, Z.; Liu, H. Green synthesis of tannic acid functionalized graphene hydrogel to efficiently adsorb methylene blue. *Colloids Surf. A Physicochem. Eng. Asp.* **2021**, *625*, 126972. [CrossRef]

96. Phiri, J.; Johansson, L.-S.; Gane, P.; Maloney, T. A comparative study of mechanical, thermal and electrical properties of graphene-, graphene oxide- and reduced graphene oxide-doped microfibrillated cellulose nanocomposites. *Compos. Part B Eng.* **2018**, *147*, 104–113. [CrossRef]

97. Cao, X.; Zhang, J.; Chen, S.; Varley, R.J.; Pan, K. 1D/2D nanomaterials synergistic, compressible, and response rapidly 3D graphene aerogel for piezoresistive sensor. *Adv. Funct. Mater.* **2020**, *30*, 2003618. [CrossRef]

98. Deng, M.; Zhao, L.; Wang, Z.; Yang, P.; Sun, Y. Preparation of phosphoric-modified aloe vera/chitosan aerogels and their efficient adsorption of U(VI). *Environ. Sci. Pollut. Res.* **2023**, *30*, 33229–33242. [CrossRef] [PubMed]

99. Nundy, S.; Ghosh, A.; Nath, R.; Paul, A.; Tahir, A.A.; Mallick, T.K. Reduced graphene oxide (rGO) aerogel: Efficient adsorbent for the elimination of antimony (III) and (V) from wastewater. *J. Hazard. Mater.* **2021**, *420*, 126554. [CrossRef] [PubMed]

100. Sreedevi, P.R.; Suresh, K.; Jiang, G. Bacterial bioremediation of heavy metals in wastewater: A review of processes and applications. *J. Water Process Eng.* **2022**, *48*, 102884. [CrossRef]

101. Bodrud-Doza, M.; Islam, S.M.D.-U.; Hasan, M.T.; Alam, F.; Haque, M.M.; Rakib, M.A.; Asad, M.A.; Rahman, M.A. Groundwater pollution by trace metals and human health risk assessment in central west part of Bangladesh. *Groundw. Sustain. Dev.* **2019**, *9*, 100219. [CrossRef]

102. Manzoor, Q.; Shahab, M.R.; Sajid, A.; Yaseen, H.M.; Alqahtani, F.O.; Malik, Q.M.; Nazir, A.; Arif, K.; Iqbal, M. Eco-benign preparation of biosorbent using momordica charantia for the efficient removal of Cr(VI) ions from wastewater. *Z. Für Phys. Chem.* **2022**, *236*, 1461–1491. [CrossRef]

103. Ghosal, P.S.; Kattil, K.V.; Yadav, M.K.; Gupta, A.K. Adsorptive removal of arsenic by novel iron/olivine composite: Insights into preparation and adsorption process by response surface methodology and artificial neural network. *J. Environ. Manag.* **2018**, *209*, 176–187. [CrossRef]

104. da Silva, E.B.; Mussoline, W.A.; Wilkie, A.C.; Ma, L.Q. Arsenic removal and biomass reduction of As-hyperaccumulator Pteris vittata: Coupling ethanol extraction with anaerobic digestion. *Sci. Total Environ.* **2019**, *666*, 205–211. [CrossRef]

105. Criscuoli, A.; Figoli, A. Pressure-driven and thermally-driven membrane operations for the treatment of arsenic-contaminated waters: A comparison. *J. Hazard. Mater.* **2019**, *370*, 147–155. [CrossRef]

106. Nieto-Delgado, C.; Gutiérrez-Martínez, J.; Rangel-Méndez, J.R. Modified activated carbon with interconnected fibrils of iron-oxyhydroxides using Mn^{2+} as morphology regulator, for a superior arsenic removal from water. *J. Environ. Sci.* **2019**, *76*, 403–414. [CrossRef]

107. Su, H.; Ye, Z.; Hmidi, N. High-performance iron oxide-graphene oxide nanocomposite adsorbents for arsenic removal. *Colloids Surf. A Physicochem. Eng. Asp.* **2017**, *522*, 161–172. [CrossRef]

108. Tang, S.C.N.; Lo, I.M.C. Magnetic nanoparticles: Essential factors for sustainable environmental applications. *Water Res.* **2013**, *47*, 2613–2632. [CrossRef]

109. Qu, G.; Li, R.; Zhou, Y.; Wu, B.; Cai, Y.; Ning, P. Preparation of ferric nitrate-graphene nanocomposite and its adsorption of arsenic(V) from simulated arsenic-containing wastewater. *Appl. Organomet. Chem.* **2019**, *33*, e5221. [CrossRef]

110. Ren, L.; Xu, J.; Zhang, Y.; Zhou, J.; Chen, D.; Chang, Z. Preparation and characterization of porous chitosan microspheres and adsorption performance for hexavalent chromium. *Int. J. Biol. Macromol.* **2019**, *135*, 898–906. [CrossRef]

111. Pavesi, T.; Moreira, J.C. Mechanisms and individuality in chromium toxicity in humans. *J. Appl. Toxicol.* **2020**, *40*, 1183–1197. [CrossRef]

112. Ben Khalifa, E.; Rzig, B.; Chakroun, R.; Nouagui, H.; Hamrouni, B. Application of response surface methodology for chromium removal by adsorption on low-cost biosorbent. *Chemom. Intell. Lab. Syst.* **2019**, *189*, 18–26. [CrossRef]

113. Panda, H.; Tiadi, N.; Mohanty, M.; Mohanty, C.R. Studies on adsorption behavior of an industrial waste for removal of chromium from aqueous solution. *S. Afr. J. Chem. Eng.* **2017**, *23*, 132–138. [CrossRef]

114. Govindaraju, K.; Vinu, R.; Gautam, R.; Vasantharaja, R.; Niranjan, M.; Sundar, I. Microwave-assisted torrefaction of biomass kappaphycus alvarezii based biochar and magnetic biochar for removal of hexavalent chromium Cr(VI) from aqueous solution. *Biomass Convers. Biorefinery* **2024**, *14*, 3643–3653. [CrossRef]

115. Mondal, N.K.; Chakraborty, S. Adsorption of Cr(VI) from aqueous solution on graphene oxide prepared from graphite: Equilibrium, kinetic and thermodynamic studies. *Appl. Water Sci.* **2020**, *10*, 61. [CrossRef]

116. Heidari, A.; Younesi, H.; Mehraban, Z.; Heikkinen, H. Selective adsorption of Pb(II), Cd(II), and Ni(II) ions from aqueous solution using chitosan–MAA nanoparticles. *Int. J. Biol. Macromol.* **2013**, *61*, 251–263. [CrossRef]

117. Kołodyńska, D. Chitosan as an effective low-cost sorbent of heavy metal complexes with the polyaspartic acid. *Chem. Eng. J.* **2011**, *173*, 520–529. [CrossRef]

118. Jia, B.; Li, G.; Cao, E.; Luo, J.; Zhao, X.; Huang, H. Recent progress of antibacterial hydrogels in wound dressings. *Mater. Today Bio* **2023**, *19*, 100582. [CrossRef]

119. Shang, M.-R.; Liu, Y.-G.; Liu, S.-B.; Zeng, G.-M.; Tan, X.-F.; Jiang, L.-H.; Huang, X.-X.; Ding, Y.; Guo, Y.-M.; Wang, S.-F. A novel graphene oxide coated biochar composite: Synthesis, characterization and application for Cr(VI) removal. *RSC Adv.* **2016**, *6*, 85202–85212. [CrossRef]

120. Kumar, P.; Chauhan, M.S. Adsorption of chromium (VI) from the synthetic aqueous solution using chemically modified dried water hyacinth roots. *J. Environ. Chem. Eng.* **2019**, *7*, 103218. [CrossRef]

121. Worku, Z.; Tibebu, S.; Nure, J.F.; Tibebu, S.; Moyo, W.; Ambaye, A.D.; Nkambule, T.T.I. Adsorption of chromium from electroplating wastewater using activated carbon developed from water hyacinth. *BMC Chem.* **2023**, *17*, 85. [CrossRef] [PubMed]

122. Wang, J.; Chen, Y.; Sun, T.; Saleem, A.; Wang, C. Enhanced removal of Cr(III)-EDTA chelates from high-salinity water by ternary complex formation on DETA functionalized magnetic carbon-based adsorbents. *Ecotoxicol. Environ. Saf.* **2021**, *209*, 111858. [CrossRef] [PubMed]

123. Kinuthia, G.K.; Ngure, V.; Beti, D.; Lugalia, R.; Wangila, A.; Kamau, L. Levels of heavy metals in wastewater and soil samples from open drainage channels in Nairobi, Kenya: Community health implication. *Sci. Rep.* **2020**, *10*, 8434. [CrossRef]

124. Narayana, P.L.; Lingamdinne, L.P.; Karri, R.R.; Devanesan, S.; AlSalhi, M.S.; Reddy, N.S.; Chang, Y.-Y.; Koduru, J.R. Predictive capability evaluation and optimization of Pb(II) removal by reduced graphene oxide-based inverse spinel nickel ferrite nanocomposite. *Environ. Res.* **2022**, *204*, 112029. [CrossRef]

125. Yu, J.-G.; Yu, L.-Y.; Yang, H.; Liu, Q.; Chen, X.-H.; Jiang, X.-Y.; Chen, X.-Q.; Jiao, F.-P. Graphene nanosheets as novel adsorbents in adsorption, preconcentration and removal of gases, organic compounds and metal ions. *Sci. Total Environ.* **2015**, *502*, 70–79. [CrossRef] [PubMed]

126. Akhavan, O.; Bijanzad, K.; Mirsepah, A. Synthesis of graphene from natural and industrial carbonaceous wastes. *RSC Adv.* **2014**, *4*, 20441–20448. [CrossRef]

127. Azam, M.G.; Kabir, M.H.; Shaikh, M.A.A.; Ahmed, S.; Mahmud, M.; Yasmin, S. A rapid and efficient adsorptive removal of lead from water using graphene oxide prepared from waste dry cell battery. *J. Water Process Eng.* **2022**, *46*, 102597. [CrossRef]

128. Lingamdinne, L.P.; Godlaveeti, S.K.; Angaru, G.K.R.; Chang, Y.-Y.; Nagireddy, R.R.; Somala, A.R.; Koduru, J.R. Highly efficient surface sequestration of Pb^{2+} and Cr^{3+} from water using a Mn_3O_4 anchored reduced graphene oxide: Selective removal of Pb^{2+} from real water. *Chemosphere* **2022**, *299*, 134457. [CrossRef]

129. Mu, R.; Liu, B.; Chen, X.; Wang, N.; Yang, J. Adsorption of Cu (II) and Co (II) from aqueous solution using lignosulfonate/chitosan adsorbent. *Int. J. Bio. Macromol.* **2020**, *163*, 120–127. [CrossRef]

130. Ranjith, K.S.; Manivel, P.; Rajendrakumar, R.T.; Uyar, T. Multifunctional ZnO nanorod-reduced graphene oxide hybrids nanocomposites for effective water remediation: Effective sunlight driven degradation of organic dyes and rapid heavy metal adsorption. *Chem. Eng. J.* **2017**, *325*, 588–600. [CrossRef]

131. Santos, S.; Ungureanu, G.; Boaventura, R.; Botelho, C. Selenium contaminated waters: An overview of analytical methods, treatment options and recent advances in sorption methods. *Sci. Total Environ.* **2015**, *521*, 246–260. [CrossRef] [PubMed]

132. Awual, M.R.; Yaita, T.; Suzuki, S.; Shiwaku, H. Ultimate selenium(IV) monitoring and removal from water using a new class of organic ligand based composite adsorbent. *J. Hazard. Mater.* **2015**, *291*, 111–119. [CrossRef] [PubMed]

133. Qureshi, S.S.; Memon, S.A.; Rafi ul, Z.; Ram, N.; Saeed, S.; Mubarak, N.M.; Karri, R.R. Rapid adsorption of selenium removal using iron manganese-based micro adsorbent. *Sci. Rep.* **2022**, *12*, 17207. [CrossRef]

134. Qi, Z.; Liu, R.; Joshi, T.P.; Peng, J.; Qu, J. Highly efficient removal of selenite by electrolysis-assisted nano-zerovalent iron (nZVI): Implication for corrosion and reduction. *Chem. Eng. J.* **2021**, *405*, 126564. [CrossRef]

135. Okonji, S.O.; Dominic, J.A.; Pernitsky, D.; Achari, G. Removal and recovery of selenium species from wastewater: Adsorption kinetics and co-precipitation mechanisms. *J. Water Process Eng.* **2020**, *38*, 101666. [CrossRef]

136. Latva, S.; Peräniemi, S.; Ahlgrén, M. Study of metal-loaded activated charcoals for the separation and determination of selenium species by energy dispersive X-ray fluorescence analysis. *Anal. Chim. Acta* **2003**, *478*, 229–235. [CrossRef]

137. Dobrowolski, R.; Otto, M. Preparation and evaluation of Fe-loaded activated carbon for enrichment of selenium for analytical and environmental purposes. *Chemosphere* **2013**, *90*, 683–690. [CrossRef]

138. Jankovský, O.; Šimek, P.; Klímová, K.; Sedmidubský, D.; Pumera, M.; Sofer, Z. Highly selective removal of Ga^{3+} ions from Al^{3+}/Ga^{3+} mixtures using graphite oxide. *Carbon* **2015**, *89*, 121–129. [CrossRef]

139. Xiao, W.; Yan, B.; Zeng, H.; Liu, Q. Dendrimer functionalized graphene oxide for selenium removal. *Carbon* **2016**, *105*, 655–664. [CrossRef]

140. Lu, Z.; Yu, J.; Zeng, H.; Liu, Q. Polyamine-modified magnetic graphene oxide nanocomposite for enhanced selenium removal. *Sep. Purif. Technol.* **2017**, *183*, 249–257. [CrossRef]

141. Sun, F.; Zhu, Y.; Liu, X.; Chi, Z. Highly efficient removal of Se(IV) using reduced graphene oxide-supported nanoscale zero-valent iron (nZVI/rGO): Selenium removal mechanism. *Environ. Sci. Pollut. Res.* **2023**, *30*, 27560–27569. [CrossRef] [PubMed]

142. Yoon, Y.; Park, W.K.; Hwang, T.-M.; Yoon, D.H.; Yang, W.S.; Kang, J.-W. Comparative evaluation of magnetite–graphene oxide and magnetite-reduced graphene oxide composite for As(III) and As(V) removal. *J. Hazard. Mater.* **2016**, *304*, 196–204. [CrossRef]

143. Ye, Y.; Yin, D.; Wang, B.; Zhang, Q. Synthesis of three-dimensional Fe_3O_4 graphene aerogels for the removal of Arsenic Ions from Water. *J. Nanomater.* **2015**, *2015*, 864864. [CrossRef]

144. Singh, N.; Naseh, M.F.; Ansari, J.R.; Sarkar, T.; Datta, A. Removal of aqueous arsenic (III) by graphene-based systems at micro-trace level. *Carbon Lett.* **2023**, *33*, 233–243. [CrossRef]

145. Chen, H.; Liu, F.; Cai, C.; Wu, H.; Yang, L. Removal of Hg^{2+} from desulfurization wastewater by tannin-immobilized graphene oxide. *Environ. Sci. Pollut. Res.* **2022**, *29*, 17964–17976. [CrossRef] [PubMed]

146. Li, L.; Luo, C.; Li, X.; Duan, H.; Wang, X. Preparation of magnetic ionic liquid/chitosan/graphene oxide composite and application for water treatment. *Int. J. Biol. Macromol.* **2014**, *66*, 172–178. [CrossRef] [PubMed]

147. Lingamdinne, L.P.; Koduru, J.R.; Choi, Y.-L.; Chang, Y.-Y.; Yang, J.-K. Studies on removal of Pb(II) and Cr(III) using graphene oxide based inverse spinel nickel ferrite nano-composite as sorbent. *Hydrometallurgy* **2016**, *165*, 64–72. [CrossRef]

148. Huang, Y.; Huang, W.; Chen, Y.; Sun, J.; Liang, M.; Guo, Y.; Liu, X.; Liu, M.; Wei, Y.; Wei, J.; et al. Effective removal of hexavalent chromium from aqueous solutions using quaternary ammonium-functionalized magnetic graphene oxide composites. *Separations* **2023**, *10*, 463. [CrossRef]
149. Fan, L.; Luo, C.; Sun, M.; Li, X.; Qiu, H. Highly selective adsorption of lead ions by water-dispersible magnetic chitosan/graphene oxide composites. *Colloids Surf. B Biointerfaces* **2013**, *103*, 523–529. [CrossRef]
150. Bao, S.; Yang, W.; Wang, Y.; Yu, Y.; Sun, Y. One-pot synthesis of magnetic graphene oxide composites as an efficient and recoverable adsorbent for Cd(II) and Pb(II) removal from aqueous solution. *J. Alloys Compd.* **2020**, *381*, 120914. [CrossRef]
151. Zhao, D.; Gao, X.; Wu, C.; Xie, R.; Feng, S.; Chen, C. Facile preparation of amino functionalized graphene oxide decorated with Fe3O4 nanoparticles for the adsorption of Cr(VI). *Appl. Surf. Sci.* **2016**, *384*, 1–9. [CrossRef]
152. Wu, W.P.; Ge, H.C. Preparation of amino-silane and thiosemicarbazide modified graphene oxide composite for high uptake adsorption of Hg(II) and Pb(II). *J. Alloys Compd.* **2024**, 2312839. [CrossRef]
153. Joya-Cárdenas, D.R.; Rodríguez-Caicedo, J.P.; Corona-Rivera, M.A.; Saldaña-Robles, N.; Damián-Ascencio, C.E.; Saldaña-Robles, A. Removal of As(V) in the presence of Cr(VI) in contaminated water from the Bajio region of Mexico using ferrihydrite-functionalized graphene oxide (GOFH): A case study. *Emerg. Contam.* **2024**, *10*, 100312. [CrossRef]
154. Wu, Z.; Deng, W.; Zhou, W.; Luo, J. Novel magnetic polysaccharide/graphene oxide @Fe$_3$O$_4$ gel beads for adsorbing heavy metal ions. *Carbohydr. Polym.* **2019**, *216*, 119–128. [CrossRef]
155. Verma, M.; Lee, I.; Oh, J.; Kumar, V.; Kim, H. Synthesis of EDTA-functionalized graphene oxide-chitosan nanocomposite for simultaneous removal of inorganic and organic pollutants from complex wastewater. *Chemosphere* **2022**, *287*, 132385. [CrossRef]
156. Zhang, H.; Liu, X.; Han, J.; Niu, W.; Wang, B.; Wu, Z.; Wei, Z.; Zhu, Y.; Guo, Q.; Wang, X. Acid-resistant chitosan/graphene oxide adsorbent for Cu^{2+} removal: The role of mixed cross-linking and amino-functionalized. *Int. J. Biol. Macromol.* **2024**, *273*, 133096. [CrossRef] [PubMed]
157. Azfar Shaida, M.; Daniyal; Ali, S.; Saalim Badar, M.; Salim Mahtab, M.; Umar Khan, M.; Ullah Khan, S.; Ahmad, I.; Atika; Haq Farooqi, I.; et al. Synthesis, characterization, and breakthrough modeling of low-cost graphene oxide-sand supported adsorbent filter for the separation of lead and chromium ions. *J. Mol. Liq.* **2024**, *403*, 124611. [CrossRef]
158. Bhardwaj, M.; Tewari, S.; Kumari, N.; Bhardwaj, A.; Misra, N.; Shukla, S.; Dwivedi, J.; Sharma, S. Adsorption of Pb(II) and Cd(II) by functionalized graphene oxide (GO-MBT): Mechanisms, antibacterial activity, and DFT studies. *Ind. Eng. Chem. Res.* **2024**, *164*, 112464. [CrossRef]
159. Elumalai, N.S.; Jaisankar, S.M.; Kumaran, C. Utilization of graphene oxide-chitosan nanocomposite for the removal of heavy metals: Kinetics, isotherm, and error analysis. *Water Conserv. Sci. Eng.* **2024**, *9*, 9. [CrossRef]
160. Zhang, C.-Z.; Chen, B.; Bai, Y.; Xie, J. A new functionalized reduced graphene oxide adsorbent for removing heavy metal ions in water via coordination and ion exchange. *Sep. Sci. Technol.* **2018**, *53*, 2896–2905. [CrossRef]
161. Attia, N.F.; Diab, M.A.; Attia, A.S.; El-Shahat, M.F. Greener approach for fabrication of antibacterial graphene-polypyrrole nanoparticle adsorbent for removal of Mn^{2+} from aqueous solution. *Synth. Met.* **2021**, *282*, 107132. [CrossRef]
162. Hadadian, M.; Goharshadi, E.K.; Fard, M.M.; Ahmadzadeh, H. Synergistic effect of graphene nanosheets and zinc oxide nanoparticles for effective adsorption of Ni(II) ions from aqueous solutions. *ACS Biomater. Sci. Eng.* **2018**, *124*, 239. [CrossRef]
163. Pan, L.; Wang, Z.; Yang, Q.; Huang, R. Efficient removal of lead, copper and cadmium ions from water by a porous calcium alginate/graphene oxide composite aerogel. *Nanomaterials* **2018**, *8*, 957. [CrossRef] [PubMed]
164. Cao, Z.-f.; Wen, X.; Wang, J.; Yang, F.; Zhong, H.; Wang, S.; Wu, Z.-k. In situ nano-Fe$_3$O$_4$/triisopropanolamine functionalized graphene oxide composites to enhance Pb^{2+} ions removal. *Colloids Surf. A Physicochem. Eng. Asp.* **2019**, *561*, 209–217. [CrossRef]
165. Ibrahim, A.I.; Onaizi, S.A.; Vohra, M.S. Novel CTAB functionalized graphene oxide for selenium removal: Adsorption results and ANN & RSM modeling. *Emergent Mater.* **2024**, *7*, 547–564. [CrossRef]
166. Liu, H.; Zhou, Y.; Yang, Y.; Zou, K.; Wu, R.; Xia, K.; Xie, S. Synthesis of polyethylenimine/graphene oxide for the adsorption of U(VI) from aqueous solution. *Appl. Surf. Sci.* **2019**, *471*, 88–95. [CrossRef]
167. Nan, Y.; Wang, J.; Chang, X.; Shao, K.; Lin, Y.; Qian, L.; Li, Z.; Hu, P. Functionalized graphene oxide/sodium alginate beads with ion responsiveness for uranium trapping. *Carbohydr. Polym.* **2023**, *300*, 120259. [CrossRef]
168. Wu, F.; Huang, H.; Sun, X.; Xie, S.; Yuan, H.; Liu, Y.; Guo, Y. Persimmon tannin-modified graphene oxide/chitosan microsphere for removing U(VI) in rare earth wastewater. *J. Radioanal. Nucl. Chem.* **2023**, *332*, 3617–3633. [CrossRef]
169. Kim, Y.; Eom, H.H.; Kim, Y.K.; Harbottle, D.; Lee, J.W. Effective removal of cesium from wastewater via adsorptive filtration with potassium copper hexacyanoferrate-immobilized and polyethyleneimine-grafted graphene oxide. *Chemosphere* **2020**, *250*, 126262. [CrossRef]
170. Kadam, A.A.; Jang, J.; Lee, D.S. Facile synthesis of pectin-stabilized magnetic graphene oxide Prussian blue nanocomposites for selective cesium removal from aqueous solution. *Bioresour. Technol.* **2016**, *216*, 391–398. [CrossRef]
171. Huang, T.; Qu, J.; Tan, L.; Yao, R.; Jiao, W.; Wang, Y.; Lin, T.; Hao, Y.; Yang, H.; Yang, H.; et al. Efficient adsorption of Ce (III) using cellulose graft poly (2-acrylamido-2-methyl-1-propanesulfonic acid)/graphene oxide composite. *Colloids Surf. A Physicochem. Eng. Asp.* **2024**, *682*, 132981. [CrossRef]
172. Abu Elgoud, E.M.; Abd-Elhamid, A.I.; Aly, H.F. Modification of graphene oxide with imidazolium-based ionic liquid for significant sorption of La(III) and Pr(III) from aqueous solutions. *Appl. Water Sci.* **2023**, *13*, 152. [CrossRef]
173. Gbadebo, A.M. Groundwater fluoride and dental fluorosis in southwestern Nigeria. *Environ. Geochem. Health* **2012**, *34*, 597–604. [CrossRef] [PubMed]

174. Liu, M.; Zang, Z.; Zhang, S.; Ouyang, G.; Han, R. Enhanced fluoride adsorption from aqueous solution by zirconium (IV)-impregnated magnetic chitosan graphene oxide. *Int. J. Biol. Macromol.* **2021**, *182*, 1759–1768. [CrossRef]

175. Rashid, U.S.; Das, T.K.; Sakthivel, T.S.; Seal, S.; Bezbaruah, A.N. GO-CeO₂ nanohybrid for ultra-rapid fluoride removal from drinking water. *Sci. Total Environ.* **2021**, *793*, 148547. [CrossRef]

176. Vasudevan, S.; Lakshmi, J. The adsorption of phosphate by graphene from aqueous solution. *RSC Adv.* **2012**, *2*, 5234–5242. [CrossRef]

177. Eltaweil, A.S.; Ibrahim, K.; El-Monaem, E.M.A.; El-Subruiti, G.M.; Omer, A.M. Phosphate removal by Lanthanum-doped aminated graphene oxide@aminated chitosan microspheres: Insights into the adsorption mechanism. *J. Clean. Prod.* **2023**, *385*, 135640. [CrossRef]

178. Wang, P.; Li, L.; Tian, Y.; Sun, L.; Zhan, W.; Chen, S.; Zhang, J.; Zuo, W. Three-dimensional graphene/La(OH)₃-nanorod aerogel adsorbent by self-assembly process for enhanced removal and recovery of phosphate in wastewater. *Sci. Total Environ.* **2022**, *809*, 152124. [CrossRef]

179. He, J.; Du, Y.-e.; Bai, Y.; An, J.; Cai, X.; Chen, Y.; Wang, P.; Yang, X.; Feng, Q. Facile formation of anatase/rutile TiO₂ nanocomposites with enhanced photocatalytic activity. *Molecules* **2019**, *24*, 2996. [CrossRef]

180. Shooto, N.D.; Thabede, P.M.; Bhila, B.; Moloto, H.; Naidoo, E.B. Lead ions and methylene blue dye removal from aqueous solution by mucuna beans (velvet beans) adsorbents. *J. Environ. Chem. Eng.* **2020**, *8*, 103557. [CrossRef]

181. Cao, Z.-f.; Wen, X.; Chen, P.; Yang, F.; Ou, X.-l.; Wang, S.; Zhong, H. Synthesis of a novel heterogeneous fenton catalyst and promote the degradation of methylene blue by fast regeneration of Fe²⁺. *Colloids Surf. A Physicochem. Eng. Asp.* **2018**, *549*, 94–104. [CrossRef]

182. Raees, A.; Jamal, M.; Ahmed, I.; Silanpaa, M.; Saad Algarni, T. Synthesis and characterization of CeO₂/CuO nanocomposites for photocatalytic degradation of methylene blue in visible light. *Coatings* **2021**, *11*, 305. [CrossRef]

183. Tabish, T.A.; Memon, F.A.; Gomez, D.E.; Horsell, D.W.; Zhang, S. A facile synthesis of porous graphene for efficient water and wastewater treatment. *Sci. Rep.* **2018**, *8*, 1817. [CrossRef]

184. Joshi, B.; Khalil, A.M.E.; Zhang, S.; Memon, F.A. Investigating the potential of greener-porous graphene for the treatment of organic pollutants in wastewater. *C* **2023**, *9*, 97. [CrossRef]

185. Naeem, H.; Tofil, H.M.; Soliman, M.; Hai, A.; Zaidi, S.H.H.; Kizilbash, N.; Alruwaili, D.; Ajmal, M.; Siddiq, M. Reduced graphene oxide-zinc sulfide nanocomposite decorated with silver nanoparticles for wastewater treatment by adsorption, photocatalysis and antimicrobial action. *Molecules* **2023**, *28*, 926. [CrossRef] [PubMed]

186. Jayawardena, R.; Eldridge, D.S.; Malherbe, F. Sonochemical synthesis of improved graphene oxide for enhanced adsorption of methylene blue. *Colloids Surf. A Physicochem. Eng. Asp.* **2022**, *650*, 129587. [CrossRef]

187. Dang, A.; Yuan, Z.; Liu, X.; Ma, S.; Yang, Y.; Zada, A.; Gao, Y.; Liu, Y.; Li, T.; Han, Y. Graphene oxide mediated carbon foam/CNTs composites for highly efficient adsorption of methylene blue and mechanism insight. *Ceram. Int.* **2023**, *49*, 36970–36978. [CrossRef]

188. Rashad, M.; Helali, S.; Shaalan, N.M.; Albalawi, A.E.; Alatawi, N.S.; Al-Faqiri, B.; Al-Belwi, M.M.; Alsharari, A.M. Dual studies of photo degradation and adsorptions of Congo red in wastewater on graphene–copper oxide heterostructures. *Materials* **2023**, *16*, 3721. [CrossRef]

189. Zheng, Y.; Zhou, X.; Luo, H.; Ling, H.; Mo, W.; Fang, H.; Shen, C.; Lei, J.; Sun, M.; Li, J. Efficient removal of Congo red with graphene aerogel derived from recycled anode of lithium-ion battery. *Int. J. Environ. Sci. Technol.* **2021**, *18*, 3995–4006. [CrossRef]

190. Yang, Z.; He, C.; Liao, W.; Zhang, X.; Liu, W.; Zou, B. Adsorption of orange G in liquid solution by the amino functionalized GO. *Separations* **2022**, *9*, 391. [CrossRef]

191. Labiadh, L.; Kamali, A.R. 3D graphene nanoedges as efficient dye adsorbents with ultra-high thermal regeneration performance. *Appl. Surf. Sci.* **2019**, *490*, 383–394. [CrossRef]

192. Yang, Z.; Liu, X.; Liu, X.; Wu, J.; Zhu, X.; Bai, Z.; Yu, Z. Preparation of β-cyclodextrin/graphene oxide and its adsorption properties for methylene blue. *Colloids Surf. B Biointerfaces* **2021**, *200*, 111605. [CrossRef]

193. Wu, Z.; Zhong, H.; Yuan, X.; Wang, H.; Wang, L.; Chen, X.; Zeng, G.; Wu, Y. Adsorptive removal of methylene blue by rhamnolipid-functionalized graphene oxide from wastewater. *Water Res.* **2014**, *67*, 330–344. [CrossRef]

194. Bu, J.; Yuan, L.; Zhang, N.; Liu, D.; Meng, Y.; Peng, X. High-efficiency adsorption of methylene blue dye from wastewater by a thiosemicarbazide functionalized graphene oxide composite. *Diam. Relat. Mater.* **2020**, *101*, 107604. [CrossRef]

195. Banaei, A.; Saadat, A.; Javadi, R.; Pargolghasemi, P. Preparation magnetic graphene oxide/diethylenetriamine composite for removal of methylene blue from aqueous solutions. *Sci. Rep.* **2024**, *14*, 15457. [CrossRef] [PubMed]

196. Liu, X.; Jing, K.; Peng, S.; Shi, Q.; Liu, H. Facile preparation of graphene oxide-based composite aerogel to efficiently adsorb methylene blue. *Colloids Surf. A Physicochem. Eng. Asp.* **2024**, *681*, 132754. [CrossRef]

197. Zhao, Q.; Zhu, X.; Chen, B. Stable graphene oxide/poly(ethyleneimine) 3D aerogel with tunable surface charge for high performance selective removal of ionic dyes from water. *Chem. Eng. J.* **2018**, *334*, 1119–1127. [CrossRef]

198. Xu, W.; Li, Y.; Wang, H.; Du, Q.; Li, M.; Sun, Y.; Cui, M.; Li, L. Study on the adsorption performance of casein/graphene oxide aerogel for methylene blue. *ACS Omega* **2021**, *6*, 29243–29253. [CrossRef] [PubMed]

199. Fu, Y.; Wang, Z.; Tian, T.; Li, G.; Gu, J.; Zhou, J.; Dong, S. Preparation of carboxymethyl cellulose/graphene oxide/ZIF-8 aerogels for efficient methylene blue adsorption. *Colloids Surf. A Physicochem. Eng. Asp.* **2024**, *696*, 134338. [CrossRef]

200. Zhou, S.; Yin, J.; Ma, Q.; Baihetiyaer, B.; Sun, J.; Zhang, Y.; Jiang, Y.; Wang, J.; Yin, X. Montmorillonite-reduced graphene oxide composite aerogel (M−rGO): A green adsorbent for the dynamic removal of cadmium and methylene blue from wastewater. *Sep. Purif. Technol.* **2022**, *296*, 121416. [CrossRef]

201. E, T.; Ma, D.; Yang, S.; Hao, X. Graphene oxide-montmorillonite/sodium alginate aerogel beads for selective adsorption of methylene blue in wastewater. *J. Alloys Compd.* **2020**, *832*, 154833. [CrossRef]

202. Li, Y.; Ni, M.; He, Q.; Li, X.; Zhang, W.; Wang, H. Adsorption of rhodamine B and Cr^{3+} ion onto graphene/chitosan composite. *J. Comput. Methods Sci. Eng.* **2021**, *21*, 927–938. [CrossRef]

203. Natasha; Khan, A.; Rahman, U.U.; Sadaf; Yaseen, M.; Abumousa, R.A.; Khattak, R.; Rehman, N.; Bououdina, M.; Humayun, M. Effective removal of nile blue dye from wastewater using silver-decorated reduced graphene oxide. *ACS Omega* **2024**, *9*, 19461–19480. [CrossRef] [PubMed]

204. Sharma, G.; AlGarni, T.S.; Kumar, P.S.; Bhogal, S.; Kumar, A.; Sharma, S.; Naushad, M.; Alothman, Z.A.; Stadler, F.J. Utilization of Ag_2O-Al_2O_3-ZrO_2 decorated onto rGO as adsorbent for the removal of Congo red from aqueous solution. *Environ. Res.* **2021**, *197*, 111179. [CrossRef]

205. Dissanayake, N.S.L.; Pathirana, M.A.; Wanasekara, N.D.; Mahltig, B.; Nandasiri, G.K. Removal of methylene blue and congo red using a chitosan–graphene oxide-electrosprayed functionalized polymeric nanofiber membrane. *Nanomaterials* **2023**, *13*, 1350. [CrossRef]

206. Su, J.; He, S.; Zhao, Z.; Liu, X.; Li, H. Efficient preparation of cetyltrimethylammonium bromide-graphene oxide composite and its adsorption of Congo red from aqueous solutions. *Colloids Surf. A Physicochem. Eng. Asp.* **2018**, *554*, 227–236. [CrossRef]

207. Mahmood, T.; Noreen, U.; Ali, R.; Ullah, A.; Naeem, A.; Aslam, M. Adsorptive removal of Congo red from aqueous phase using graphene–tin oxide composite as a novel adsorbent. *Int. J. Environ. Sci. Technol.* **2022**, *19*, 10275–10290. [CrossRef]

208. Li, Y.; Liu, H.; Nie, R.; Li, Y.; Li, Q.; Lei, Y.; Guo, M.; Zhang, Y. Highly efficient adsorption of anionic dyes on a porous graphene oxide nanosheets/chitosan composite aerogel. *Ind. Crops Prod.* **2024**, *220*, 119146. [CrossRef]

209. Dong, J.; Chen, Q.; Zhang, J.; Wang, Z.; Cai, J.; Yan, H.; Chen, C. Effects of rainfall events on behavior of tetracycline antibiotics in a receiving river: Seasonal differences in dominant processes and mechanisms. *Sci. Total Environ.* **2019**, *692*, 511–518. [CrossRef]

210. Hu, X.; Zhou, Q.; Luo, Y. Occurrence and source analysis of typical veterinary antibiotics in manure, soil, vegetables and groundwater from organic vegetable bases, northern China. *Environ. Pollut.* **2010**, *158*, 2992–2998. [CrossRef]

211. Zhao, H.; Liu, X.; Cao, Z.; Zhan, Y.; Shi, X.; Yang, Y.; Zhou, J.; Xu, J. Adsorption behavior and mechanism of chloramphenicols, sulfonamides, and non-antibiotic pharmaceuticals on multi-walled carbon nanotubes. *J. Hazard. Mater.* **2016**, *310*, 235–245. [CrossRef] [PubMed]

212. Liu, P.; Liu, W.-J.; Jiang, H.; Chen, J.-J.; Li, W.-W.; Yu, H.-Q. Modification of bio-char derived from fast pyrolysis of biomass and its application in removal of tetracycline from aqueous solution. *Bioresour. Technol.* **2012**, *121*, 235–240. [CrossRef]

213. Gao, Y.; Li, Y.; Zhang, L.; Huang, H.; Hu, J.; Shah, S.M.; Su, X. Adsorption and removal of tetracycline antibiotics from aqueous solution by graphene oxide. *J. Colloid Interface Sci.* **2012**, *368*, 540–546. [CrossRef]

214. Moussavi, G.; Hossaini, Z.; Pourakbar, M. High-rate adsorption of acetaminophen from the contaminated water onto double-oxidized graphene oxide. *Chem. Eng. J.* **2016**, *287*, 665–673. [CrossRef]

215. Peng, B.; Chen, L.; Que, C.; Yang, K.; Deng, F.; Deng, X.; Shi, G.; Xu, G.; Wu, M. Adsorption of antibiotics on graphene and biochar in aqueous solutions induced by π-π interactions. *Sci. Rep.* **2016**, *6*, 31920. [CrossRef]

216. Chen, H.; Gao, B.; Li, H. Removal of sulfamethoxazole and ciprofloxacin from aqueous solutions by graphene oxide. *J. Hazard. Mater.* **2015**, *282*, 201–207. [CrossRef] [PubMed]

217. Rostamian, R.; Behnejad, H. A comprehensive adsorption study and modeling of antibiotics as a pharmaceutical waste by graphene oxide nanosheets. *Ecotoxicol. Environ. Saf.* **2018**, *147*, 117–123. [CrossRef]

218. Li, Z.; Jiang, H.; Wang, X.; Wang, C.; Wei, X. Effect of pH on adsorption of tetracycline antibiotics on graphene oxide. *Int. J. Environ. Res. Public Health* **2023**, *20*, 2448. [CrossRef] [PubMed]

219. Shaha, C.K.; Mahmud, M.A.A.; Saha, S.; Karmaker, S.; Saha, T.K. Efficient removal of sparfloxacin antibiotic from water using sulfonated graphene oxide: Kinetics, thermodynamics, and environmental implications. *Heliyon* **2024**, *10*, e33644. [CrossRef]

220. Song, X.; Shui, B.; Wang, Y.; Zhou, J.; Wang, S.; Wu, N. Adsorption performance of GO-doped activated ATP composites towards tetracycline. *RSC Adv.* **2022**, *12*, 19917–19928. [CrossRef]

221. Parashar, D.; Harafan, A.; Achari, G.; Kumar, M. Ciprofloxacin and metronidazole adsorption on chitosan-modified graphene oxide as single-compound and binary mixtures: Kinetics, isotherm, and sorption mechanism. *J. Hazard. Toxic Radioact. Waste* **2023**, *27*, 04022042. [CrossRef]

222. Yu, H.; Zheng, K.; Xu, X.; Liu, X.; Zhao, B.; Ding, H.; Yu, Z.; Deng, C. Preparation of β-cyclodextrin/dopamine hydrochloride-graphene oxide and its adsorption properties for sulfonamide antibiotics. *Environ. Sci. Pollut. Res.* **2022**, *29*, 70192–70201. [CrossRef] [PubMed]

223. Fatholahi, P.; Salehzadeh, H.; Hosseini, K.; Wantala, K.; Shivaraju, H.P.; Jenkins, D.; Shahmoradi, B. Removal of erythromycin antibiotic from the aqueous media using magnetic graphene oxide nanoparticles. *Desalination Water Treat.* **2023**, *303*, 142–150. [CrossRef]

224. Bahar, P.; Hassani, A.H.; Panahi, H.A.; Moniri, E. Application of modified graphene oxide with thermosensitive polymers for adsorption of antibiotics from synthetic contaminated water. *Dalton Trans.* **2021**, *210*, 281–295. [CrossRef]

225. Wang, J.; Yao, Q.; Sheng, C.; Jin, C.; Sun, Q. One-step preparation of graphene oxide/cellulose nanofibril hybrid aerogel for adsorptive removal of four kinds of antibiotics. *J. Nanomater.* **2017**, *2017*, 5150613. [CrossRef]

226. Zhuang, Y.; Yu, F.; Ma, J.; Chen, J. Enhanced adsorption removal of antibiotics from aqueous solutions by modified alginate/graphene double network porous hydrogel. *J. Colloid Interface Sci.* **2017**, *507*, 250–259. [CrossRef]

227. Karaolia, P.; Michael-Kordatou, I.; Hapeshi, E.; Drosou, C.; Bertakis, Y.; Christofilos, D.; Armatas, G.S.; Sygellou, L.; Schwartz, T.; Xekoukoulotakis, N.P.; et al. Removal of antibiotics, antibiotic-resistant bacteria and their associated genes by graphene-based TiO$_2$ composite photocatalysts under solar radiation in urban wastewaters. *Appl. Catal. B-Environ.* **2018**, *224*, 810–824. [CrossRef]

228. Tang, L.; Ma, X.Y.; Wang, Y.; Zhang, S.; Zheng, K.; Wang, X.C.; Lin, Y. Removal of trace organic pollutants (pharmaceuticals and pesticides) and reduction of biological effects from secondary effluent by typical granular activated carbon. *Sci. Total Environ.* **2020**, *749*, 141611. [CrossRef]

229. Gouveia, T.I.A.; Mota, I.H.; Silva, A.M.T.; Alves, A.; Santos, M.S.F. Are cytostatic drugs in surface waters a potential threat? *Sci. Total Environ.* **2022**, *853*, 158559. [CrossRef]

230. Cao, S.; Liu, Y.; Ming, D.; Tian, J.; You, J.; Chen, Z. Evaluation of the difference in adsorption of amphetamine-type drugs on deep eutectic solvent-functionalized graphene oxide/ZIF-67 composite: Experiment and theoretical calculations. *Environ. Res.* **2024**, *249*, 118356. [CrossRef]

231. Al-Ghouti, M.A.; Sayma, J.; Munira, N.; Mohamed, D.; Da'na, D.A.; Qiblawey, H.; Alkhouzaam, A. Effective removal of phenol from wastewater using a hybrid process of graphene oxide adsorption and UV-irradiation. *Environ. Technol. Innov.* **2022**, *27*, 102525. [CrossRef]

232. Cui, Y.; Kang, W.; Hu, J. Effectiveness and mechanisms of the adsorption of phenol from wastewater onto N-doped graphene oxide aerogel. *J. Water Process Eng.* **2023**, *53*, 103665. [CrossRef]

233. Severo, L.S.; Thue, P.S.; Lima, D.R.; Didó, C.A.; Vasconcellos, M.A.Z.; Armas, L.E.G.; Lima, E.C.; Benvenutti, E.V.; de Menezes, E.W. 3D graphene sponge biomass-derived with high surface area applied as adsorbent for nitrophenols. *J. Environ. Chem. Eng.* **2023**, *11*, 109924. [CrossRef]

234. Wang, F.; Lu, X.; Peng, W.; Deng, Y.; Zhang, T.; Hu, Y.; Li, X.-y. Sorption behavior of bisphenol A and triclosan by graphene: Comparison with activated carbon. *ACS Omega* **2017**, *2*, 5378–5384. [CrossRef] [PubMed]

235. Song, T.; Tian, W.; Qiao, K.; Zhao, J.; Chu, M.; Du, Z.; Wang, L.; Xie, W. Adsorption behaviors of polycyclic aromatic hydrocarbons and oxygen derivatives in wastewater on n-doped reduced graphene oxide. *Sep. Purif. Technol.* **2021**, *254*, 117565. [CrossRef]

236. Kang, W.; Cui, Y.; Yang, Y.; Guo, M.; Zhao, Z.; Wang, X.; Liu, X. Preparation of nitrogen-doped hollow carbon nanosphere/graphene composite aerogel for efficient removal of quinoline from wastewater. *J. Hazard. Mater.* **2021**, *417*, 126160. [CrossRef]